Copy 197

NASA MEMO 12-6-58L

NASA MEMO 12-6-58L

C. 197

LOAN COPY: RETU
AFWL (WLL—
KIRTLAND AFB, N
0062969

TECH LIBRARY KAFB, NM

NASA

MEMORANDUM

AERODYNAMIC CHARACTERISTICS OF THREE VERSIONS OF A SUPERSONIC AIRPLANE MODEL WITH A 45° SWEPTBACK MIDWING AT MACH NUMBERS OF 1.57 AND 2.01

By W. H. Appich, Jr., Waldo I. Oehman, and Donald T. Gregory

Langley Research Center
Langley Field, Va.

[redacted]

NATIONAL AERONAUTICS AND SPACE ADMINISTRATION
WASHINGTON
February 1959

[redacted]

1197

2 cds removed 21 Jan 64 fa

[redacted]

NATIONAL AERONAUTICS AND SPACE ADMINISTRATION

TECH LIBRARY KAFB, NM
0062969

MEMORANDUM 12-6-58L

AERODYNAMIC CHARACTERISTICS OF THREE VERSIONS OF A SUPERSONIC AIRPLANE MODEL WITH A 45° SWEPTBACK MIDWING AT MACH NUMBERS OF 1.57 AND 2.01*

By W. H. Appich, Jr., Waldo I. Oehman, and Donald T. Gregory

Classification changed to Unclassified by authority of NASA Memo 5-27-59L dated 12/29/65

SUMMARY

An investigation has been conducted in the Langley Unitary Plan wind tunnel to determine the aerodynamic characteristics of a model of a 45° swept-wing, supersonic airplane in a Reynolds number range, based on mean aerodynamic chord of the wing, from 0.7×10^6 to 3.2×10^6 for a Mach number of 1.57 and from 0.6×10^6 to 3.4×10^6 for a Mach number of 2.01. The basic model has a wing with 45° sweepback of the quarter-chord line, aspect ratio of 3.2, taper ratio of 0.468, NACA 65A005.5 sections just outboard of the inlet, and NACA 65A003.7 sections at the tip. The configuration is essentially a midwing model with an all-movable horizontal tail located below the extended chord line of the wing. The model has twin wing-root supersonic inlets ducted to a single exit at the base of the fuselage. Modifications to this model that were also investigated include an enlarged-canopy model and a model with an enlarged canopy and a lengthened nose section. Increasing the canopy size increases the minimum drag coefficient; however, lengthening the nose of the enlarged-canopy model halves this increment in drag coefficient.

The directional stability of the enlarged-canopy configuration is markedly reduced in comparison with that of the basic model. A single ventral fin of the size used on these configurations is ineffective in overcoming directional instability at high angles of attack. Large nose strakes were the most effective means of increasing directional stability at high angles of attack at a Mach number of 2.01; however, the large-canopy configurations with large nose strakes were neutrally stable at angles of attack near 17°. Adding a center-line tank to the large-canopy configuration leads to a significant decrease in directional stability for all test conditions, and this configuration becomes directionally unstable near angles of attack of 10° and 6° at Mach numbers of 1.57 and 2.01, respectively.

*Title, Unclassified.

[redacted]

INTRODUCTION

The versatility of a supersonic fighter aircraft may be increased if, by slight modification, it can be developed for use as a trainer or for reconnaissance. A trainer aircraft would require an enlarged canopy to accommodate two persons. A reconnaissance version would probably entail the use of an enlarged fuselage for radar or photographic equipment, as well as a larger canopy for additional personnel. Determination of the effects of such modifications on the airplane aerodynamic characteristics would, of necessity, be required for the development of these configurations.

An experimental investigation has been conducted, therefore, to determine the effects of an enlarged canopy and an enlarged canopy with a lengthened nose section on the aerodynamic characteristics of a 45° swept-wing, supersonic, fighter-airplane model. The tests were performed at Mach numbers of 1.57 and 2.01 in the Langley Unitary Plan wind tunnel. In addition, tests were performed to determine the effects of external stores and stability augmentation devices on drag and stability characteristics.

The pitch tests were performed at Reynolds numbers, based on the mean aerodynamic chord of the wing, of approximately 1.4×10^6 and 1.2×10^6 at Mach numbers of 1.57 and 2.01, respectively; yaw tests were performed at Reynolds numbers of 0.7×10^6 and 0.6×10^6 at Mach numbers of 1.57 and 2.01, respectively.

SYMBOLS

The force and moment coefficients are referred to the stability-axis system (fig. 1). The reference-moment center was located longitudinally at 25 percent of the wing mean aerodynamic chord and vertically at water line 0.

α	angle of attack of wing chord, deg
β	angle of sideslip of fuselage center line, deg
b_w	wing span, 19.08 in.
$\bar{c}_w$	mean aerodynamic chord of the wing, 6.264 in.
C_D'	drag coefficient, $C_{D,t}' - C_{D,i}' - C_{D,c}'$

$C'_{D,b}$ base drag coefficient, $\frac{\text{Base axial force} \times \cos \alpha}{q_\infty S_w}$

$C'_{D,c}$ balance-chamber drag coefficient, $\frac{\text{Balance-chamber axial force} \times \cos \alpha}{q_\infty S_w}$

$C'_{D,e}$ net external drag coefficient, $C'_D - C'_{D,b}$

$C'_{D,i}$ internal-duct drag coefficient, $\frac{\text{Internal-duct force along X stability axis}}{q_\infty S_w}$

$C'_{D,min}$ minimum drag coefficient

$C'_{D,t}$ gross total drag coefficient, $\frac{\text{Force along X stability axis}}{q_\infty S_w}$

C_L lift coefficient, $\frac{\text{Lift force}}{q_\infty S_w}$

C_l rolling-moment coefficient, $\frac{\text{Rolling moment}}{q_\infty S_w b_w}$

C_m pitching-moment coefficient, $\frac{\text{Pitching moment}}{q_\infty S_w \bar{c}_w}$

C_n yawing-moment coefficient, $\frac{\text{Yawing moment}}{q_\infty S_w b_w}$

C_Y side-force coefficient, $\frac{\text{Side force}}{q_\infty S_w}$

F.S. fuselage station

$(L/D)_{max}$ maximum lift-drag ratio

M free-stream Mach number

q_∞ free-stream dynamic pressure, lb/sq ft

R	Reynolds number
S_w	projected wing area, 0.795 sq ft
W.L.	water line
$\frac{\partial C_L}{\partial \alpha}$	lift parameter (evaluated at $\alpha = 0^\circ$)
$\frac{\partial C_m}{\partial C_L}$	pitching-moment parameter (evaluated at $C_L = 0$)
C_{l_β}	rolling-moment parameter (evaluated at $\beta = 0^\circ$)
C_{n_β}	yawing-moment parameter (evaluated at $\beta = 0^\circ$)
C_{Y_β}	side-force parameter (evaluated at $\beta = 0^\circ$)
ΔC_{l_β}	increment of rolling-moment parameter provided by fixes
ΔC_{n_β}	increment of yawing-moment parameter provided by fixes
ΔC_{Y_β}	increment of side-force parameter provided by fixes

APPARATUS AND MODELS

Tunnel

The investigation was conducted in the low Mach number test section of the Langley Unitary Plan wind tunnel, which is a variable pressure return-flow type tunnel. The test section of the tunnel is 4 feet square and approximately 7 feet long. Mach number may be continuously varied from about 1.5 to 2.9 by means of an asymmetric sliding-block nozzle.

Configurations

A three-view drawing of the basic fighter-airplane model is presented in figure 2, and this configuration will be referred to as model I. Models II and III, shown in figure 3, are modifications of model I.

Model II has an enlarged canopy, whereas model III includes both an enlarged canopy and a lengthened nose.

The models have a wing with 45° sweepback of the quarter-chord line, an aspect ratio of 3.2, a taper ratio of 0.468, and a negative dihedral of 3.5°. The airfoil sections varied from NACA 65A005.5 just outboard of the engine inlets to NACA 65A003.7 at the tips.

The twin, wing-root, supersonic inlets were ducted to a single exit, and all tests were performed with air flow through the ducts. An all-movable horizontal tail was located below the extended chord line of the wing and was set at -3° angle of incidence.

Various configuration changes to models II and III included the use of external stores and directional stability control devices. The external stores were tested on model II and included a center-line tank, wing-mounted chaff dispensers, and fuselage radar blisters. These stores may be seen in figures 4 and 5. In addition, model II was tested with twin ventral fins as a directional stability control device. Model III was tested with 45° dorsal fins and small and large strakes. (See figs. 5 and 6.)

Tests of terminal fairings (fig. 7) added to model I in an attempt to improve drag characteristics were also performed. Photographs of some of the configurations tested are presented in figure 5.

Instrumentation

Forces and moments were measured by means of a six-component strain-gage balance mounted within the model.

Base pressure, balance-chamber pressure, and internal-duct pressures were measured with electrical pressure transducers.

TEST CONDITIONS, CORRECTIONS, AND ACCURACY

Test Conditions

The test conditions were as follows:

	M = 1.57	M = 2.01
Stagnation temperature, °F	125	125
Stagnation dewpoint, °F	-30	-30
Stagnation pressures (pitch tests), psia	10 and 23	10 and 29

	M = 1.57	M = 2.01
Reynolds numbers (pitch tests), based on $\bar{c}_w$ . . .	$\begin{cases} 1.4 \times 10^6 \\ 3.2 \times 10^6 \end{cases}$	$\begin{cases} 1.2 \times 10^6 \\ 3.4 \times 10^6 \end{cases}$
Stagnation pressure (sideslip tests), psia . . .	5	5
Reynolds number (sideslip tests), based on $\bar{c}_w$	0.7×10^6	0.6×10^6

Structural considerations of the model sting support limited the stagnation pressure to 5 psia for the sideslip tests. The angle of sideslip was varied from about -5° to 13° at angles of attack from 0.6° to 16.7°. The angle of attack was varied from about -2° to 18° at a sideslip angle of approximately 0°.

Corrections

The angles of attack and sideslip have been corrected for test-section flow angularity and for deflection of the balance and sting under load. Measured pressure gradients are sufficiently small to assure that model buoyancy effects are negligible.

Base-pressure measurements were obtained at the duct exit for only one pitch test at both test Mach numbers. These pressures have been converted to base drag coefficients and are shown in figure 8. Balance-chamber pressure and internal-duct pressures at the duct exit were measured for all model test points. The variation of balance-chamber and internal-duct drag coefficients with angle of attack for each test Mach number is also presented in figure 8. The drag coefficients presented in this report have been corrected for balance-chamber and internal-duct drag but have not been corrected for base drag. Net external drag coefficients may be obtained by subtracting the base drag coefficients from the drag coefficients shown on the characteristic plots for the same model angle of attack and Mach number. The drag values shown are a close approximation to the true drag level, since the base-drag values are quite small.

Accuracy

The accuracy of the individual measured quantities, based on calibrations and repeatability of data, is estimated to be within the following limits:

C_L	±0.002
C_D'	±0.001

C_m	±0.001
C_l	±0.0002
C_n	±0.0005
C_Y	±0.0015
α, deg	±0.1
β, deg	±0.1
M	±0.015

PRESENTATION OF RESULTS

The results of the investigation are presented as follows:

	Figure
Effect of angle of attack on base, chamber, and internal-duct drag coefficients	8
Typical schlieren photographs of models tested at various angles of attack	9
Effect of nose length and canopy size on aerodynamic characteristics in pitch	10
Effect of tail surfaces on aerodynamic characteristics in pitch	11
Effect of external stores on aerodynamic characteristics in pitch	12
Effect of directional stability control devices on aerodynamic characteristics in pitch	13
Summary of performance and longitudinal stability derivatives	14
Effect of terminal fairings on aerodynamic characteristics in pitch	15
Effect of Reynolds number on net external drag characteristics	16
Effect of nose length and canopy size on aerodynamic characteristics in sideslip	17
Summary of directional and lateral stability derivatives for three model configurations	18
Effect of tail surfaces and ventral fin on aerodynamic characteristics in sideslip	19
Effect of external stores on aerodynamic characteristics in sideslip	20
Summary of directional and lateral stability derivatives for the model with external stores	21
Effect of twin ventral fins on aerodynamic characteristics in sideslip for model II	22
Effect of lateral stability control devices on aerodynamic characteristics in sideslip for model III	23
Increment of directional and lateral stability parameters provided by control devices	24

DISCUSSION OF RESULTS

Longitudinal Stability and Drag

A comparison of the pitch characteristics of models I, II, and III (fig. 10) shows that forebody modifications of the magnitude tested herein have little effect on the longitudinal stability or lift-curve slopes of this type of aircraft. The increase in canopy size, however, increases the minimum drag coefficient by approximately 0.003 at both test Mach numbers. Model III, on the other hand, has a drag decrement of about 0.001 compared with model II, indicating that the lengthened nose tends to improve the performance characteristics of the configurations tested.

An examination of figure 11 shows that, for model II, the horizontal-tail contribution to $\frac{\partial C_m}{\partial C_L}$ is of the order of -0.25 at both test Mach numbers. Comparison of these data with data in reference 1 indicates that the horizontal-tail effectiveness for models I and III would be of the same order of magnitude.

Addition of any of the external stores to model II leads to significant increases in drag coefficient, particularly at the lower test Mach numbers. (See fig. 12.) The wing-mounted chaff dispensers incur the highest drag coefficients indicating that chaff can be more efficiently dispensed from fuselage-mounted stores. Addition of the external stores had little effect on lift-curve slopes or on the degree of longitudinal stability of model II at both test Mach numbers with the exception of the model with radar blisters tested at $M = 2.01$. At this higher Mach number, the radar blisters reduced the longitudinal stability level of the test configuration.

Data presented in reference 1 indicated stable directional and lateral stability characteristics of model I up to relatively large angles of attack. However, the forebody modifications made to convert model I to models II and III tend to decrease the directional and lateral stability. Accordingly, various stability augmentation devices were separately added to models II and III, and the effects of these devices on longitudinal stability are shown in figure 13; however, the effects on the directional and lateral stability characteristics will be discussed later. On model II, twin ventral fins were substituted for the single ventral fin common to the three test models. This modification had little or no effect on the longitudinal stability or drag characteristics of the model.

The 45° dorsal fins, small strakes, and large strakes were tested on model III. None of these three devices had any appreciable effect on the lift or drag characteristics of the model (figs. 13(c) and (d)).

The dorsal fins and strakes caused opposite effects on the slope of the pitching-moment curve. The dorsal fins, in effect, slightly increase the horizontal area behind the center of gravity; thus, the longitudinal stability is increased by a small amount. The strakes decrease the longitudinal stability of the model.

It is believed that the incremental effect of any of the devices on longitudinal stability will be approximately the same for either model II or model III.

The effect of model forebody configuration, external stores, and control devices are presented in figure 14.

In an effort to reduce the drag, terminal fairings were added to model I in accordance with the area rule. Essentially, these fairings reduce the slope of the area curve over the rearward portion of the model. The data presented in figure 15 indicate that no reduction in minimum drag coefficient is achieved by use of these terminal fairings at the test Mach numbers. It is possible, however, that with an underexpanded nozzle of an operating engine in the aircraft the increased pressure acting on a large base may lead to a decrease in minimum drag.

The effect of Reynolds number on minimum drag coefficient for model II is shown in figure 16. The drag beam of the strain-gage balance severely limited the Reynolds number range. The data show a slight decrease in minimum drag coefficient with Reynolds number at both test Mach numbers; however, this decrease is actually within the limits of accuracy of the balance and should be used with caution.

Directional and Lateral Stability

A comparison of the directional and lateral stability characteristics of models I, II, and III (fig. 17) shows that the enlarged canopy of model II leads to a marked decrease in directional stability at all test angles of attack and Mach numbers. The increase in nose length has no significant effect on the directional or lateral stability characteristics since the characteristic curves of models II and III are essentially coincident. The summary curves of figure 18 indicate that the decrease in directional stability with increasing angle of attack is about the same at each test Mach number for all three model configurations. The data of reference 1 showed that model I was stable up to an angle of attack of 16° at a Mach number of 2.01. However, the degree of stability was marginal at 16°. The increase in canopy size leads to directional instability at angles of attack greater than about 10° at $M = 2.01$. An extrapolation of the data of figure 18 for a Mach number of 1.57 would indicate that models II and III were directionally stable up to an angle of attack of about 15° in spite of the destabilizing effect of the large canopy.

The enlarged canopy also causes a reduction in dihedral effect at the lower angles of attack, as shown in figure 17. This reduction in dihedral effect washes out at the higher angles of attack for both test Mach numbers. An interesting point to be noted in figure 18 is that at $M = 1.57$ the dihedral effect decreases with increasing angle of attack for all three model configurations; whereas, at $M = 2.01$, the dihedral effect increases with angle of attack.

Figure 19 presents test results obtained for model II with tail surfaces removed and with tail surfaces and ventral fin removed. The ventral fin, although of small size, provides about 10 percent to 15 percent of the directional stability of the models at angles of attack near 0°. The relative effectiveness of a ventral fin would be expected to increase with increasing angle of attack. From figure 18, it may be seen that C_{n_β} for the configuration with vertical tail off does not change significantly up to an angle of attack near 11° at both test Mach numbers. The decrease in the directional stability of the three models is due, therefore, to loss of vertical-tail effectiveness with increasing Mach number and angle of attack. As previously discussed, all three model configurations show a reduction in dihedral effect with increasing angle of attack at $M = 1.57$, whereas at $M = 2.01$ the dihedral effect increases with angle of attack. Figure 18 indicates that the increase in dihedral effect at $M = 2.01$ is the result of an increase in wing-body effectiveness (denoted by the negative slope of C_{l_β} with angle of attack).

Tests of model II with center-line tank were conducted through the sideslip range at both test Mach numbers. Model II with chaff dispensers was tested only at an angle of attack of approximately 11°. The data presented in figure 20 indicate that, in general, addition of the center-line tank leads to a marked reduction in directional stability and an increase in dihedral effect at both test Mach numbers. One exception is the decrease in dihedral effect near an angle of attack of 0° at $M = 2.01$. The reduction in directional stability effected by the center-line tank causes the configuration to become unstable at an angle of attack of approximately 10° at $M = 1.57$ and at an angle of attack of approximately 6° at $M = 2.01$. These effects are more clearly illustrated in figure 21. The chaff dispensers slightly decrease the dihedral effect of the configuration at both test Mach numbers for an angle of attack near 11°. At $M = 1.57$, the chaff dispensers have essentially the same effect as the center-line tank on the directional stability of the configuration, whereas, at $M = 2.01$ they markedly increase the directional stability. From model geometry, it would be expected that the chaff dispensers will increase directional stability at both Mach numbers, and it is believed that the adverse effect of the chaff dispensers on directional stability at $M = 1.57$ is due to their being in an adverse wing-body interference field at this Mach number.

Several control devices were tested on the configurations with the enlarged canopy in an effort to improve their directional and lateral stability characteristics, and these data are presented in figures 22 and 23. Since different devices were used with two model configurations, it is believed that the effectiveness of these devices would not be altered by the difference in nose length. The effects have been plotted in incremental form. (See fig. 24.) This figure indicates that at a Mach number of 1.57, the twin ventral fins have the greatest effect in improving directional stability at all test angles of attack. From the basic figures, it may be seen that all the configurations with control devices are directionally stable at all test angles of attack. At a Mach number of 2.01, the data indicate that the large strakes would be the most effective means of improving the directional stability characteristics throughout the test angle-of-attack range. As shown in figure 23, only model III with the large strakes is stable to an angle of attack of about 17°. At this angle of attack, the other large-canopy configurations tested are directionally unstable. The addition of the devices causes only slight changes in dihedral effect at either test Mach number.

CONCLUSIONS

An investigation of the aerodynamic characteristics of a model of a 45° swept-wing, supersonic airplane at Mach numbers of 1.57 and 2.01 in the Langley Unitary Plan wind tunnel indicates the following conclusions:

1. Increasing the canopy size to that shown for these tests slightly increases the minimum drag coefficient; however, lengthening the nose halves this drag coefficient increment.

2. The directional stability of the large-canopy configurations is markedly reduced in comparison with that of the small-canopy configuration.

3. The size of the single ventral fin tested is sufficient to produce directional stability for all test configurations at a Mach number of 1.57 and for the small-canopy configuration at a Mach number of 2.01. However, at a Mach number of 2.01 the single ventral fin was too small to be effective for the large-canopy configuration at angles of attack greater than about 10°.

4. Large nose strakes are the most effective means of increasing directional stability at high angles of attack at a Mach number of 2.01; however, the large-canopy configurations are neutrally stable with this device at angles of attack near 17°.

5. Adding a center-line tank to the enlarged-canopy configuration leads to a significant decrease in directional stability for all test conditions, and this configuration becomes unstable (directionally) at angles of attack near 11° and 6° at Mach numbers of 1.57 and 2.01, respectively.

6. Terminal fairing blocks built in accordance with the supersonic area rule have no significant effect on minimum drag coefficient.

Langley Research Center,
National Aeronautics and Space Administration,
Langley Field, Va., October 1, 1958.

REFERENCE

1. Spearman, M. Leroy, Robinson, Ross B., and Driver, Cornelius: The Effects of the Addition of Small Fuselage-Mounted Fins on the Static Directional Stability Characteristics of a Model of a 45° Swept-Wing Airplane at Angles of Attack up to 15.3° at a Mach Number of 2.01. NACA RM L56D16a, 1956.

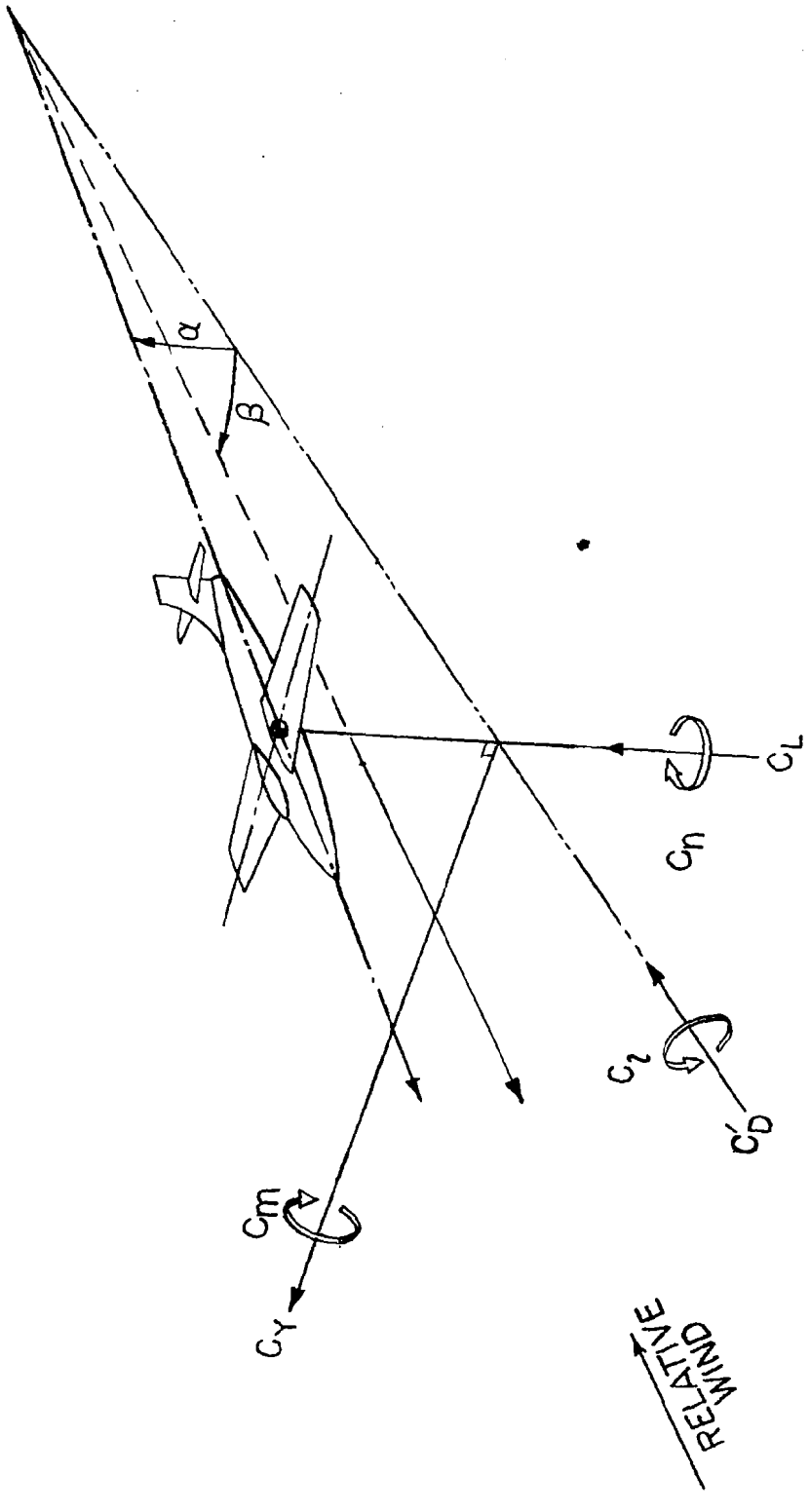

Figure 1.- Stability-axis system.

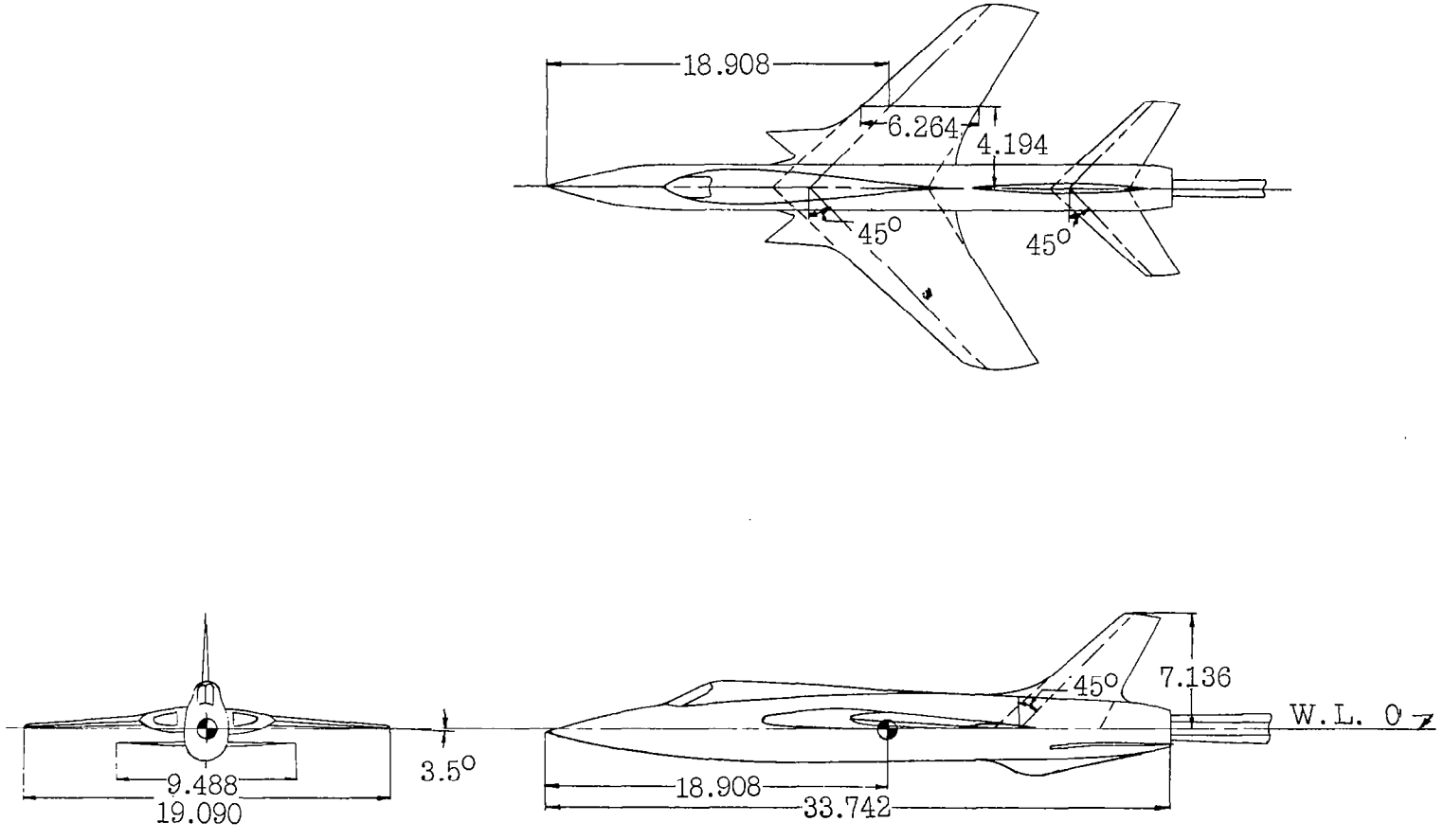

Figure 2.- Three-view drawing of 45° swept-wing, fighter-airplane model (model I). All dimensions are in inches.

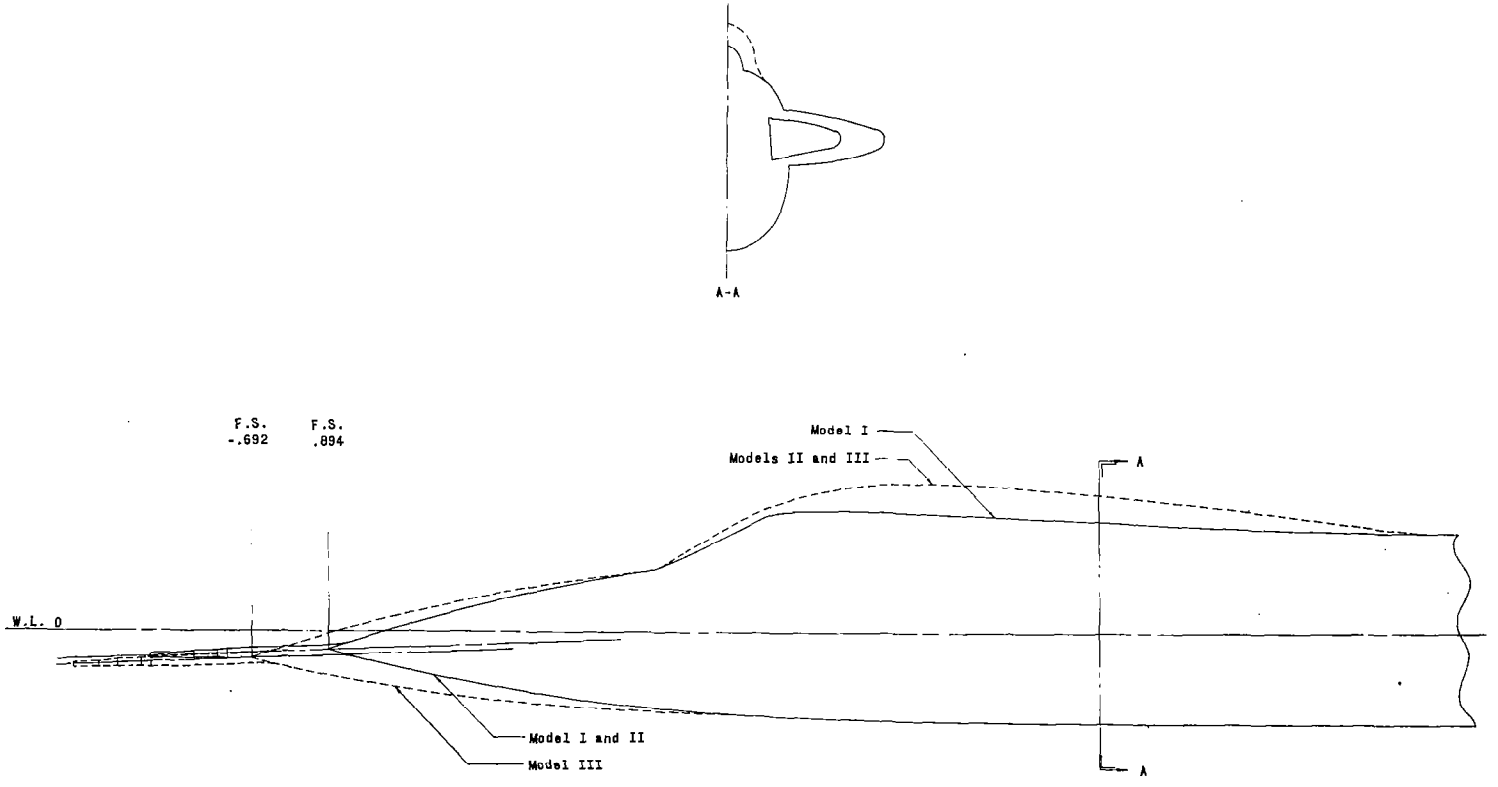

Figure 3.- Sketch showing differences between models I, II, and III. All dimensions are in inches.

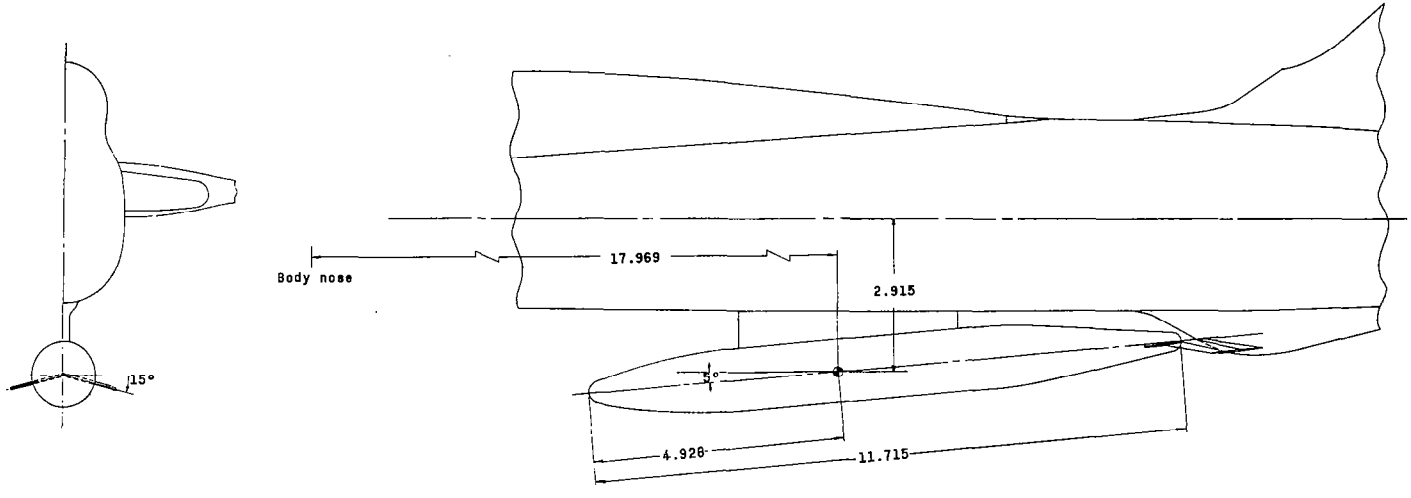

(a) Center-line tank.

Figure 4.- External stores. All dimensions are in inches.

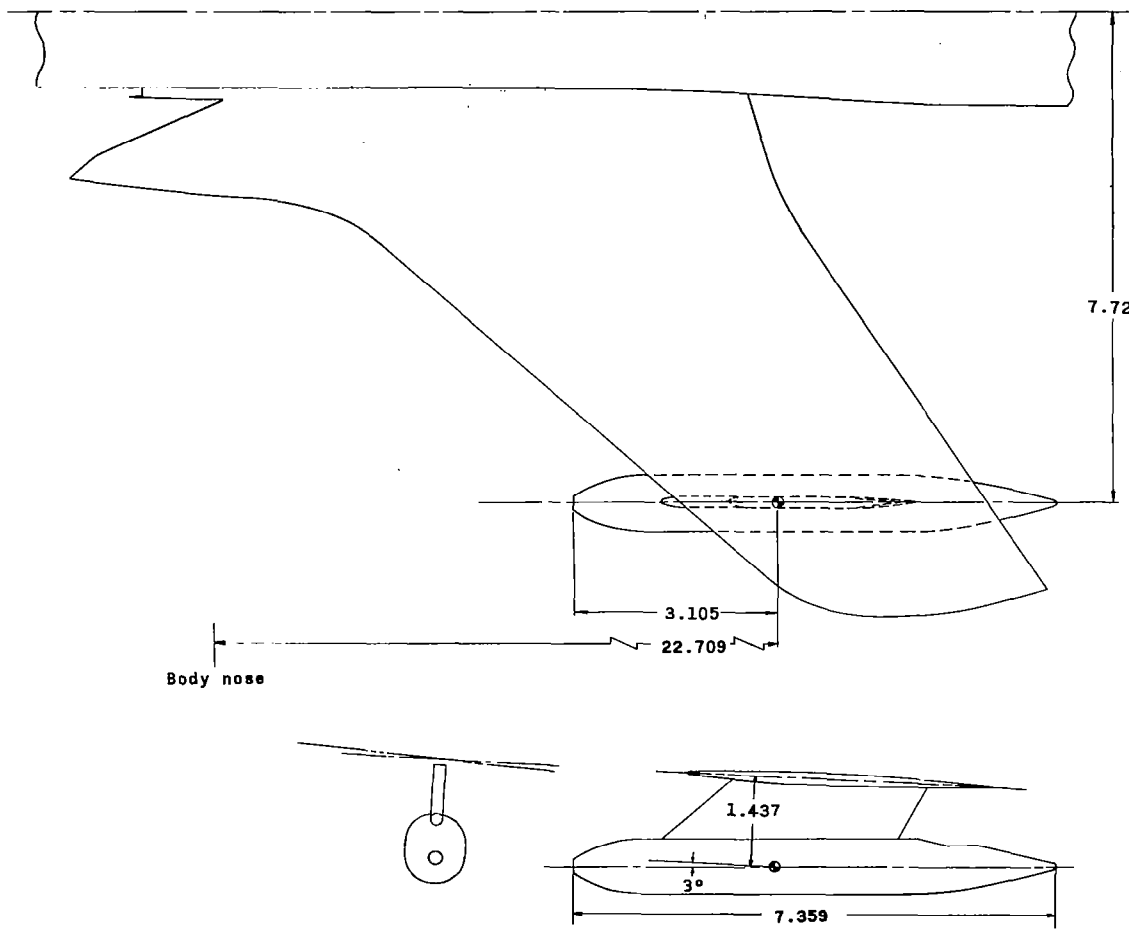

(b) Chaff dispensers.

Figure 4.- Concluded.

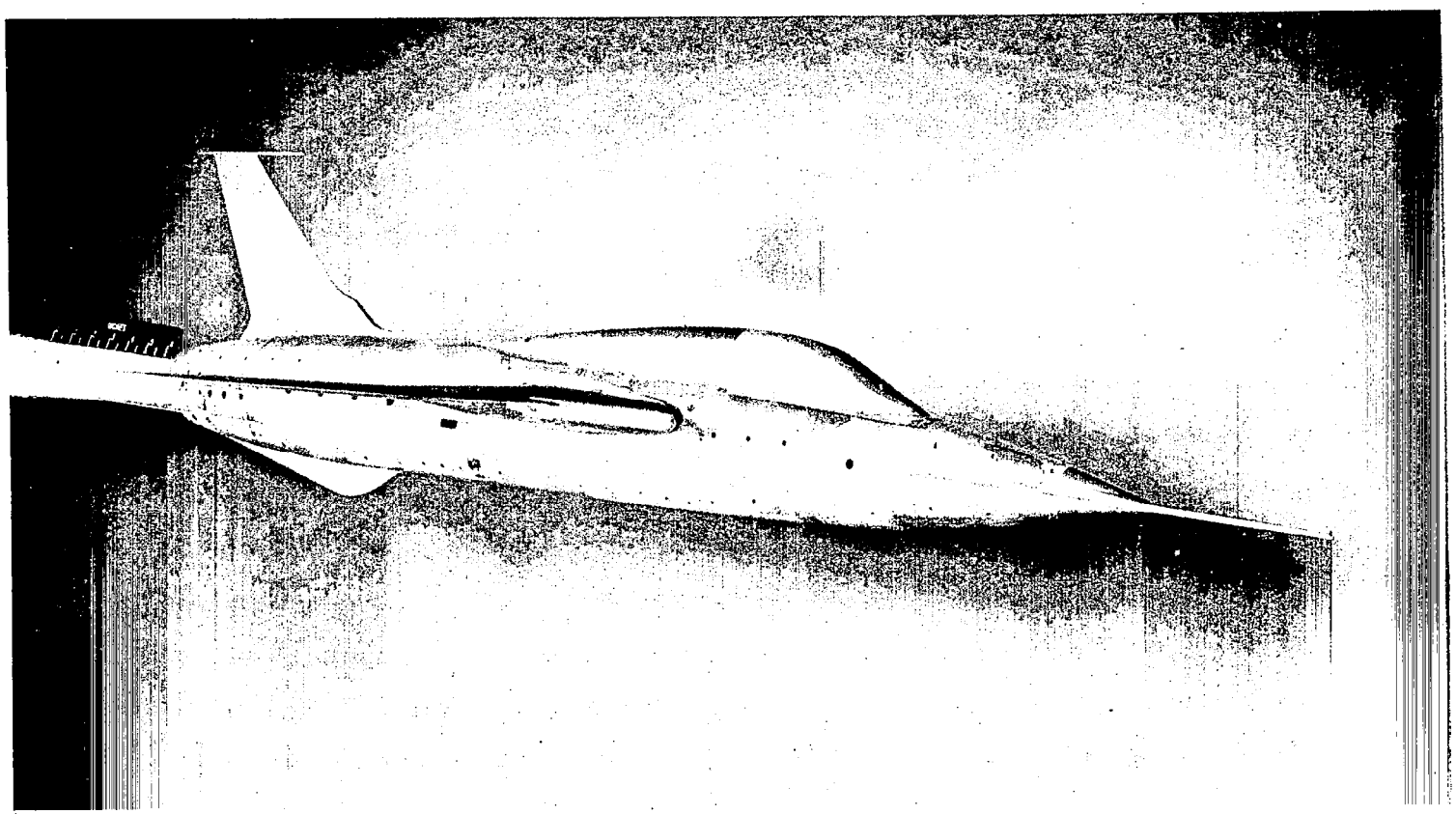

(a) Model II, three-quarter front view. L-57-1027

Figure 5.- Photographs of model configurations.

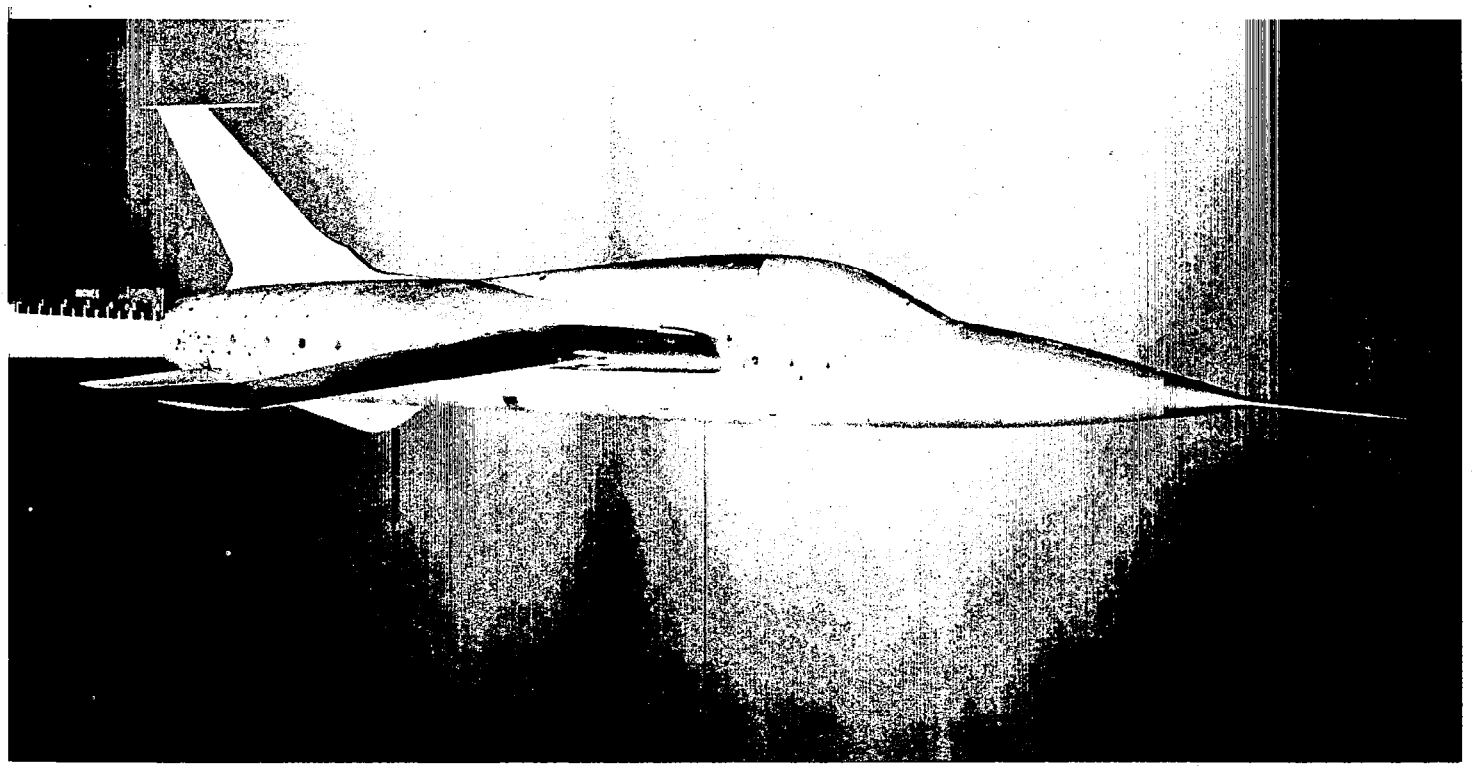

(b) Model III, side view. L-57-1017

Figure 5.- Continued.

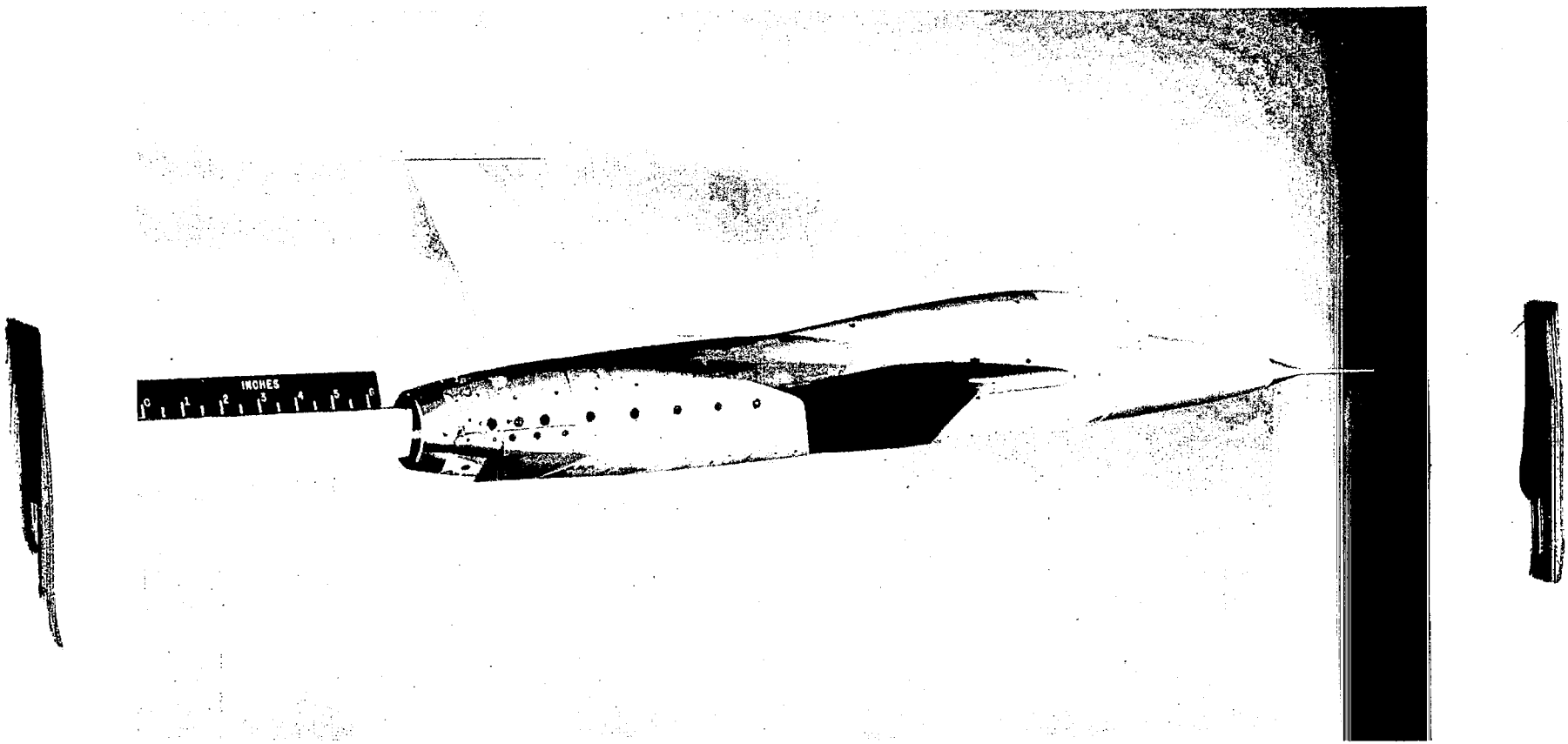

(c) Model III, three-quarter rear view. L-57-1018

Figure 5.- Continued.

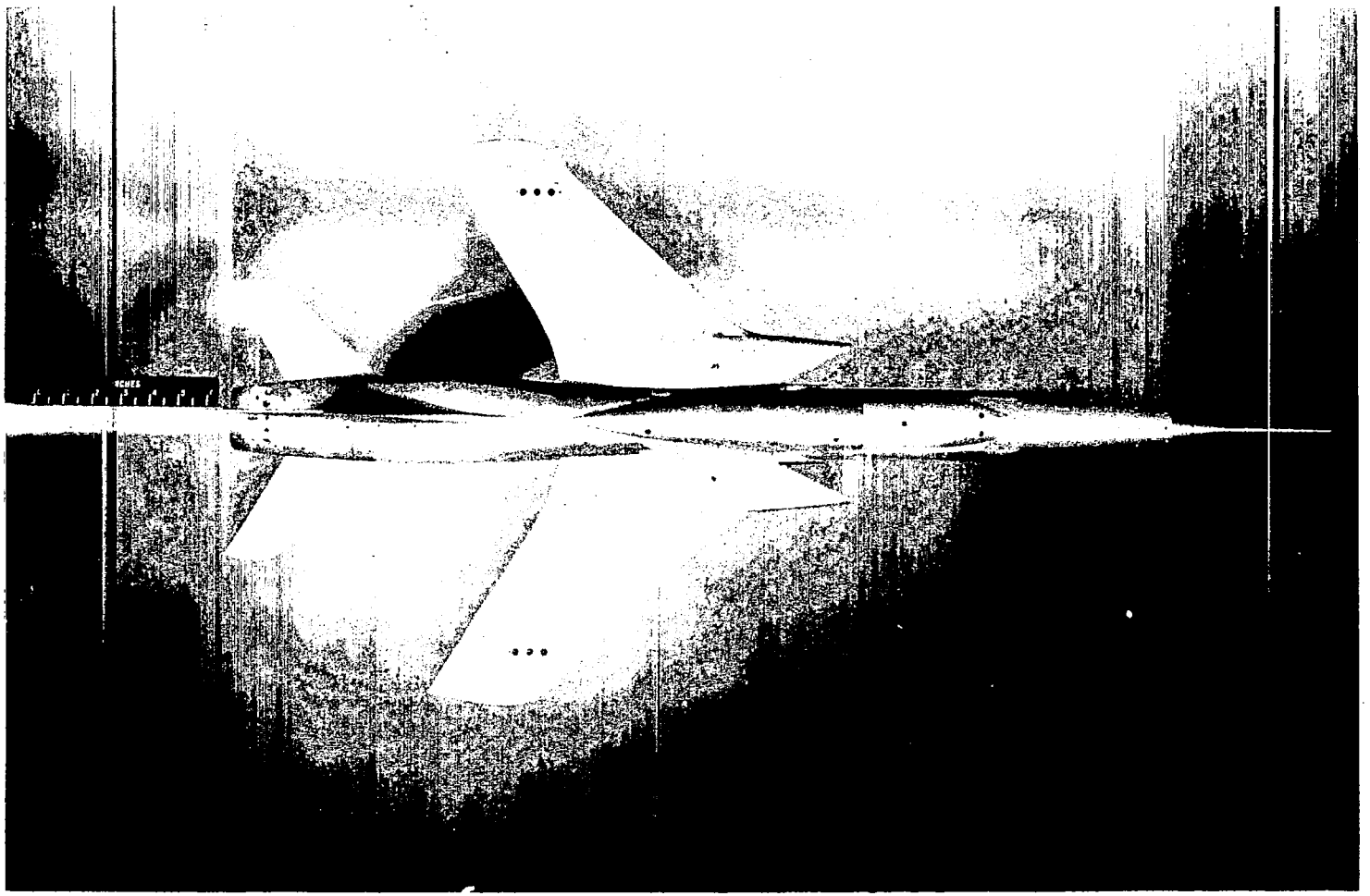

(d) Model III, top view. L-57-1029

Figure 5.- Continued.

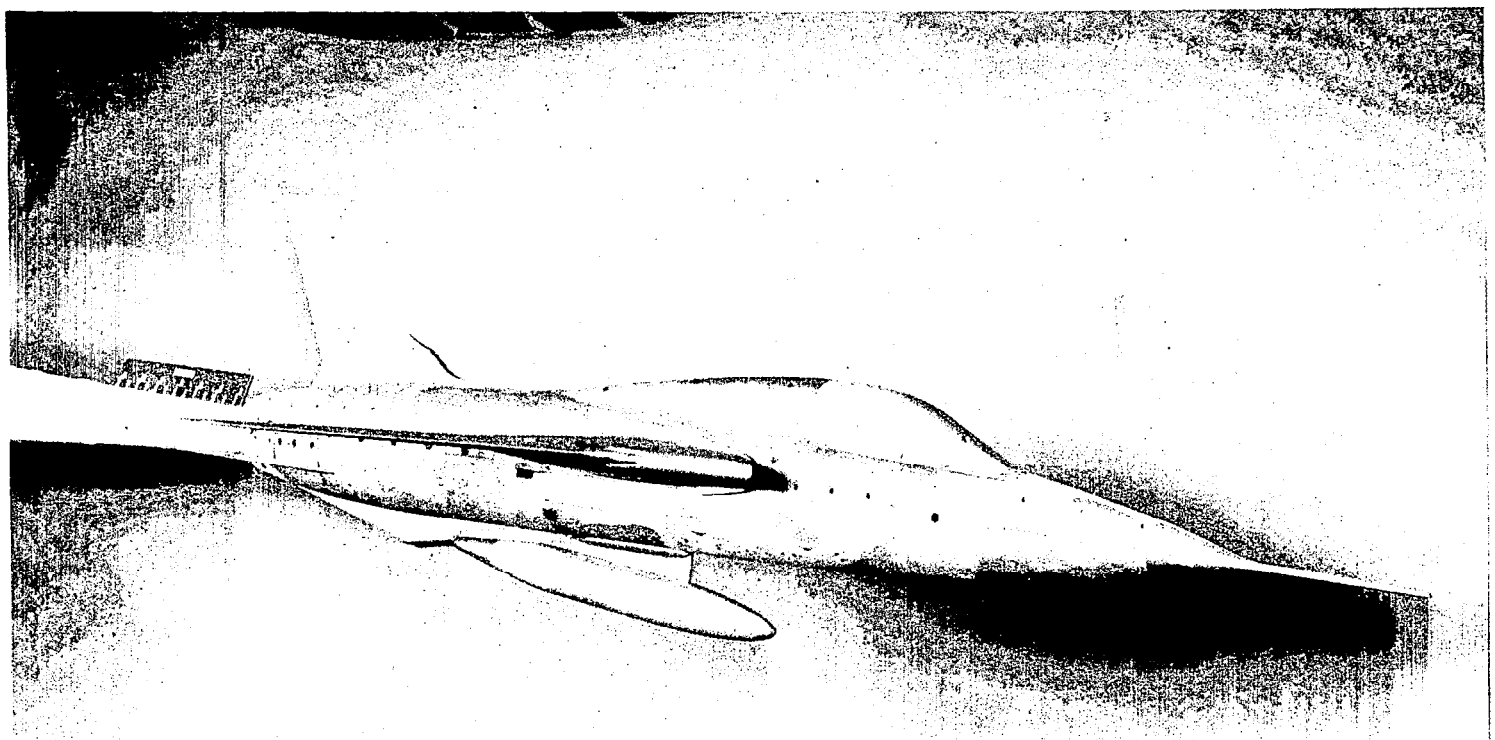

(e) Model II with center-line tank. L-57-1021

Figure 5.- Continued.

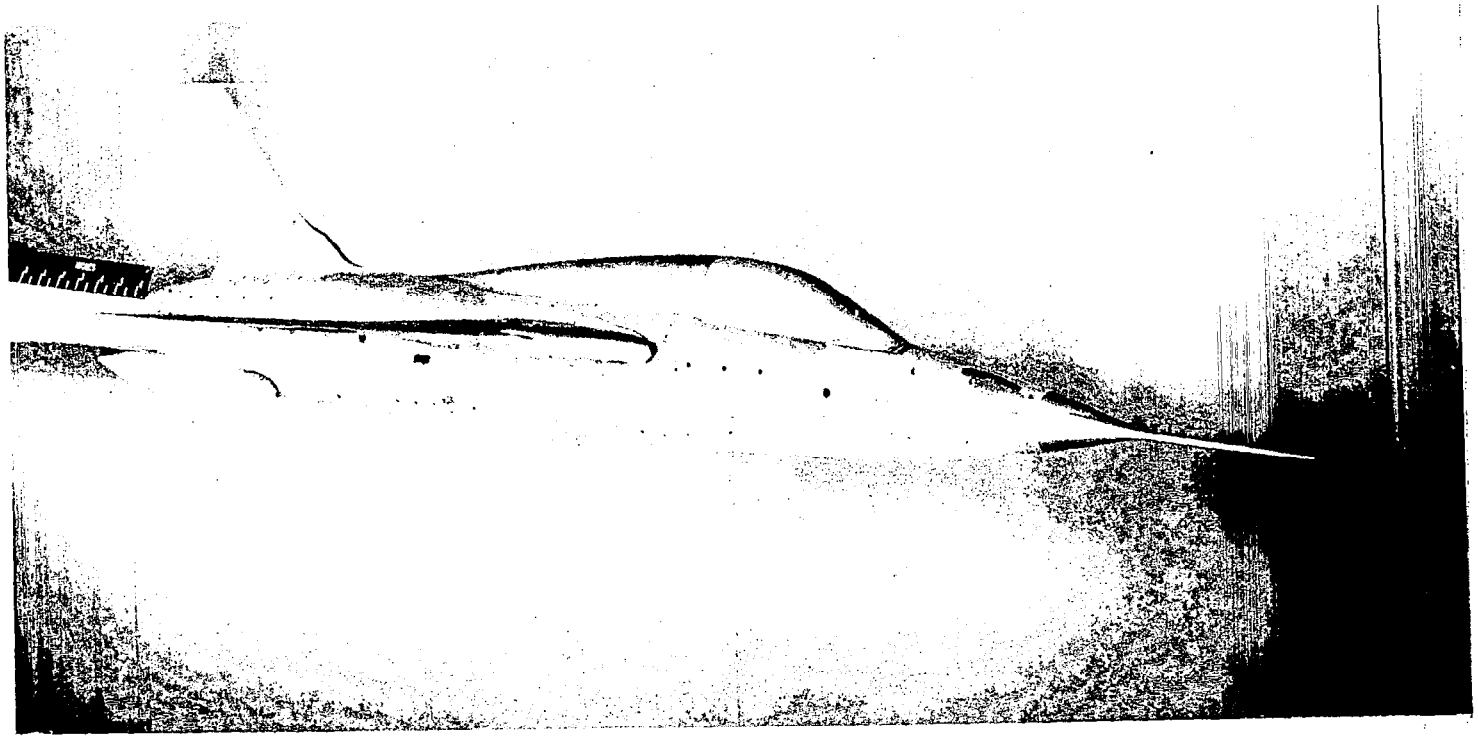

(f) Model II with chaff dispensers. L-57-1023

Figure 5.- Continued.

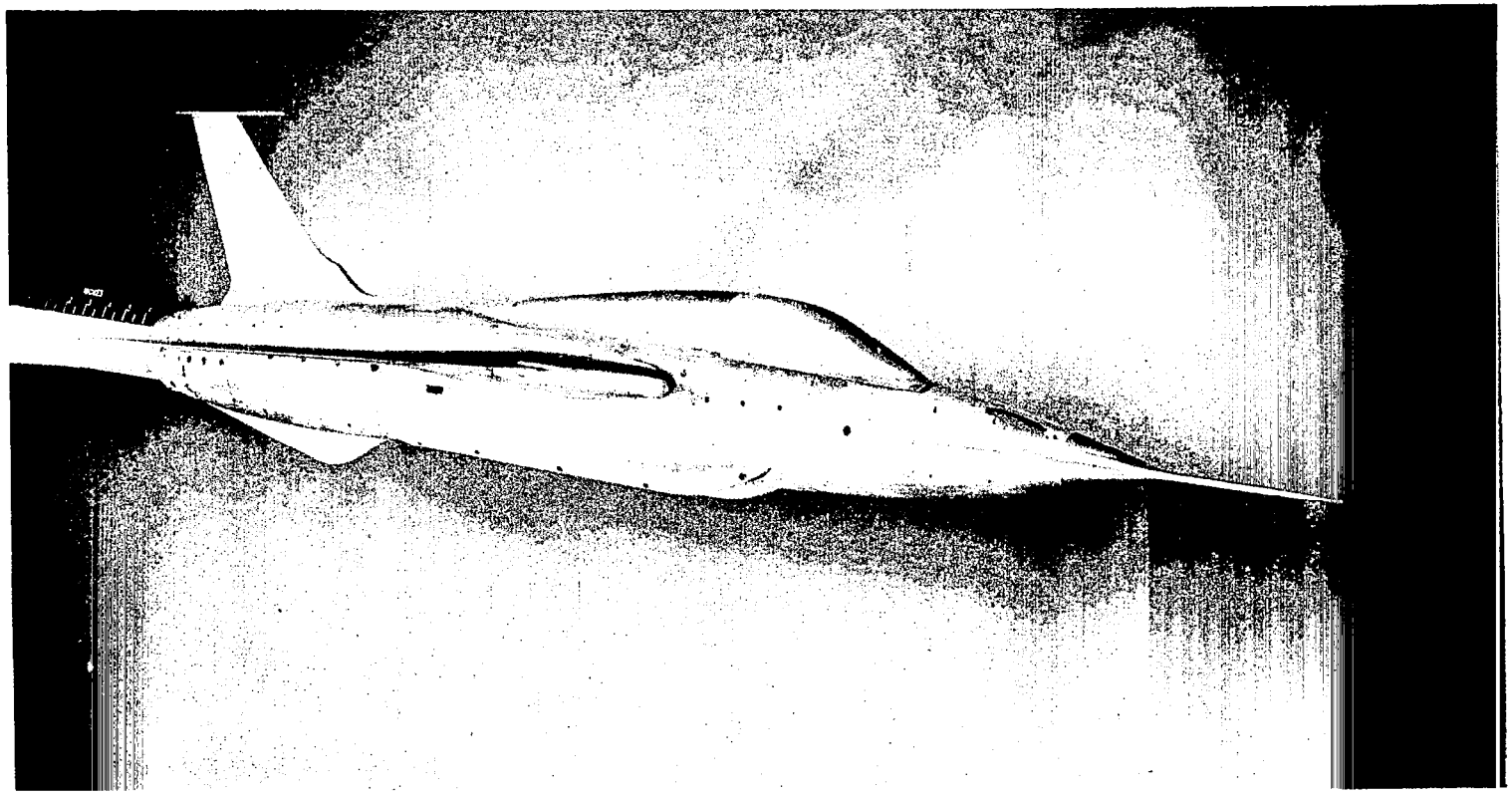

(g) Model II with fuselage radar blisters. L-57-1025

Figure 5.- Continued.

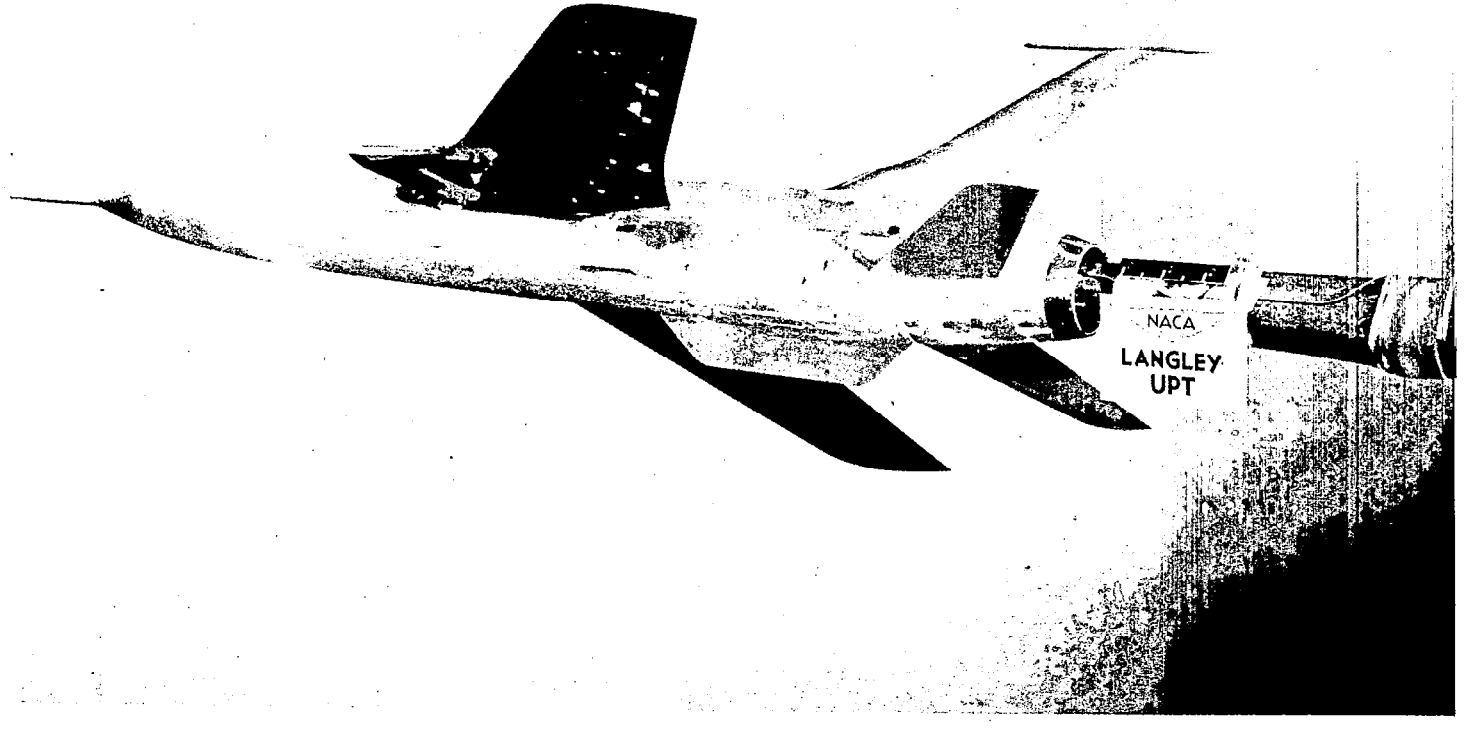

(h) Model II with twin ventral fins. L-57-4073

Figure 5.- Continued.

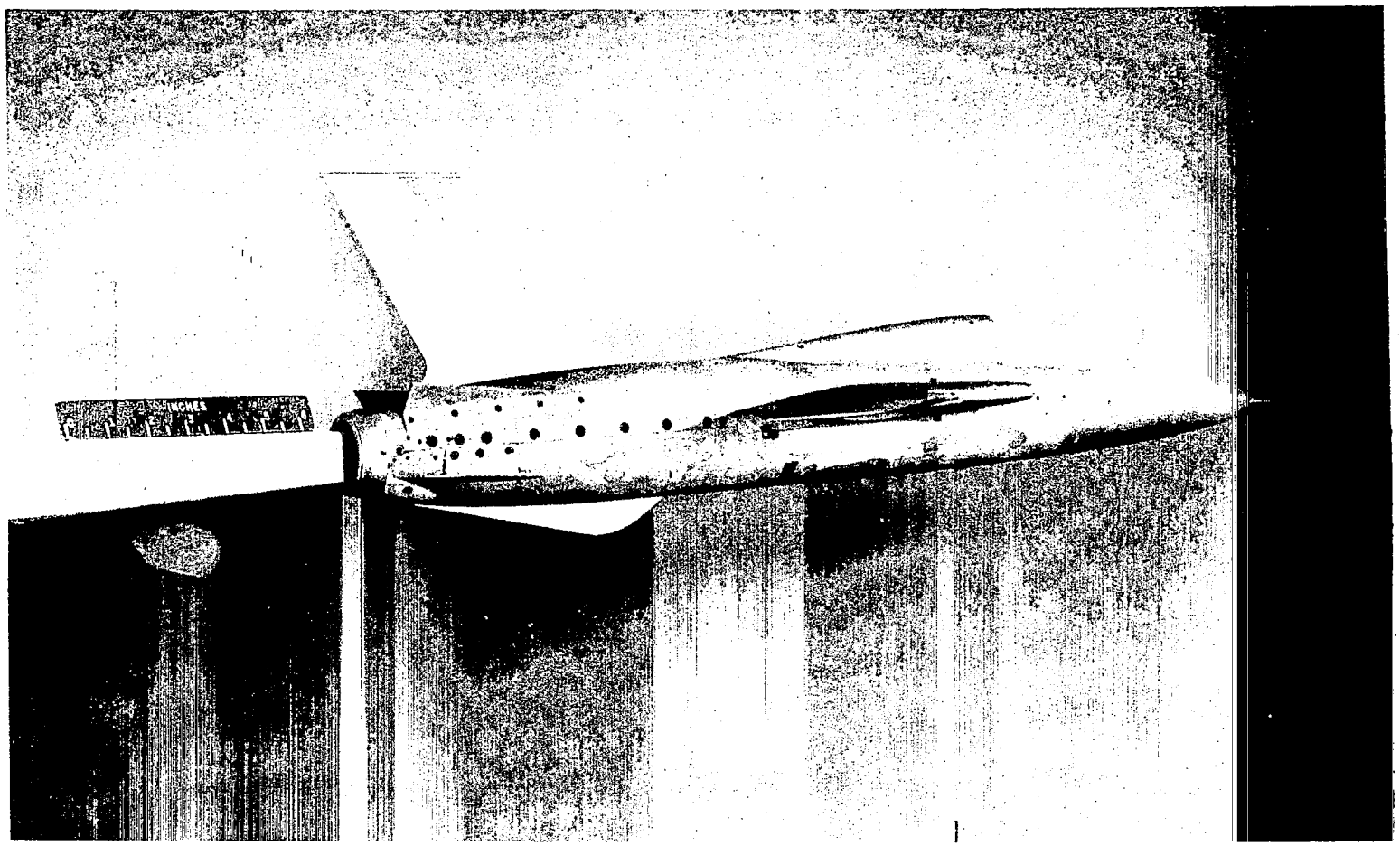

(i) Model III with 45° dorsal fins. L-57-1020

Figure 5.- Continued.

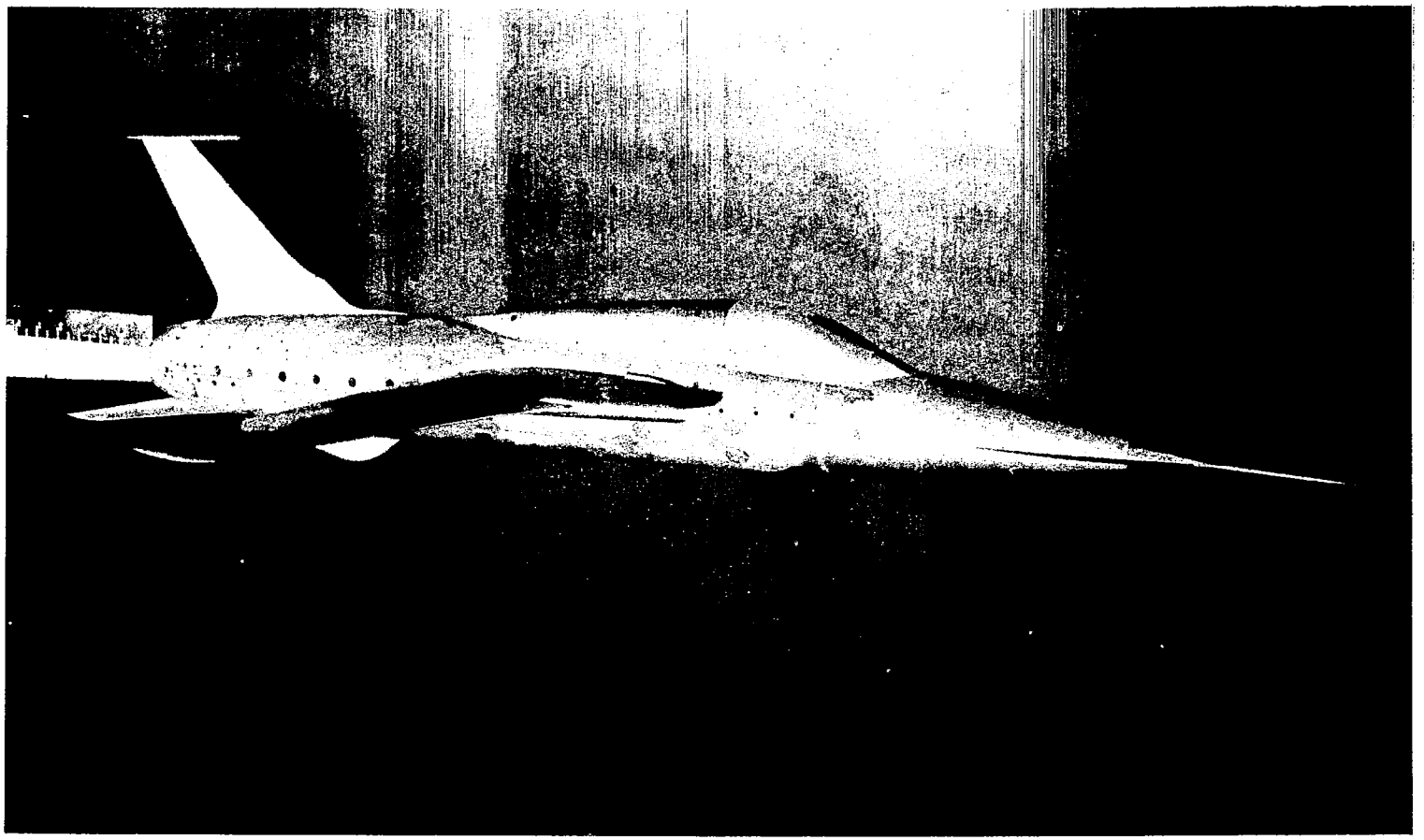

(j) Model III with small strakes. L-57-1016

Figure 5.- Concluded.

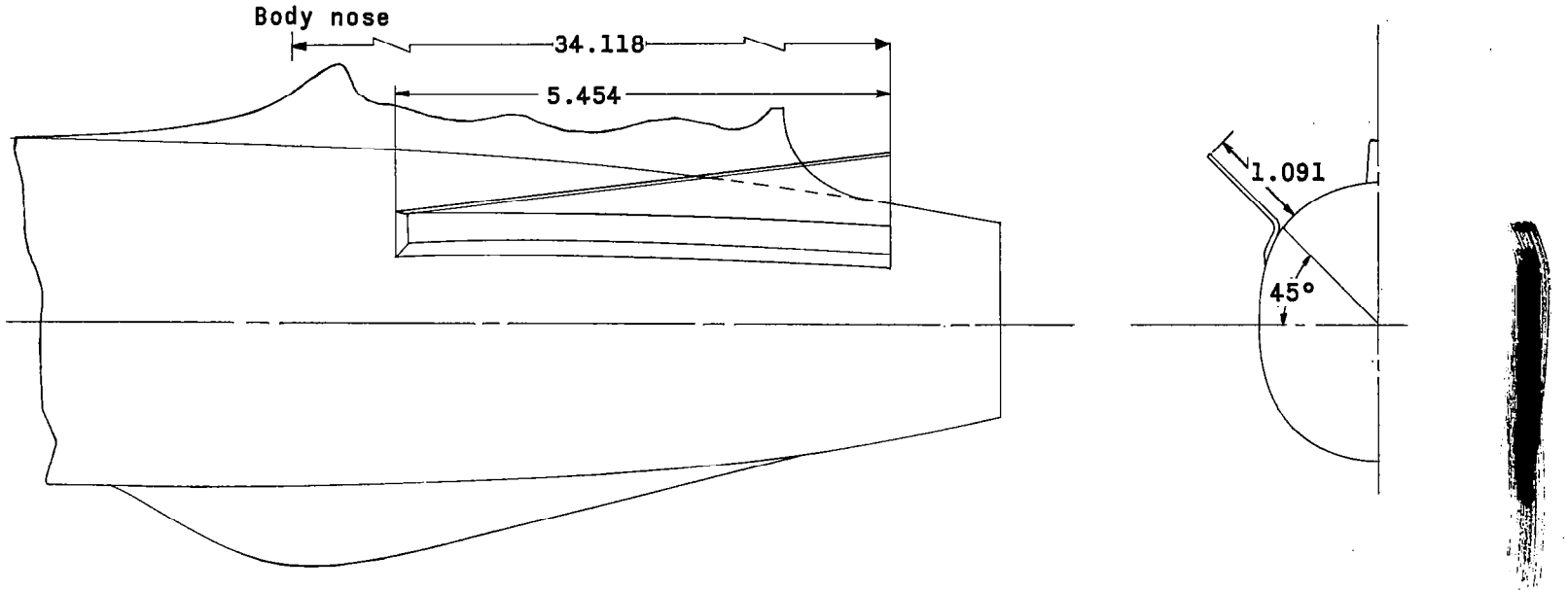

(a) 45° dorsal fins.

Figure 6.- Stability augmentation devices. All dimensions are in inches.

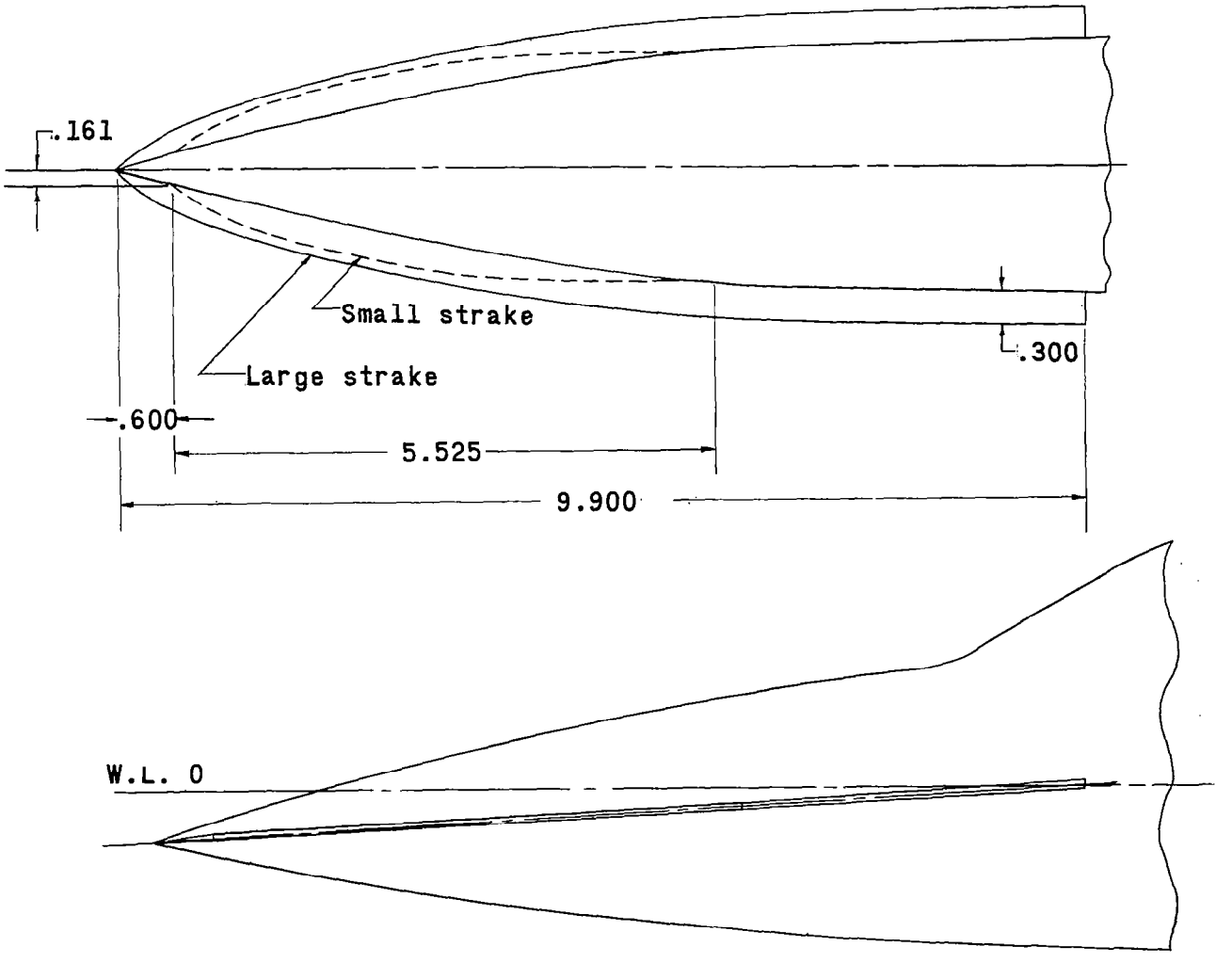

(b) Strakes.

Figure 6.- Concluded.

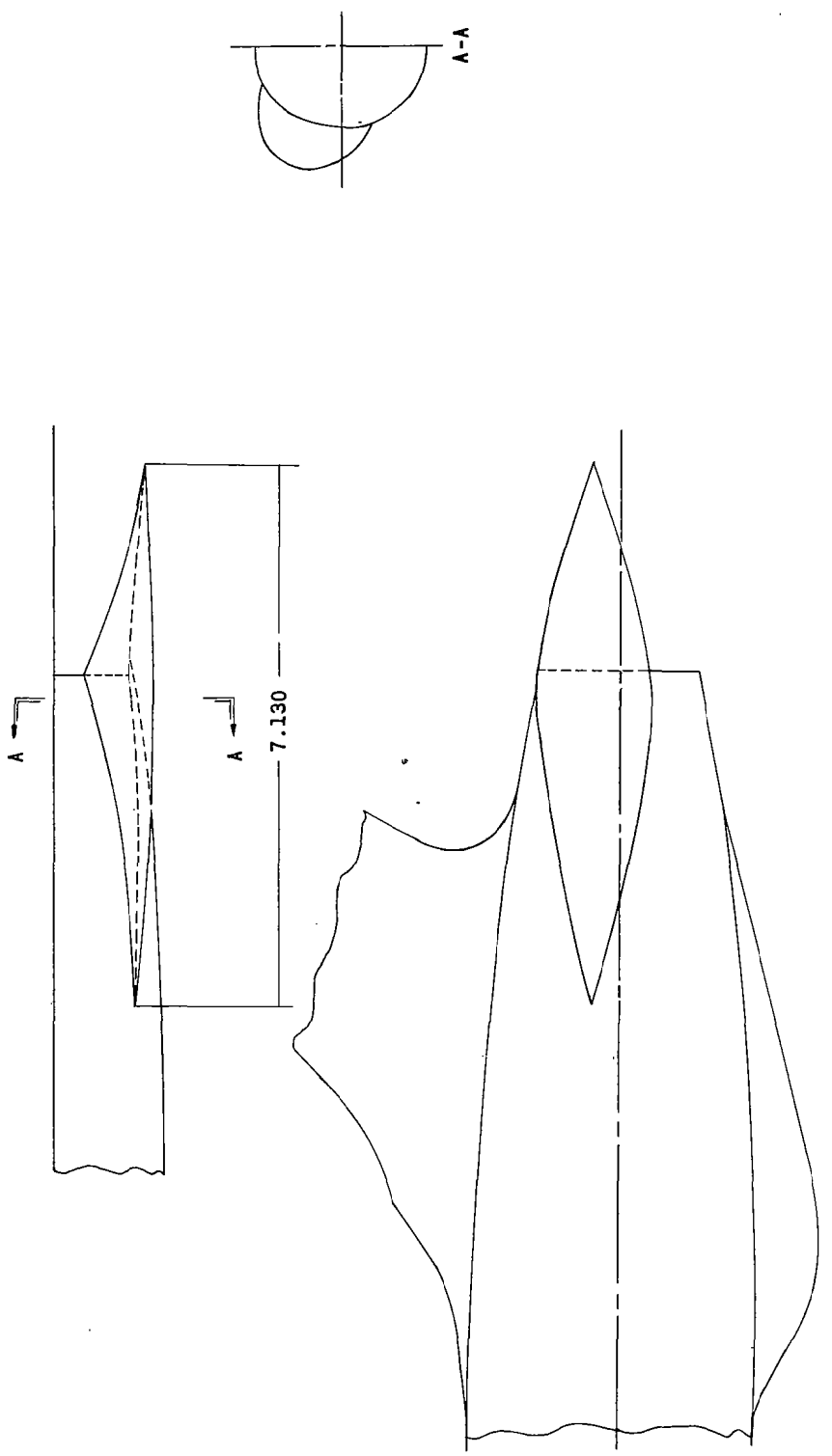

Figure 7.- Terminal fairings. All dimensions are in inches.

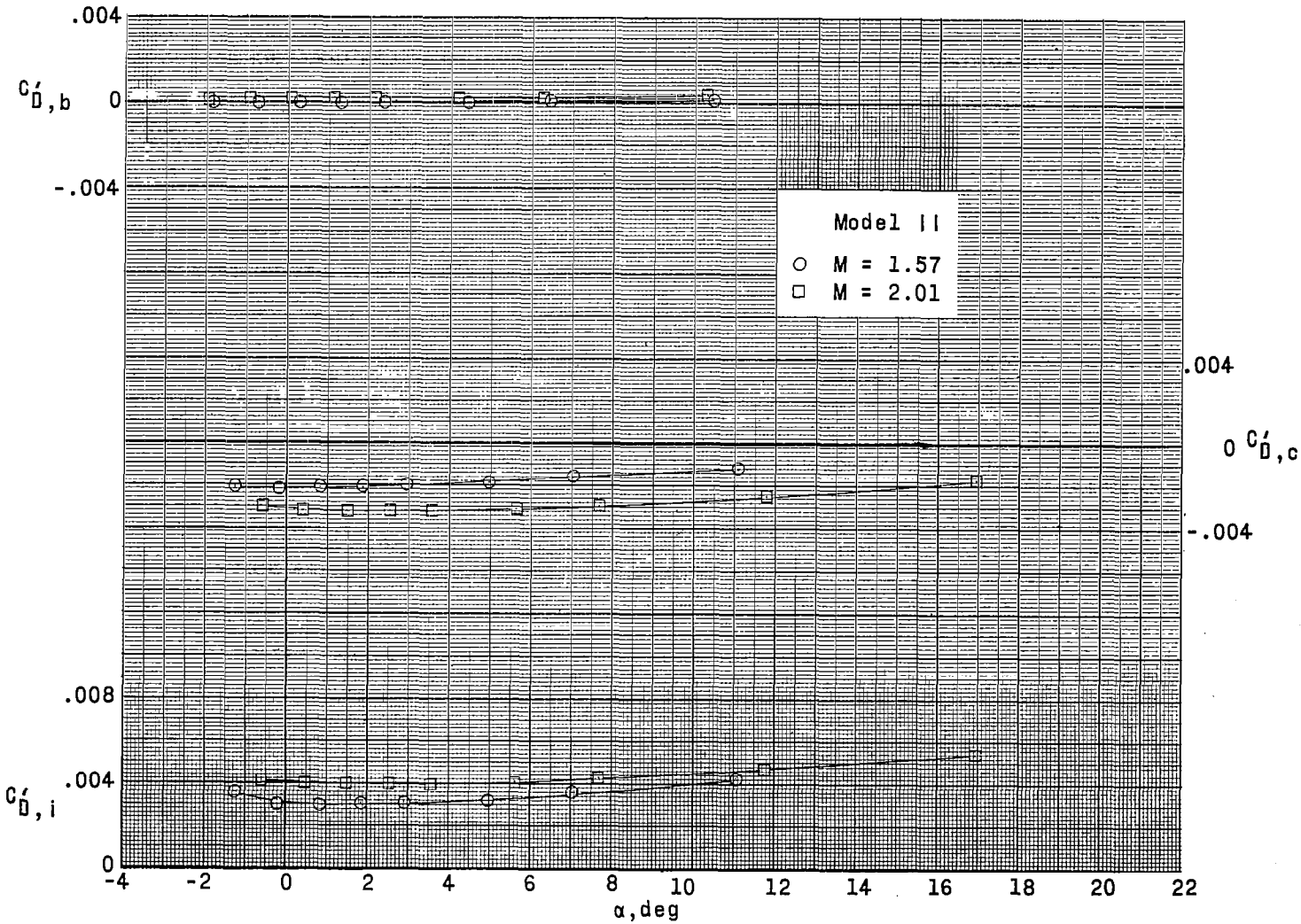

Figure 8.- Effect of angle of attack on base, chamber, and internal-duct drag coefficients. $\beta \approx 0^{\circ}$.

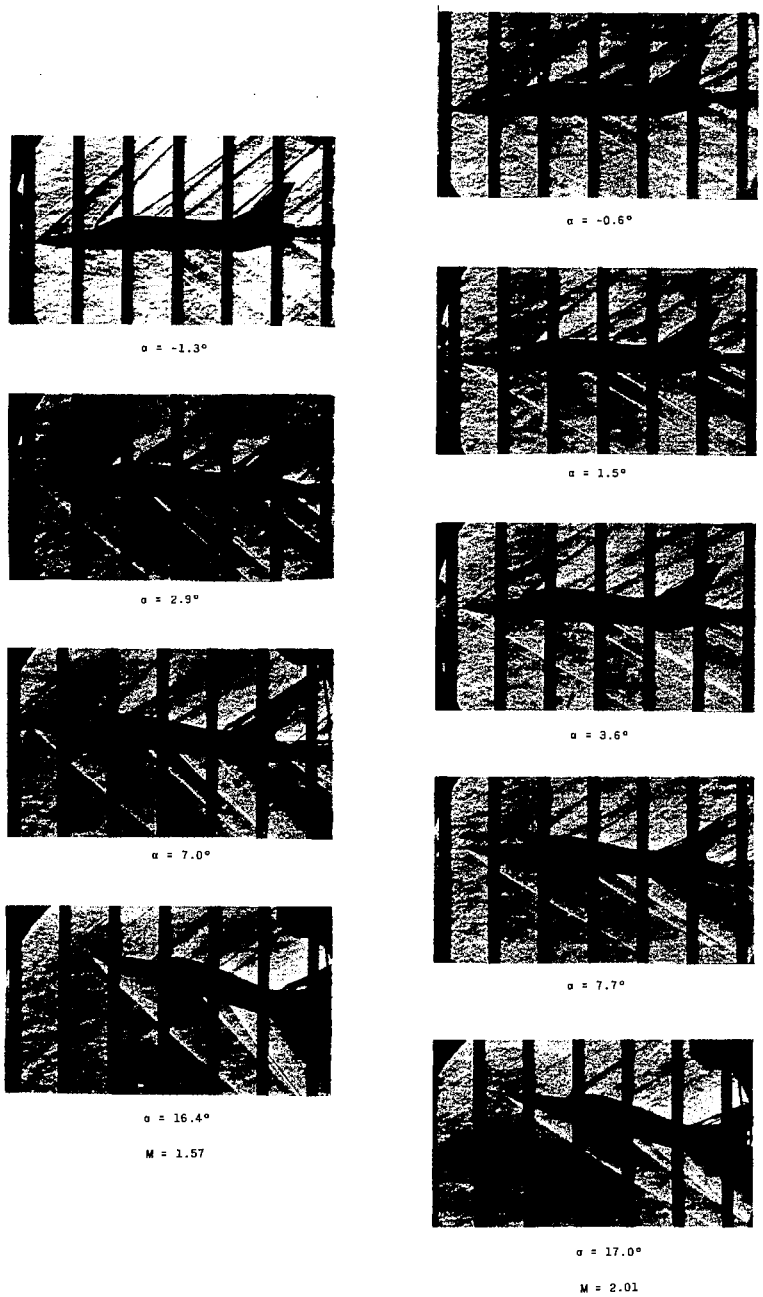

(a) Model III. L-58-2570

Figure 9.- Typical schlieren photographs of models tested at various angles of attack.

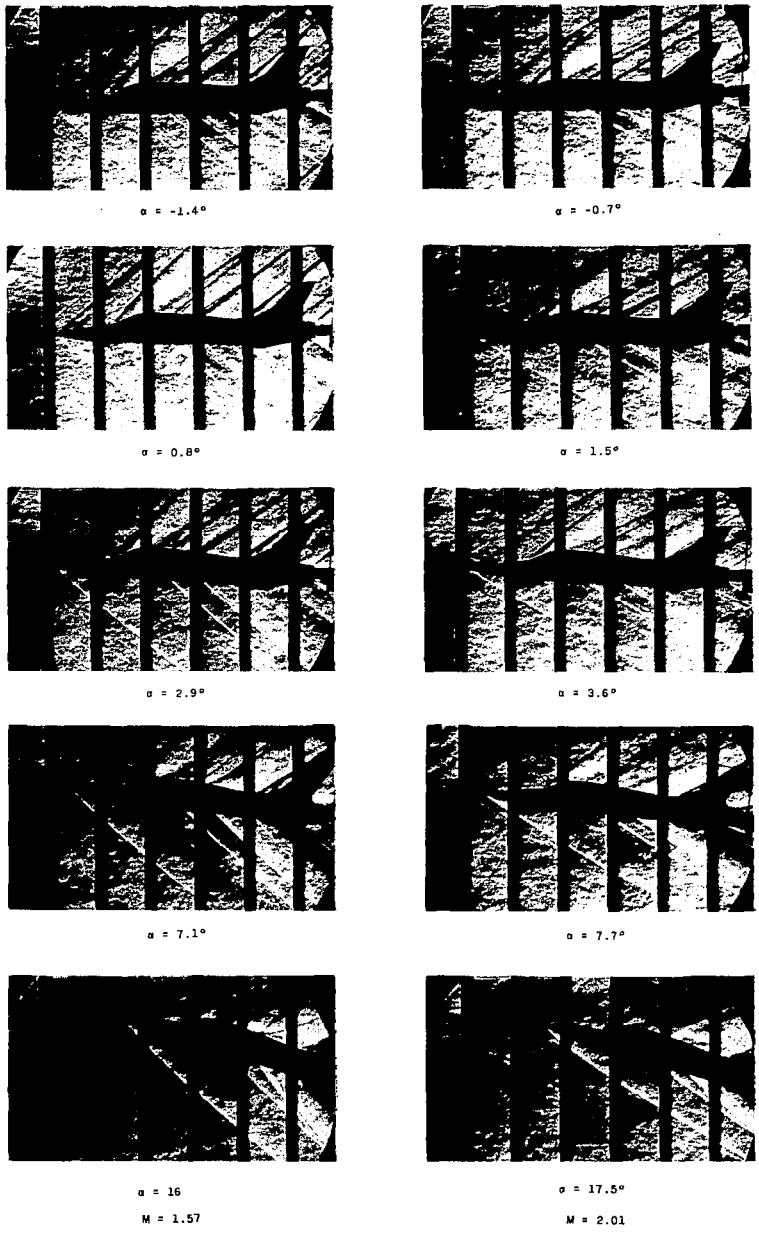

(b) Model III with large strakes. L-58-2571

Figure 9.- Concluded.

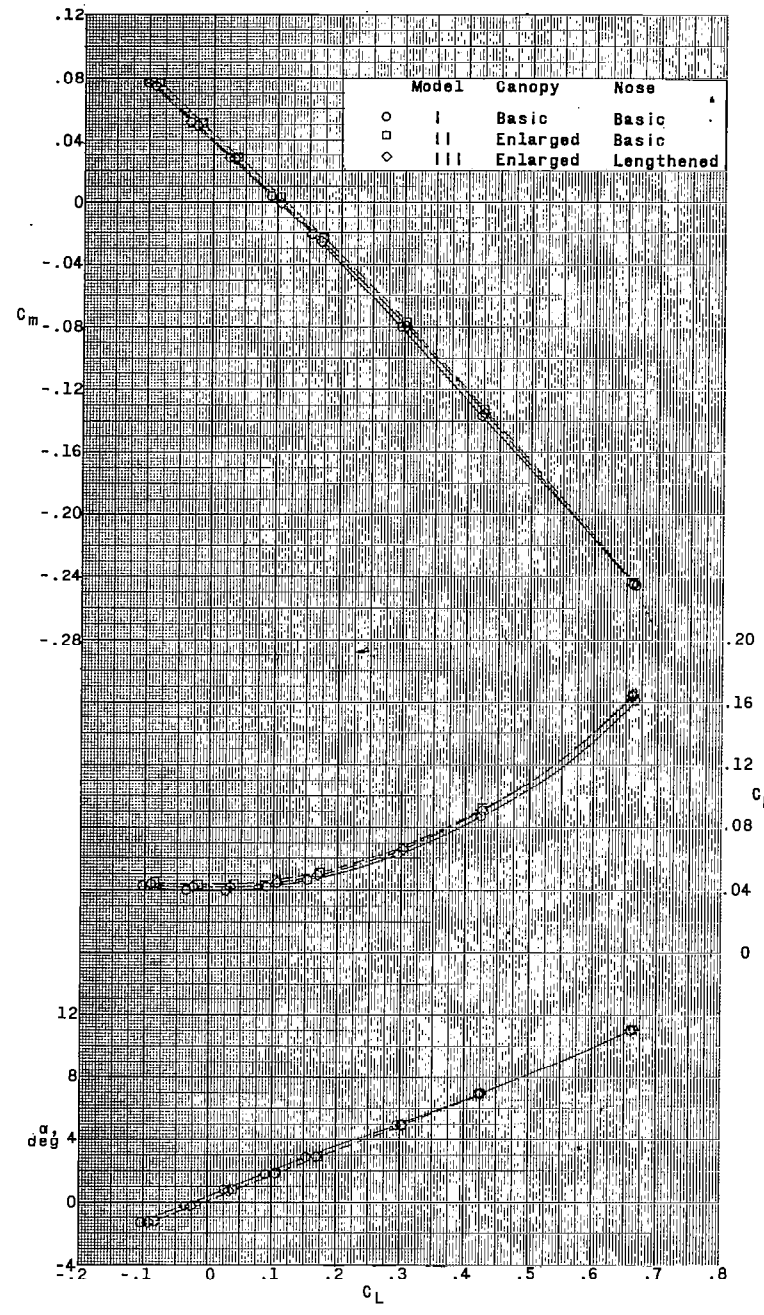

(a) M = 1.57.

Figure 10.- Effect of nose length and canopy size on aerodynamic characteristics in pitch; $\beta \approx 0^{\circ}$.

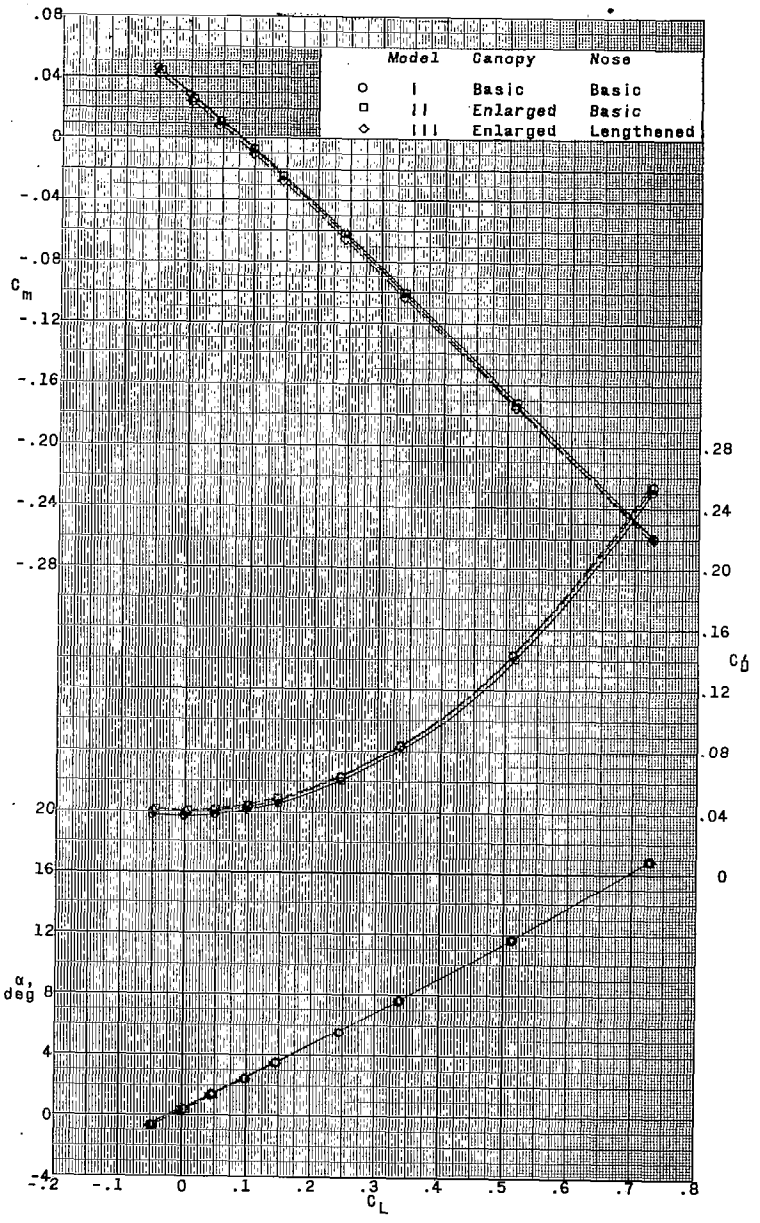

(b) M = 2.01.

Figure 10.- Concluded.

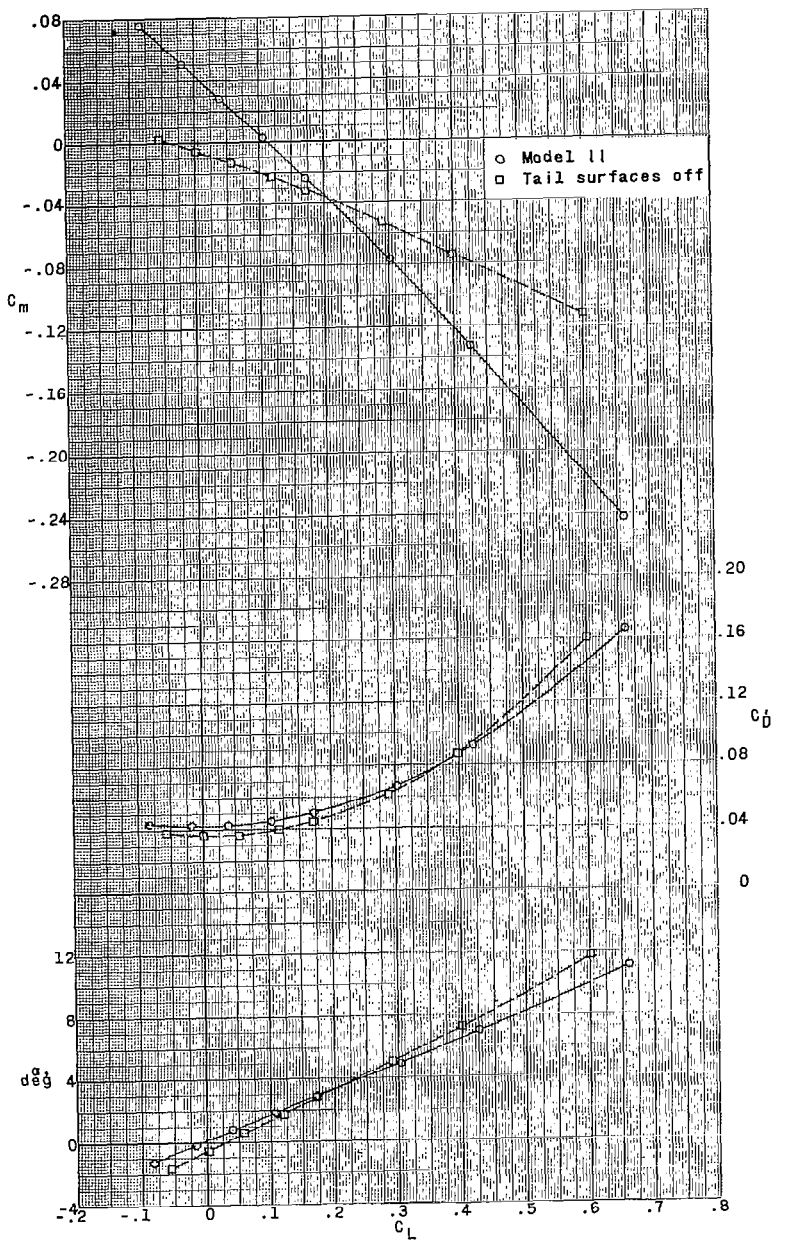

(a) M = 1.57.

Figure 11.- Effect of tail surfaces on aerodynamic characteristics in pitch; $\beta \approx 0^{\circ}$.

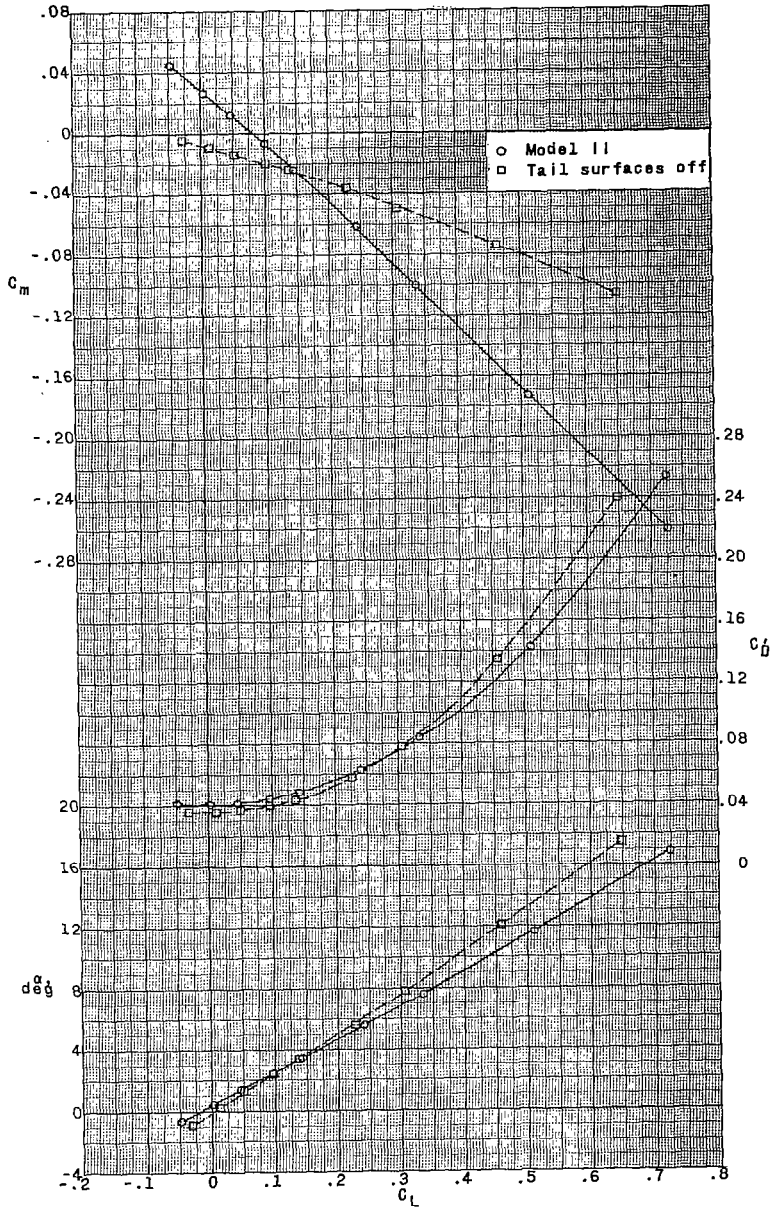

(b) M = 2.01

Figure 11.- Concluded.

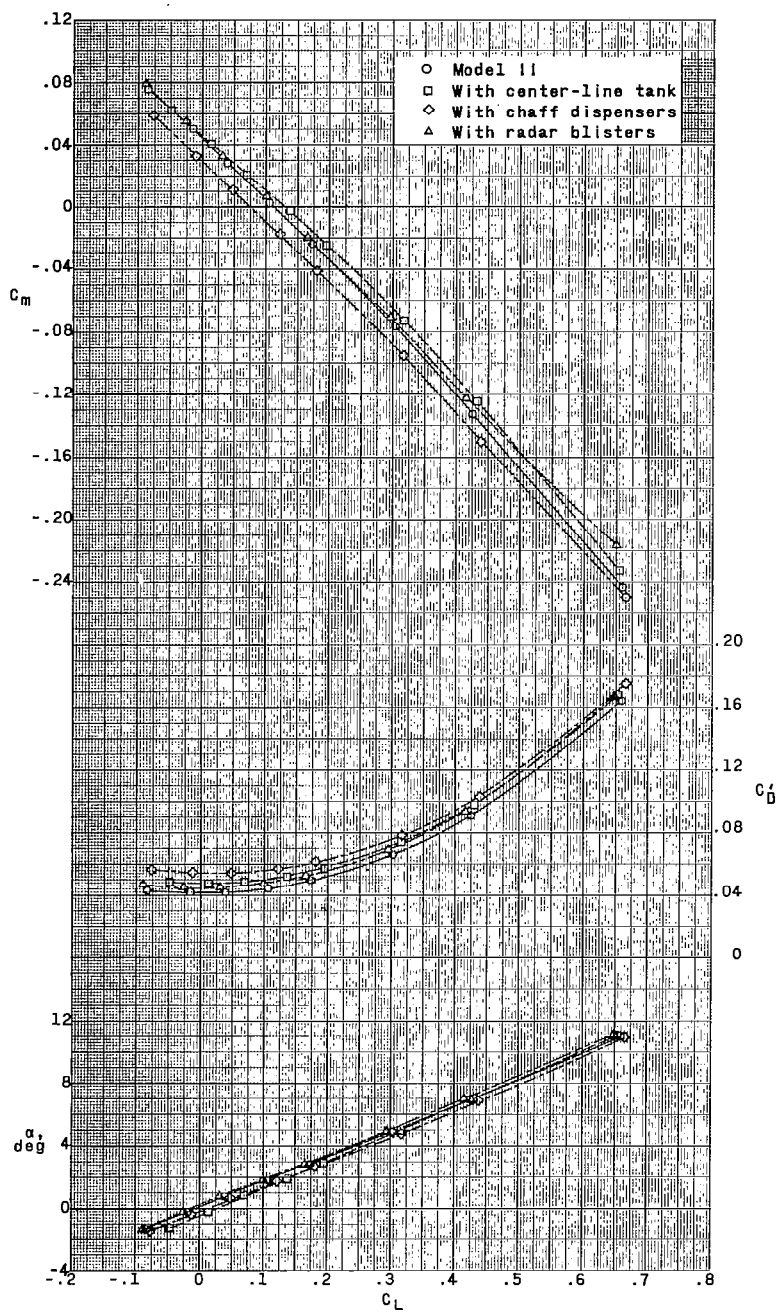

(a) M = 1.57.

Figure 12.- Effect of external stores on aerodynamic characteristics in pitch; $\beta \approx 0^{\circ}$.

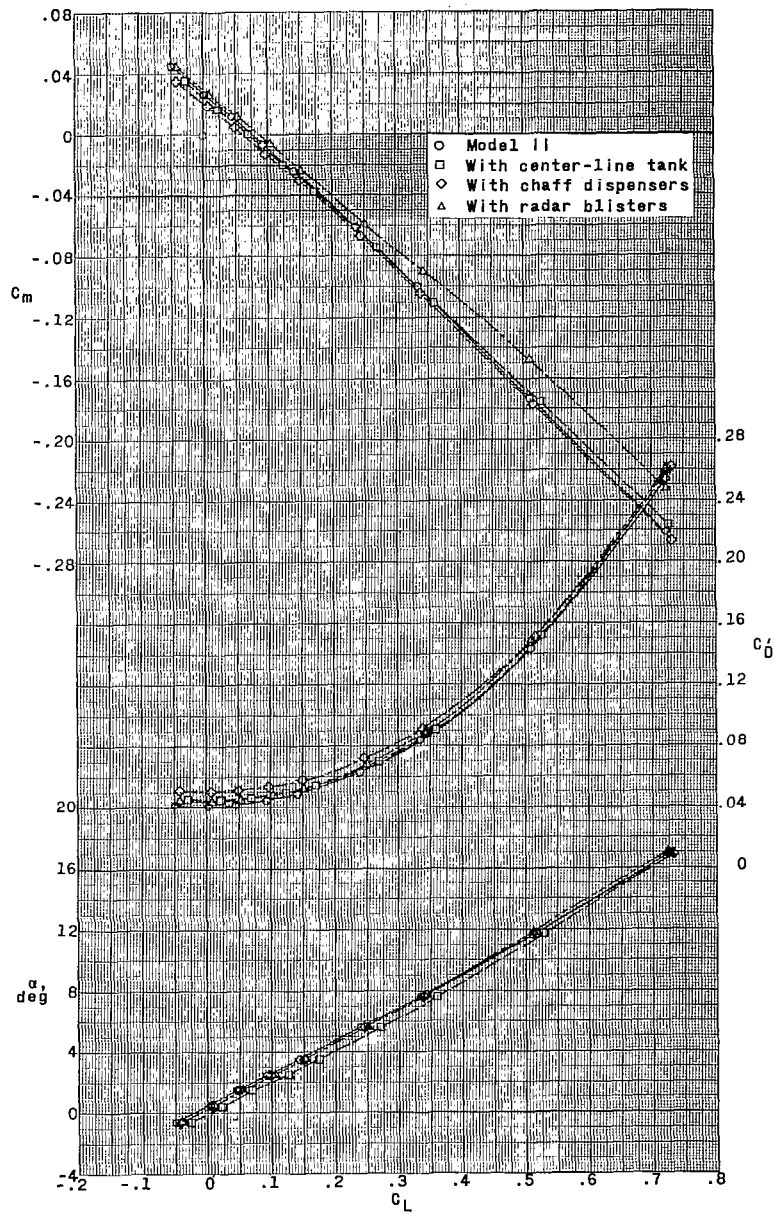

(b) M = 2.01.

Figure 12.- Concluded.

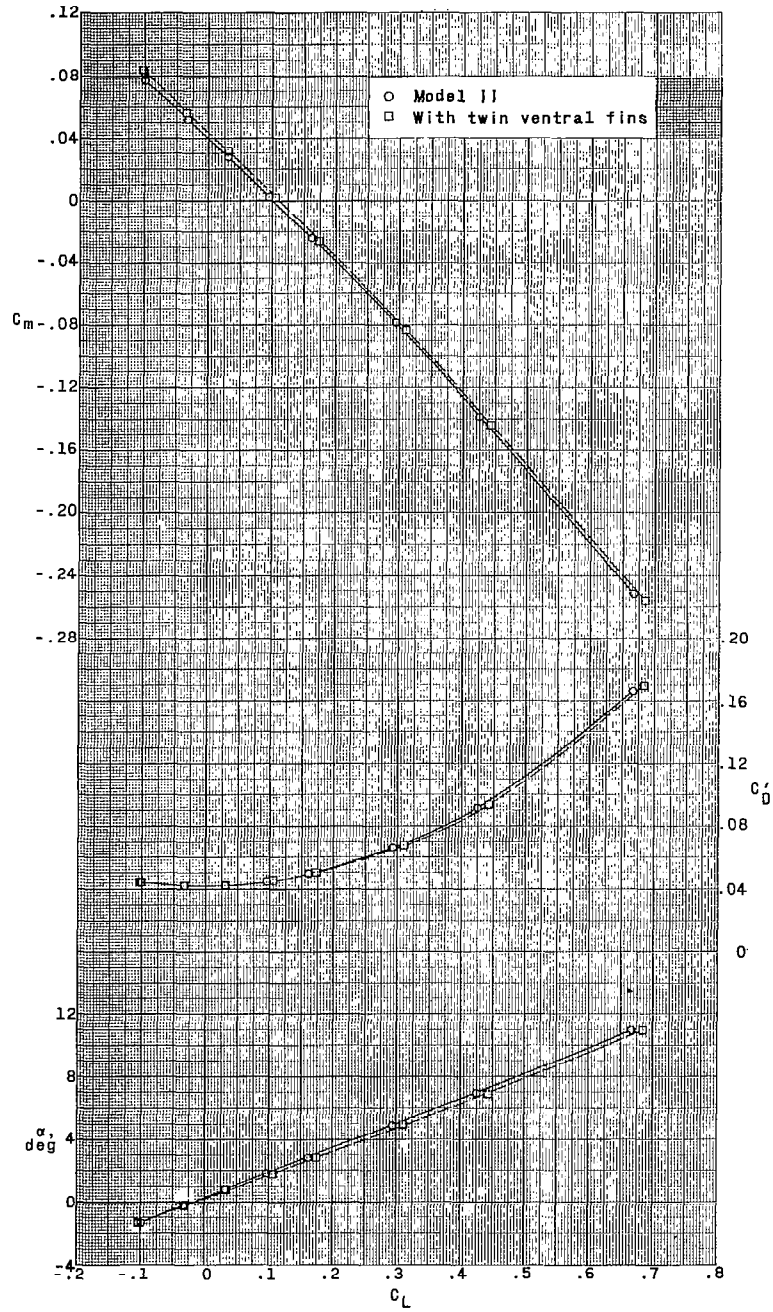

(a) M = 1.57.

Figure 13.- Effect of directional stability control devices on aerodynamic characteristics in pitch; $\beta \approx 0^{\circ}$.

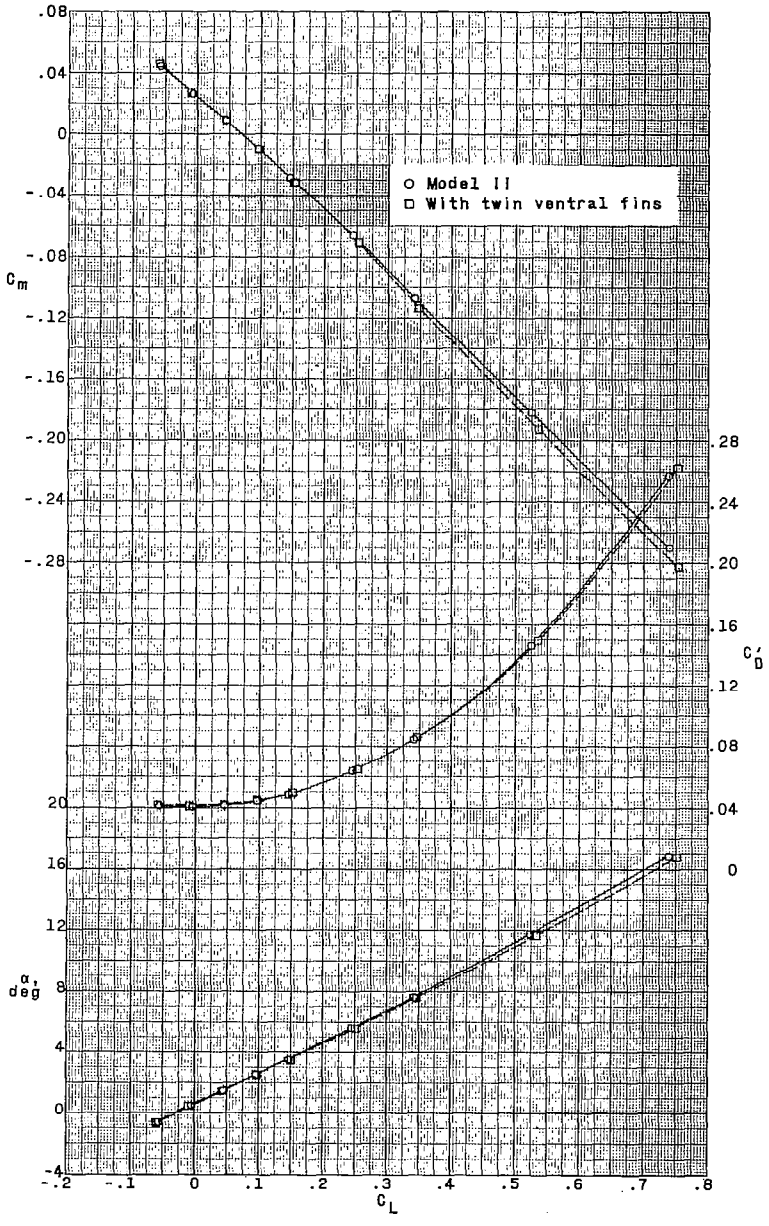

(b) M = 2.01.

Figure 13.- Continued.

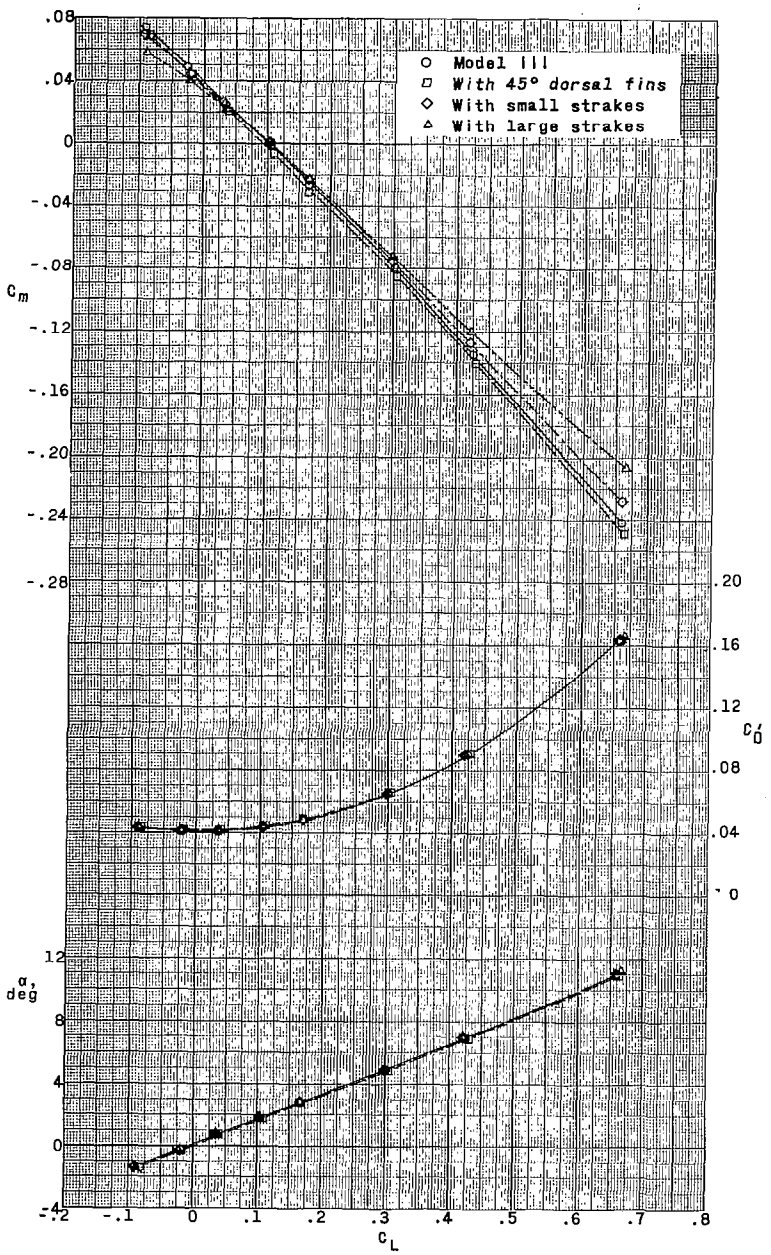

(c) M = 1.57.

Figure 13.- Continued.

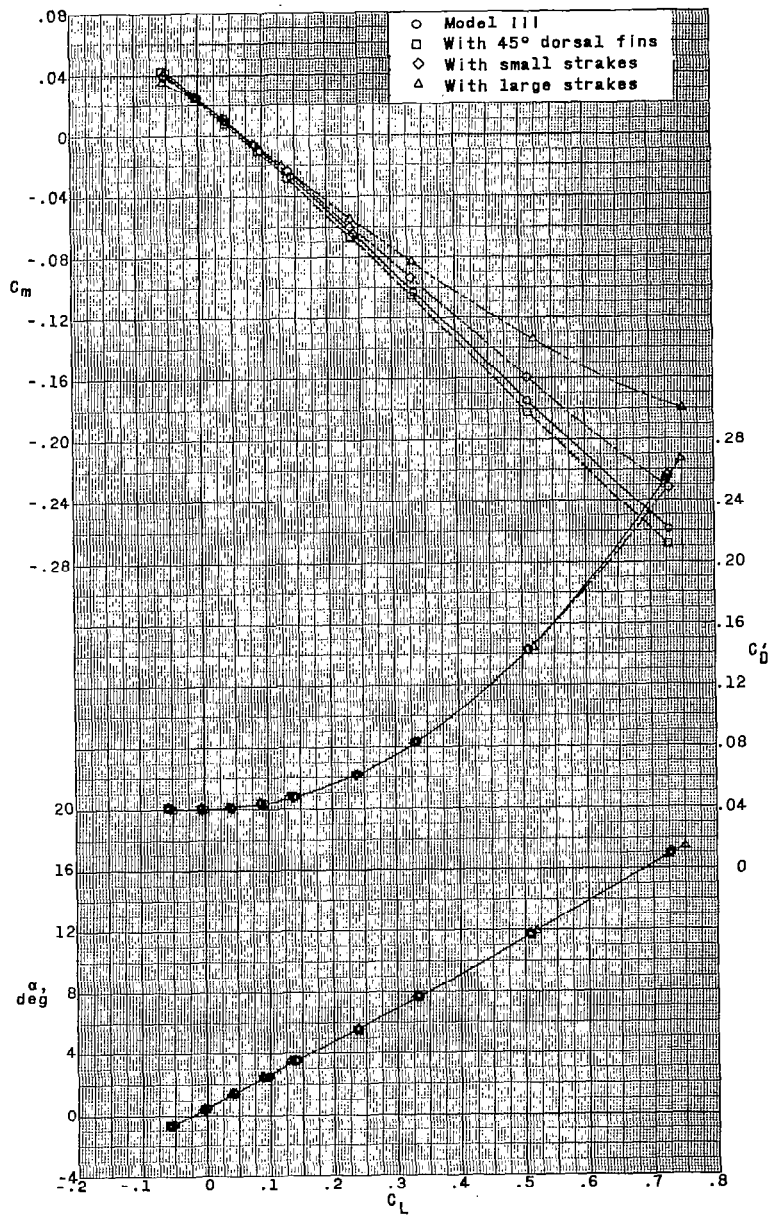

(d) M = 2.01.

Figure 13.- Concluded.

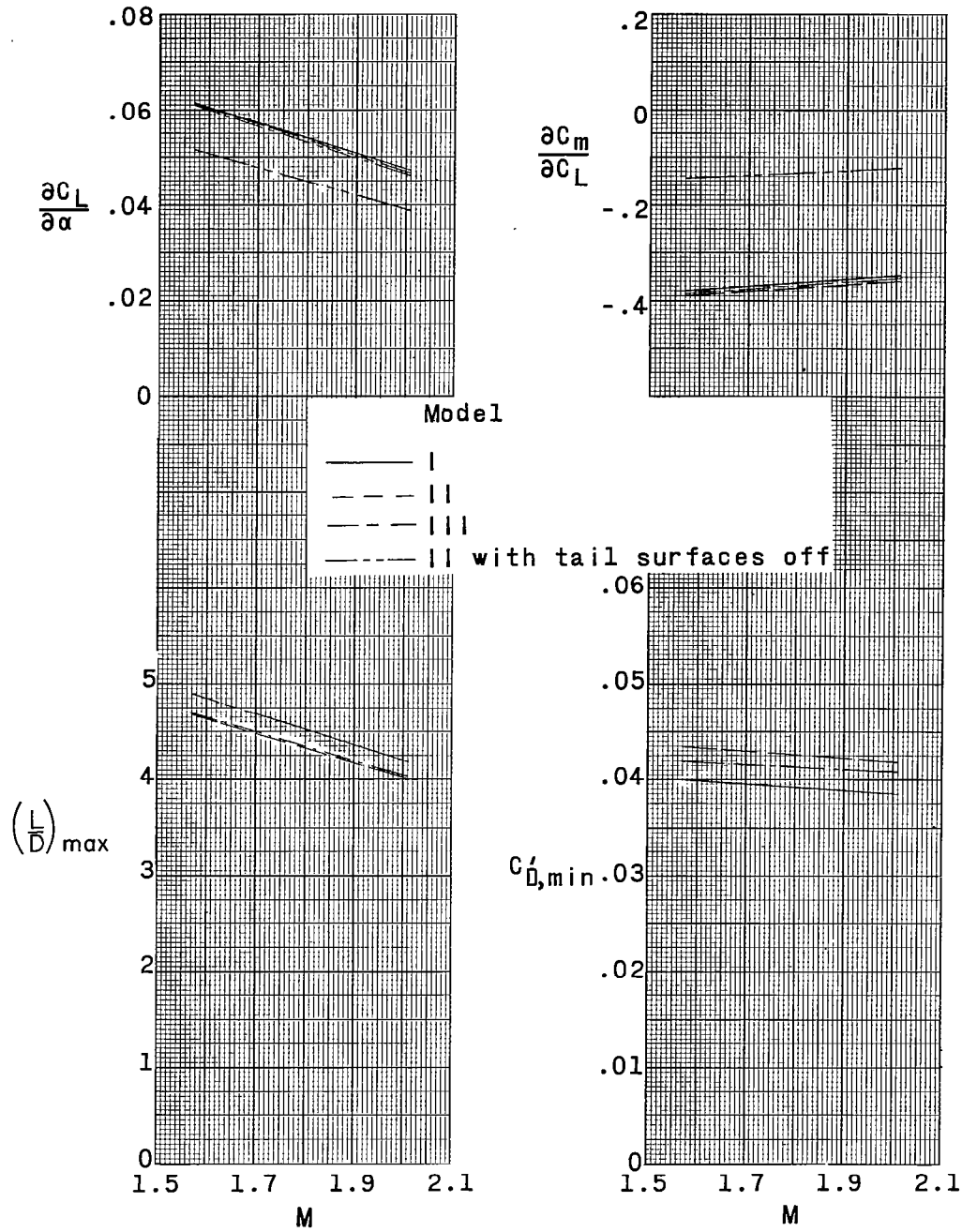

(a) Effect of forebodies.

Figure 14.- Summary of performance and longitudinal stability derivatives.

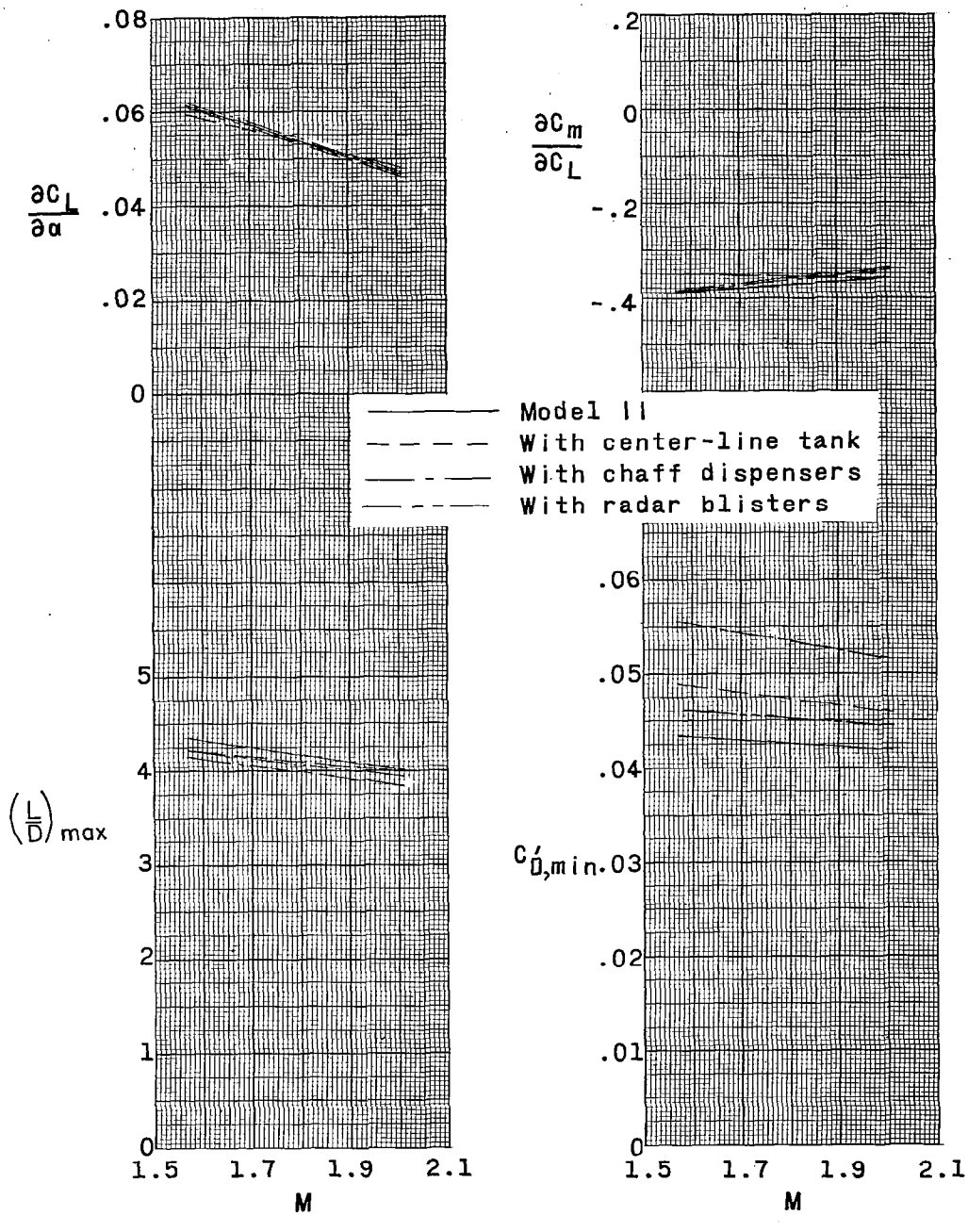

(b) Effect of external stores.

Figure 14.- Continued.

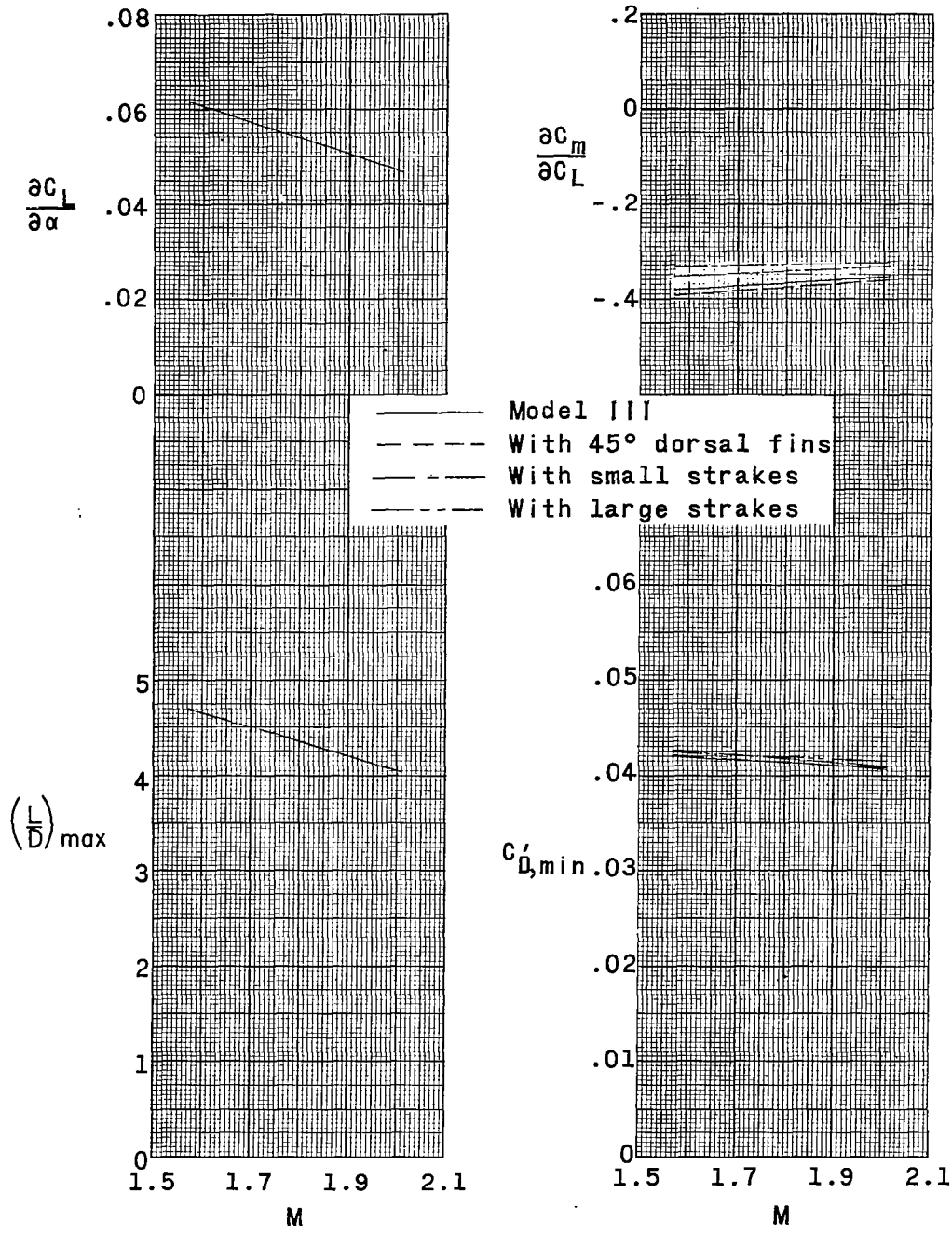

(c) Effect of control devices.

Figure 14.- Concluded.

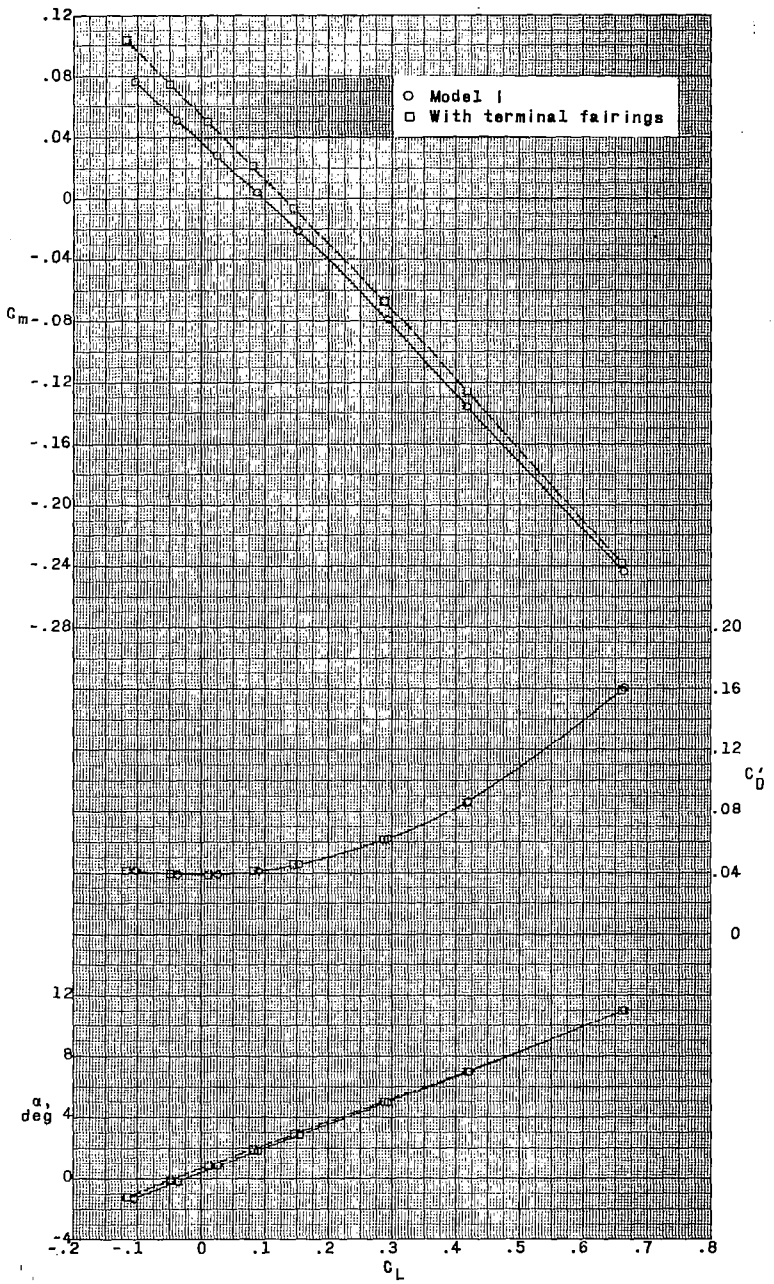

(a) M = 1.57.

Figure 15.- Effect of terminal fairings on aerodynamic characteristics in pitch; $\beta \approx 0^{\circ}$.

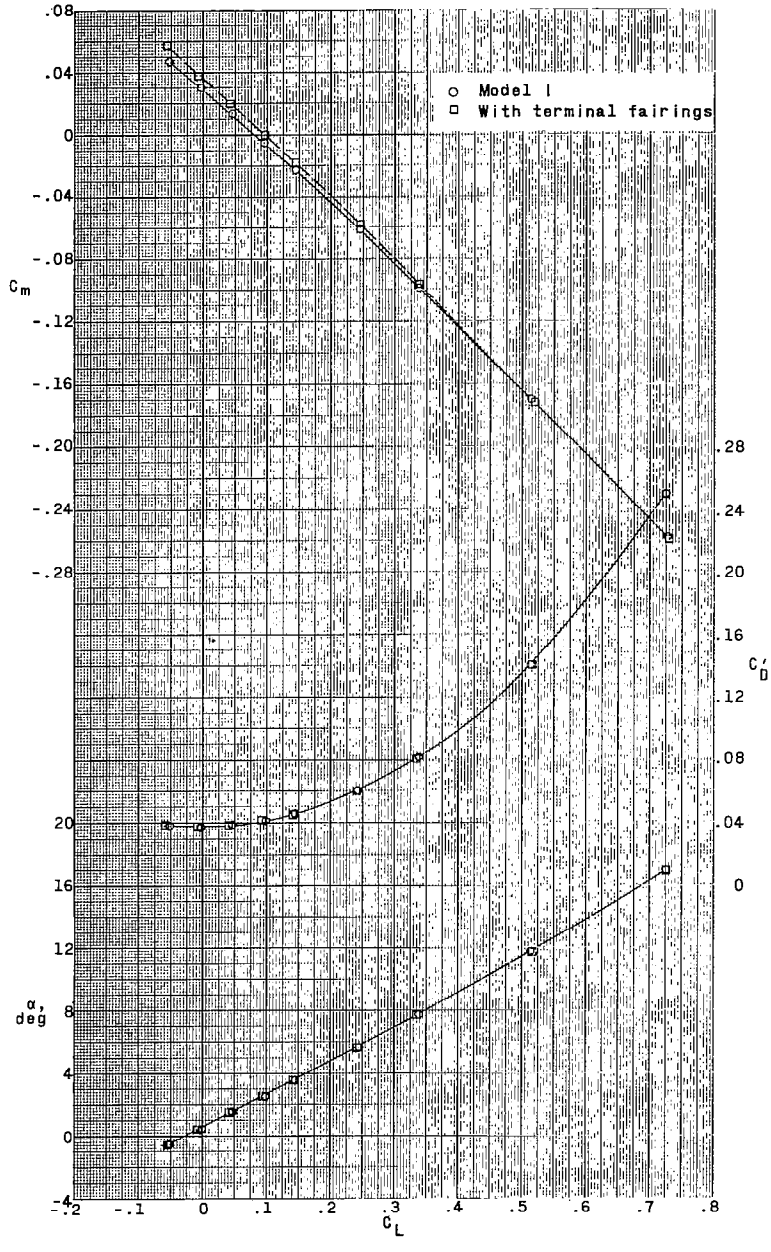

(b) M = 2.01.

Figure 15.- Concluded.

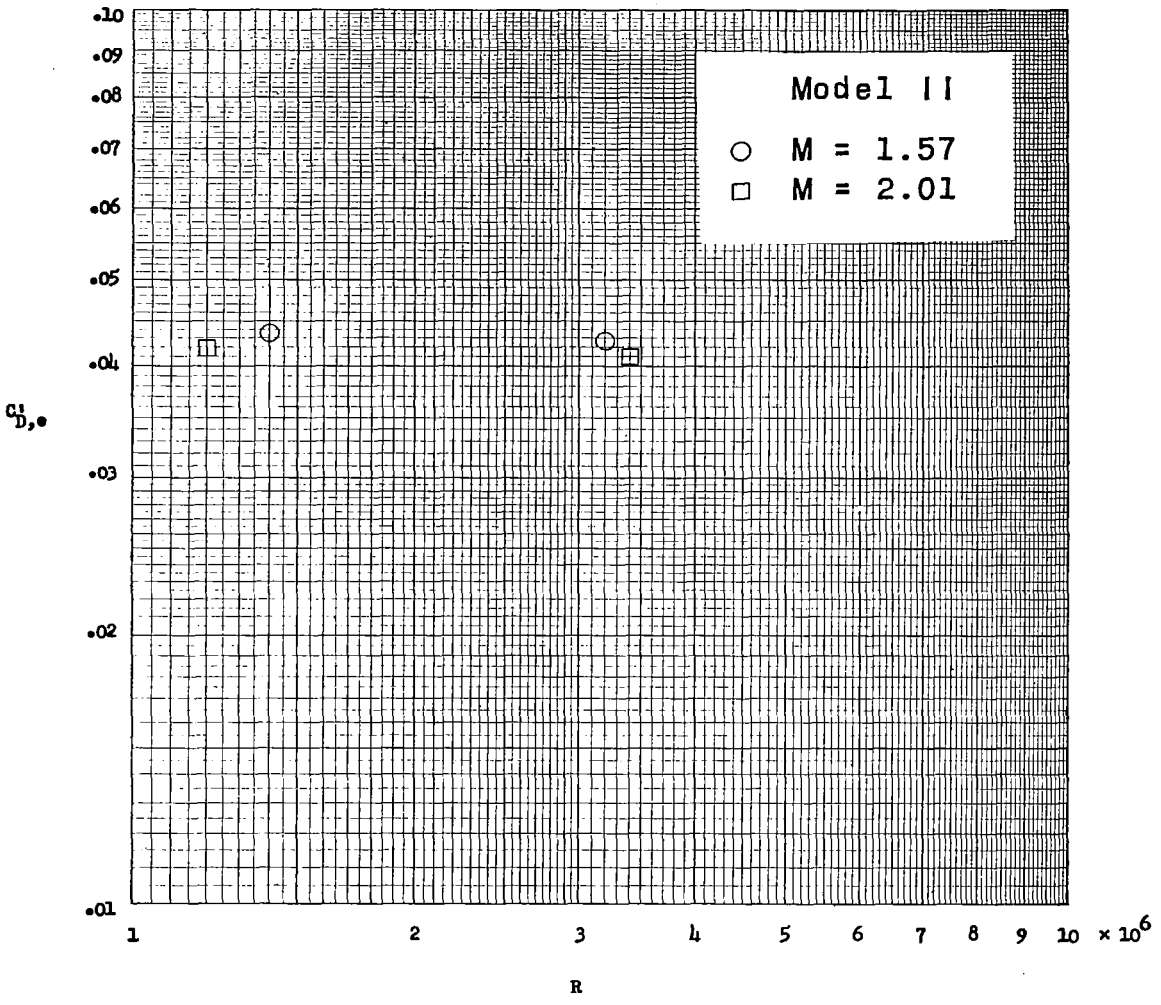

Figure 16.- Effect of Reynolds number on net external drag characteristics.

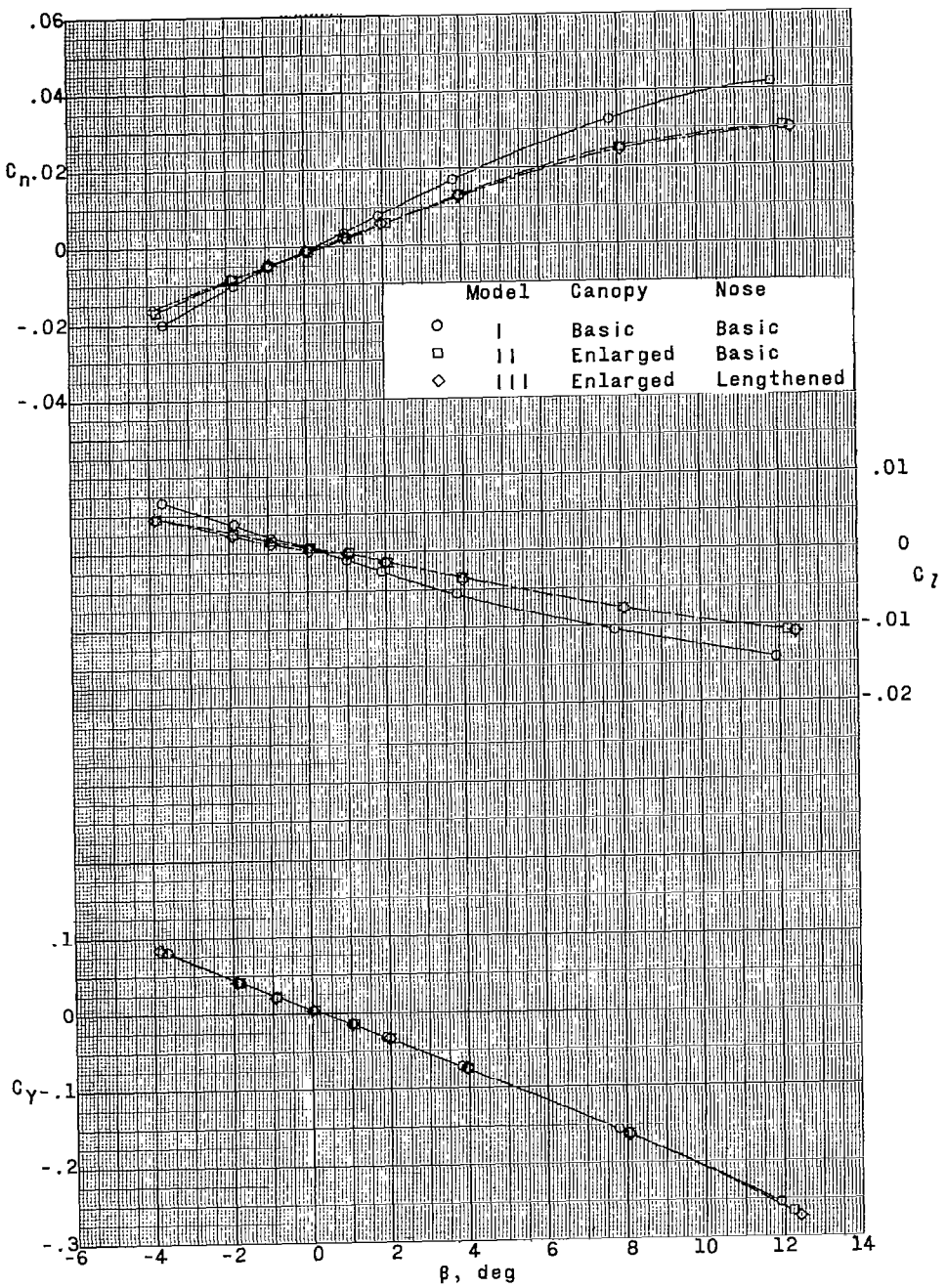

(a) M = 1.57; $\alpha \approx 0.6^{\circ}$.

Figure 17.- Effect of nose length and canopy size on aerodynamic characteristics in sideslip.

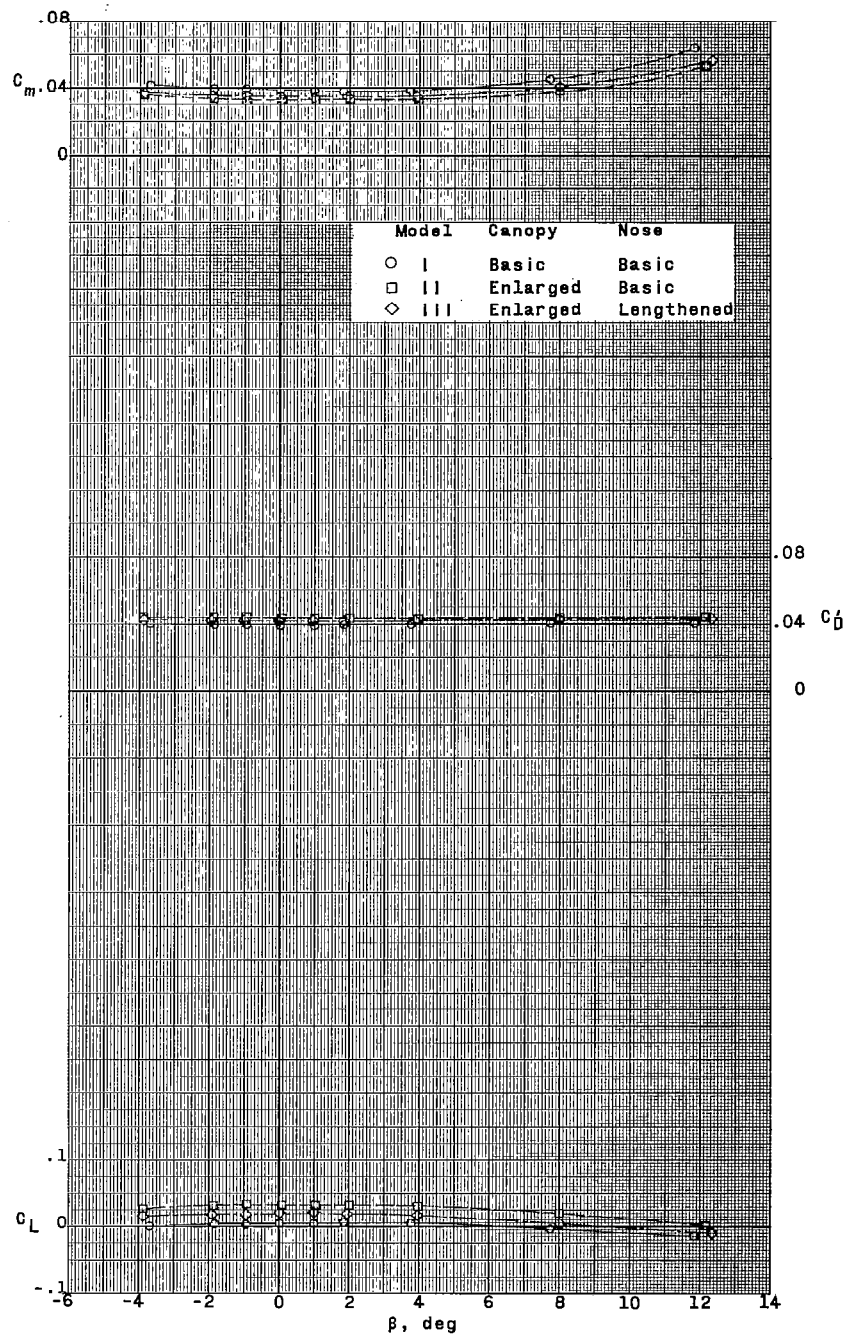

(a) Concluded.

Figure 17.- Continued.

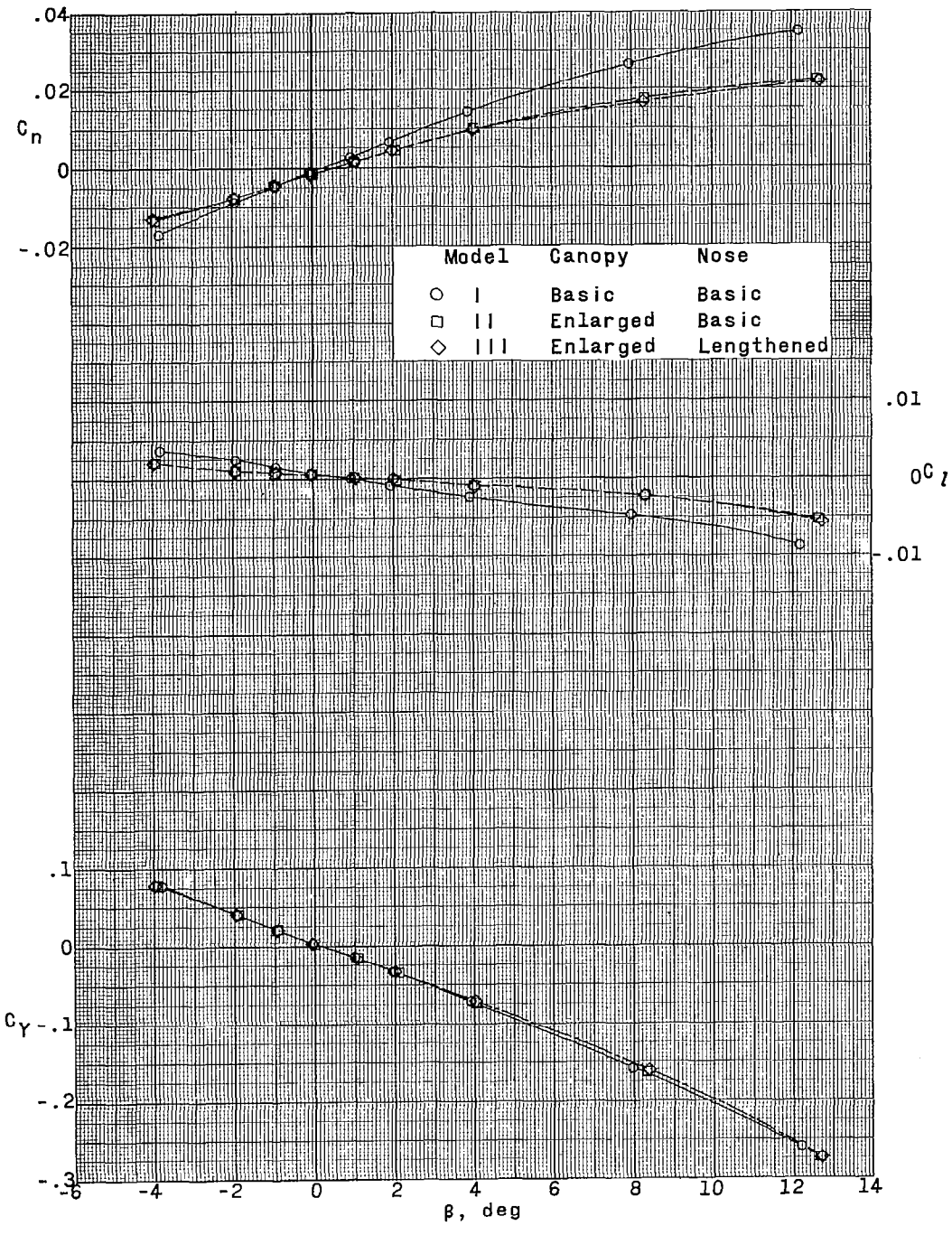

(b) M = 1.57; $\alpha \approx 5.8^{\circ}$.

Figure 17.- Continued.

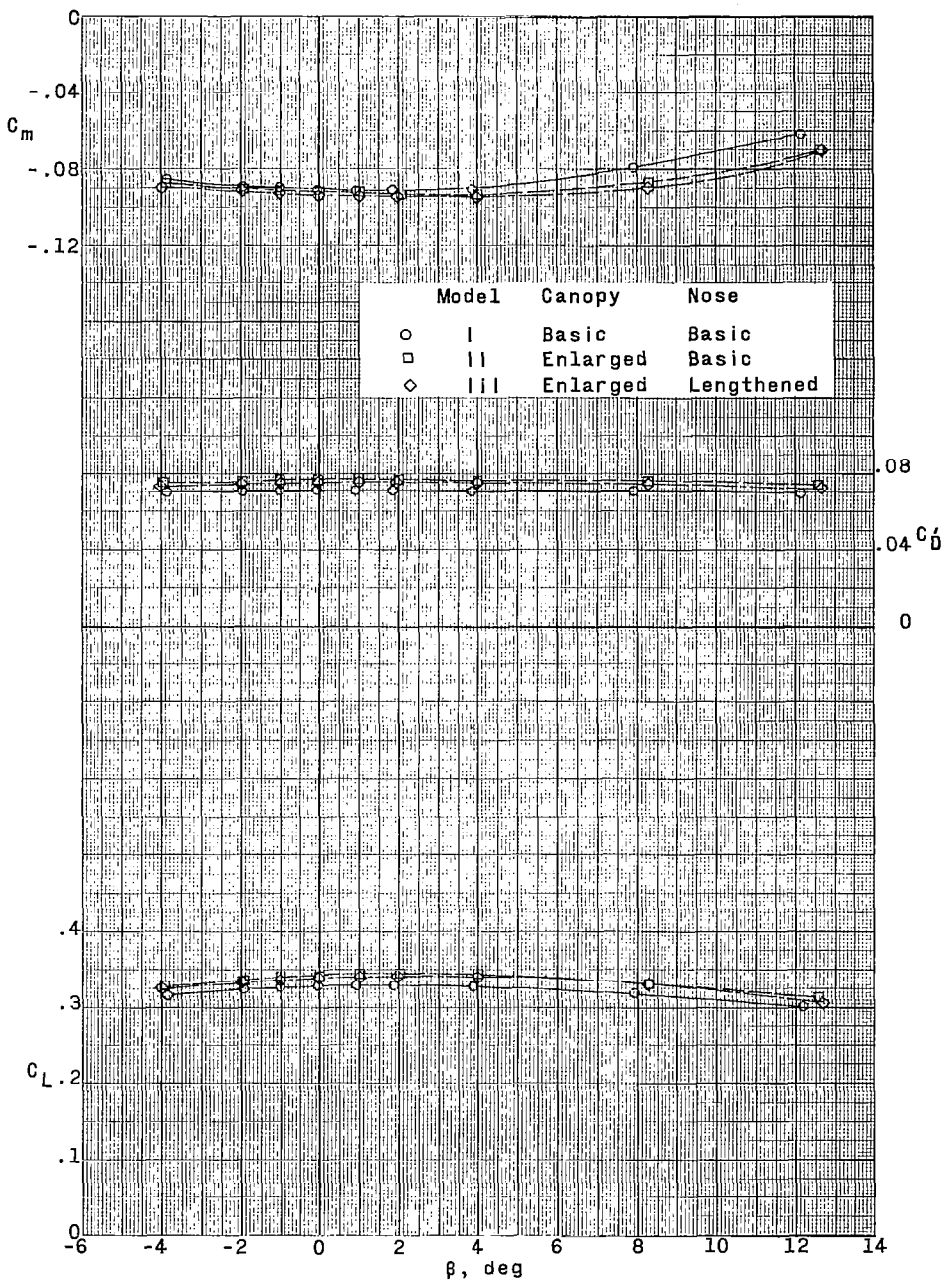

(b) Concluded.

Figure 17.- Continued.

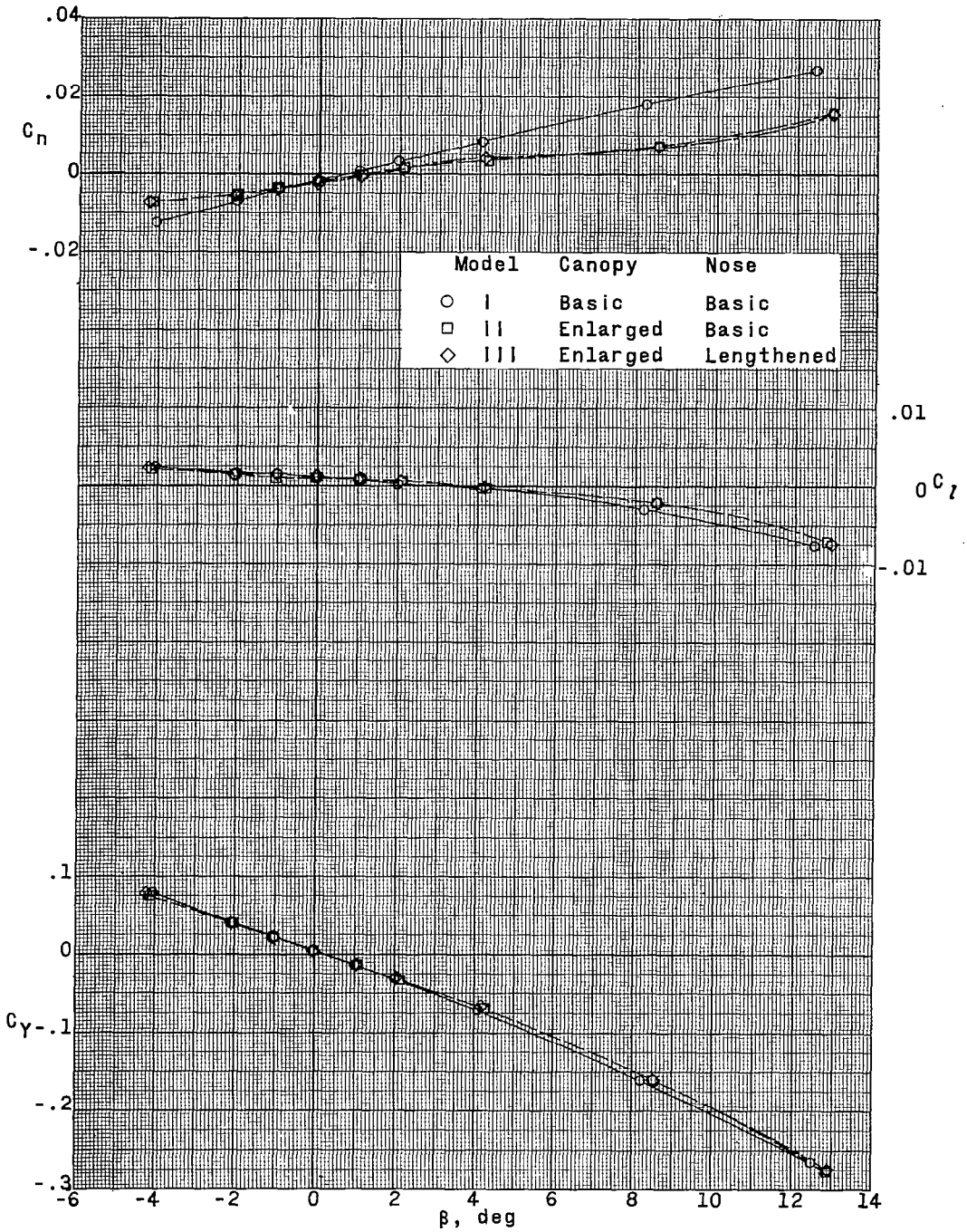

(c) $M = 1.57$; $\alpha \approx 10.8^\circ$.

Figure 17.- Continued.

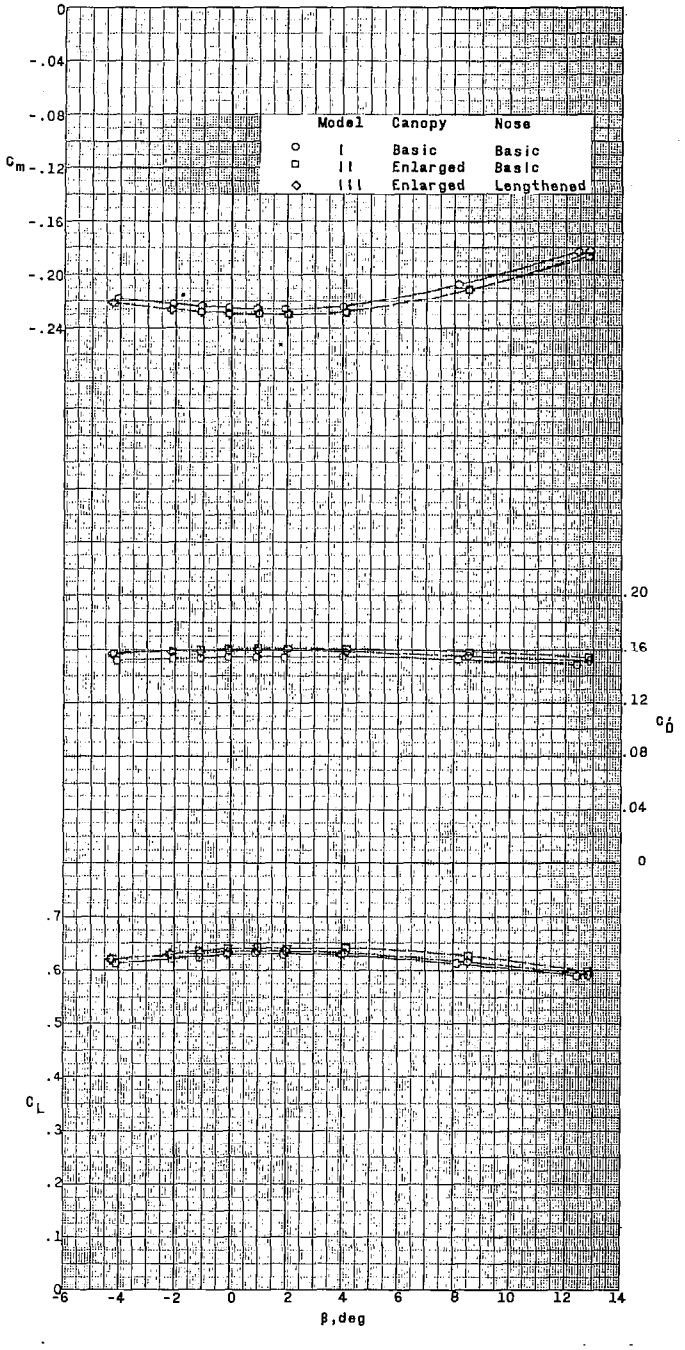

(c) Concluded.

Figure 17.- Continued.

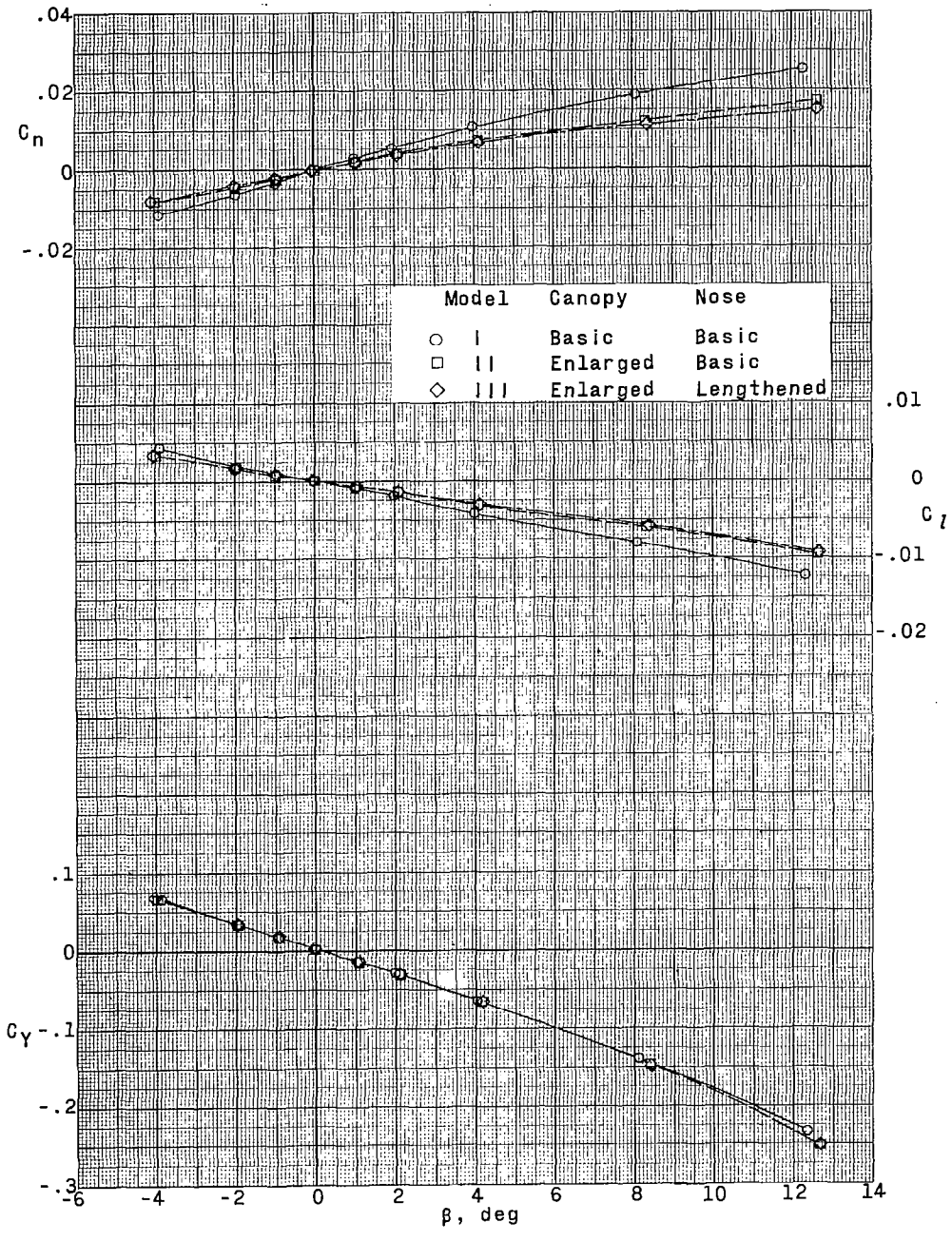

(d) M = 2.01; $\alpha \approx 1.4^{\circ}$.

Figure 17.- Continued.

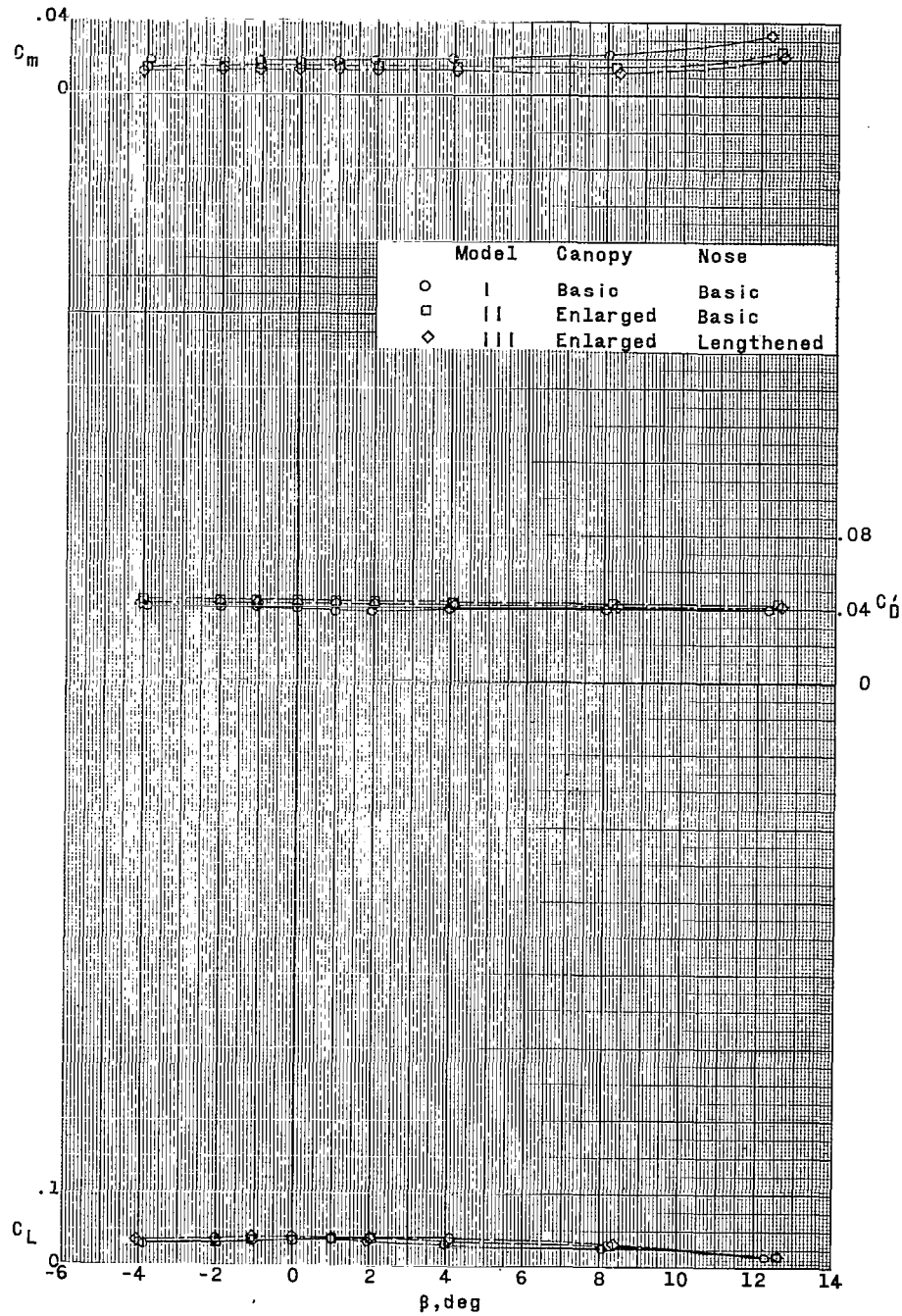

(d) Concluded.

Figure 17.- Continued.

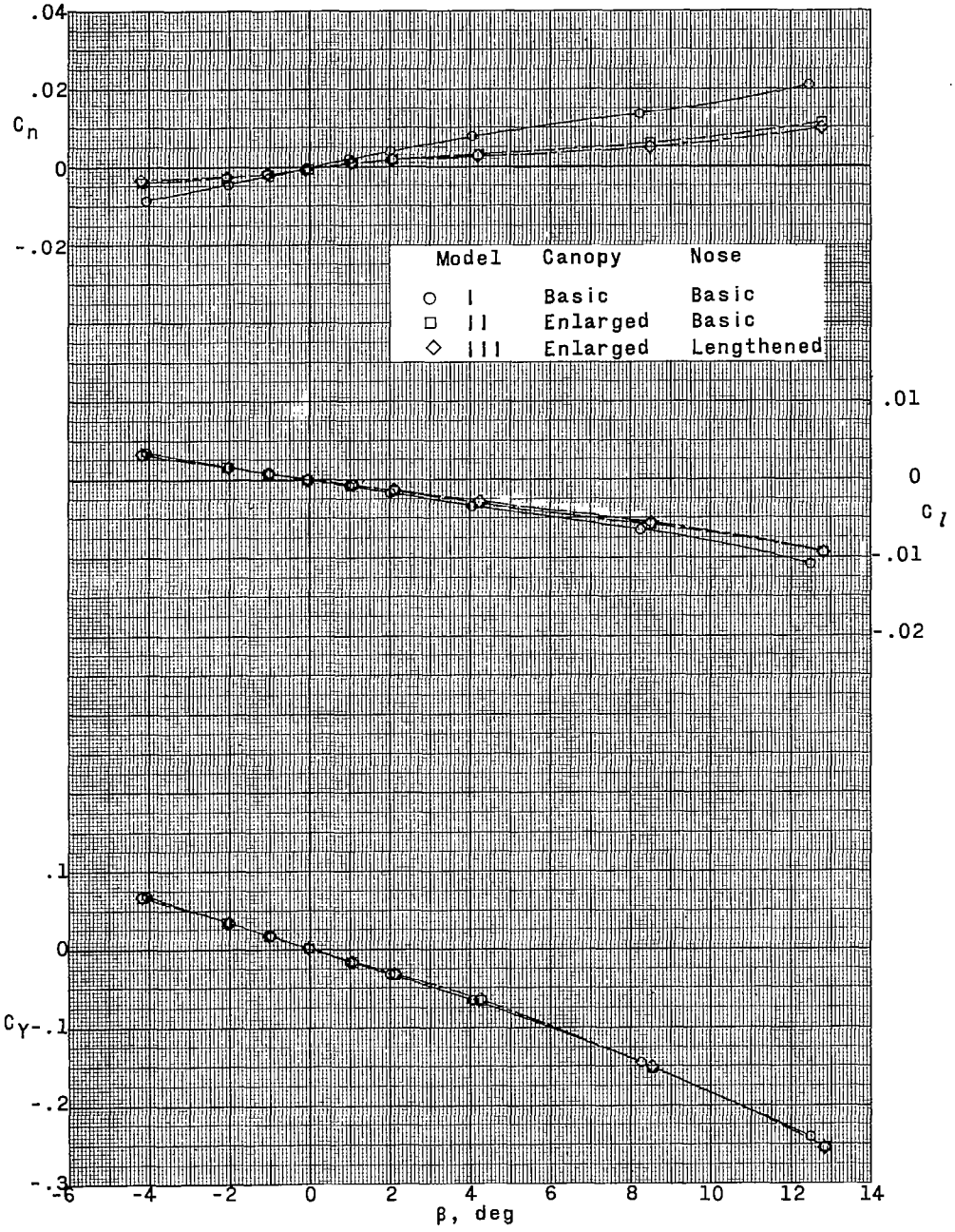

(e) M = 2.01; $\alpha \approx 6.5^{\circ}$.

Figure 17.- Continued.

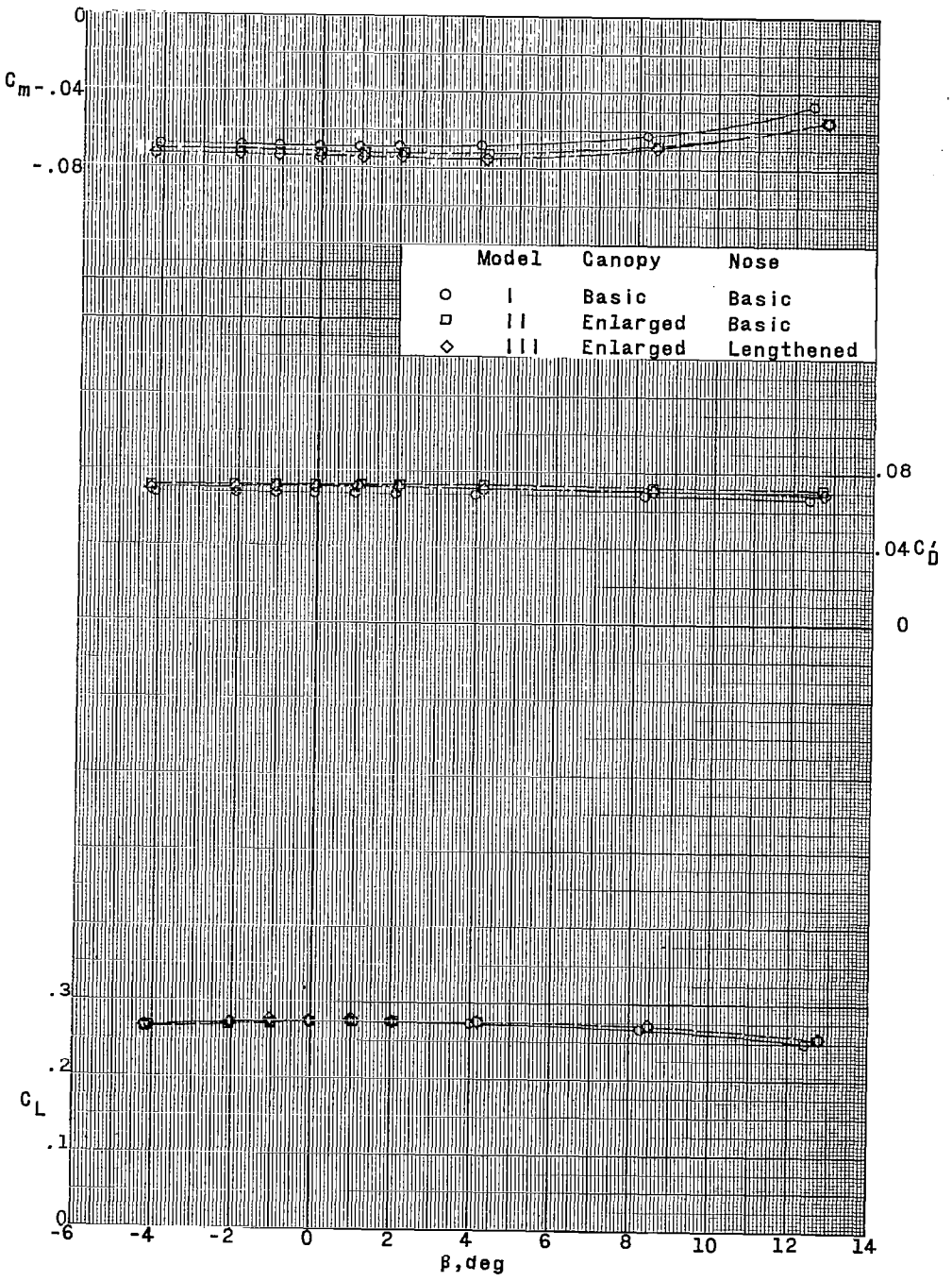

(e) Concluded.

Figure 17.- Continued.

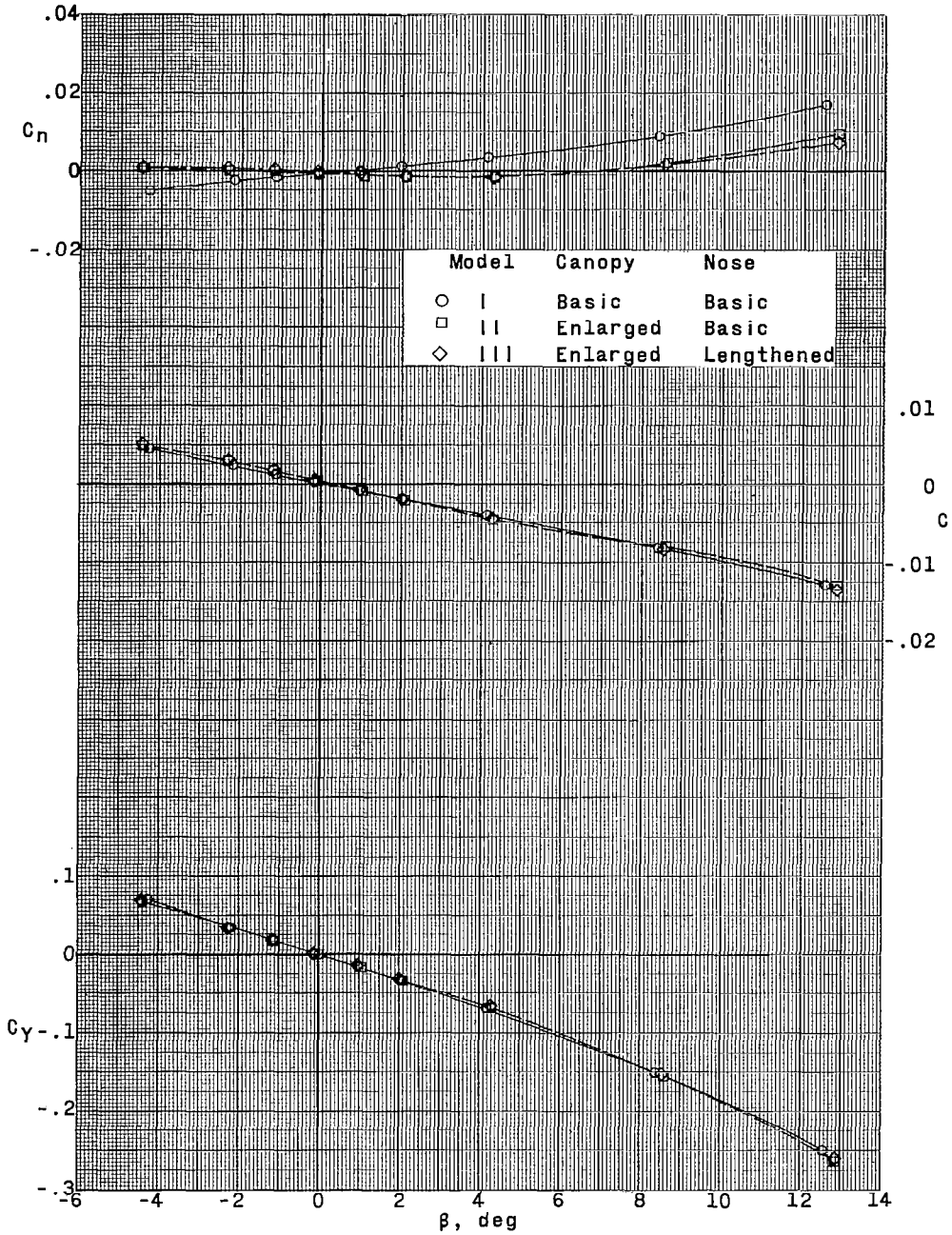

(f) M = 2.01; $\alpha \approx 11.6^{\circ}$.

Figure 17.- Continued.

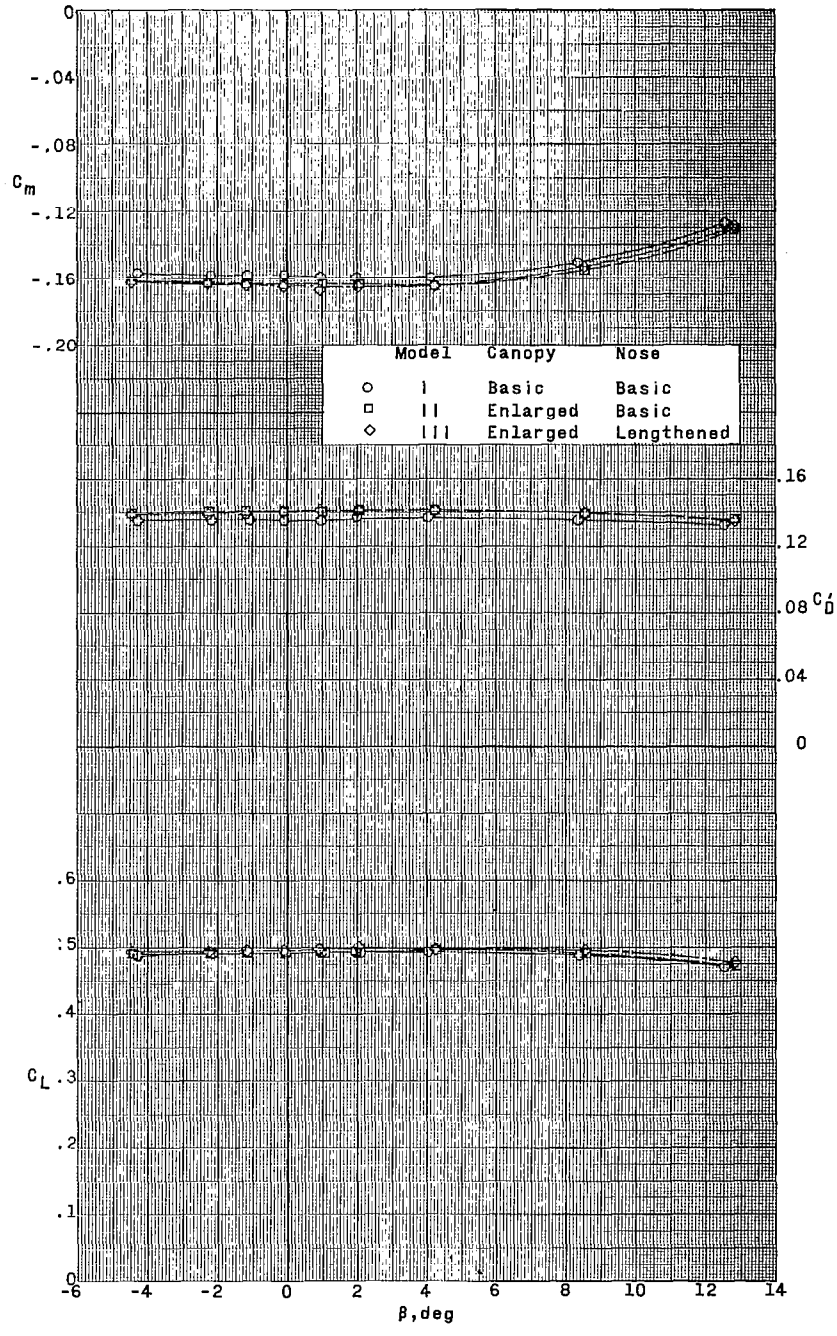

(f) Concluded.

Figure 17.- Continued.

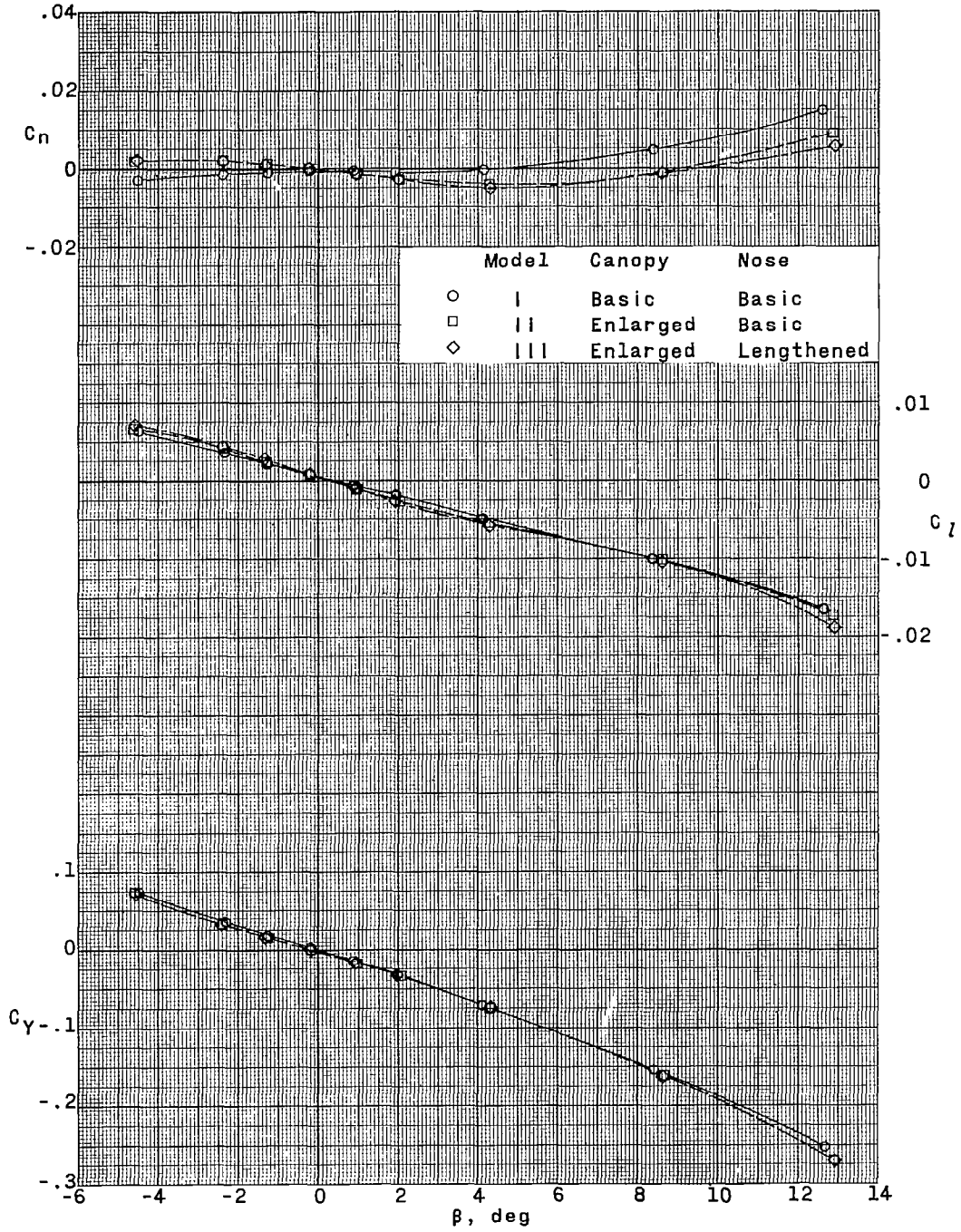

(g) M = 2.01; $\alpha \approx 16.7^{\circ}$.

Figure 17.- Continued.

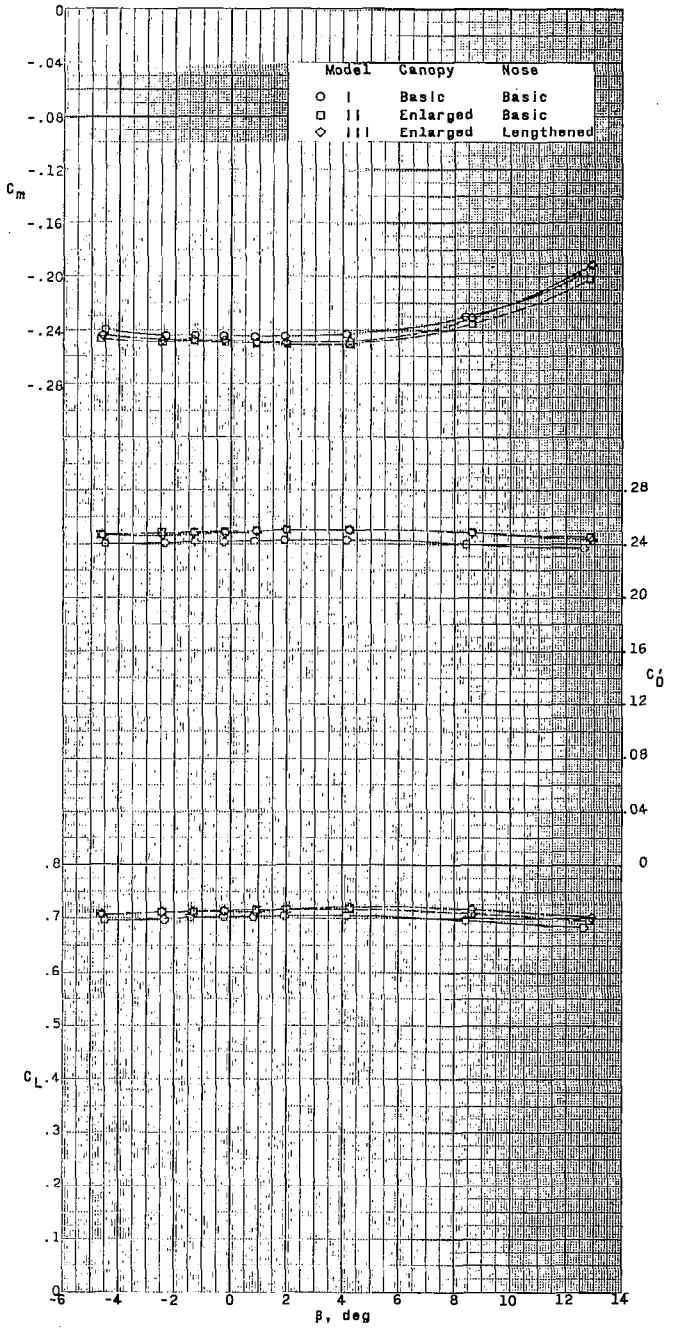

(g) Concluded.

Figure 17.- Concluded.

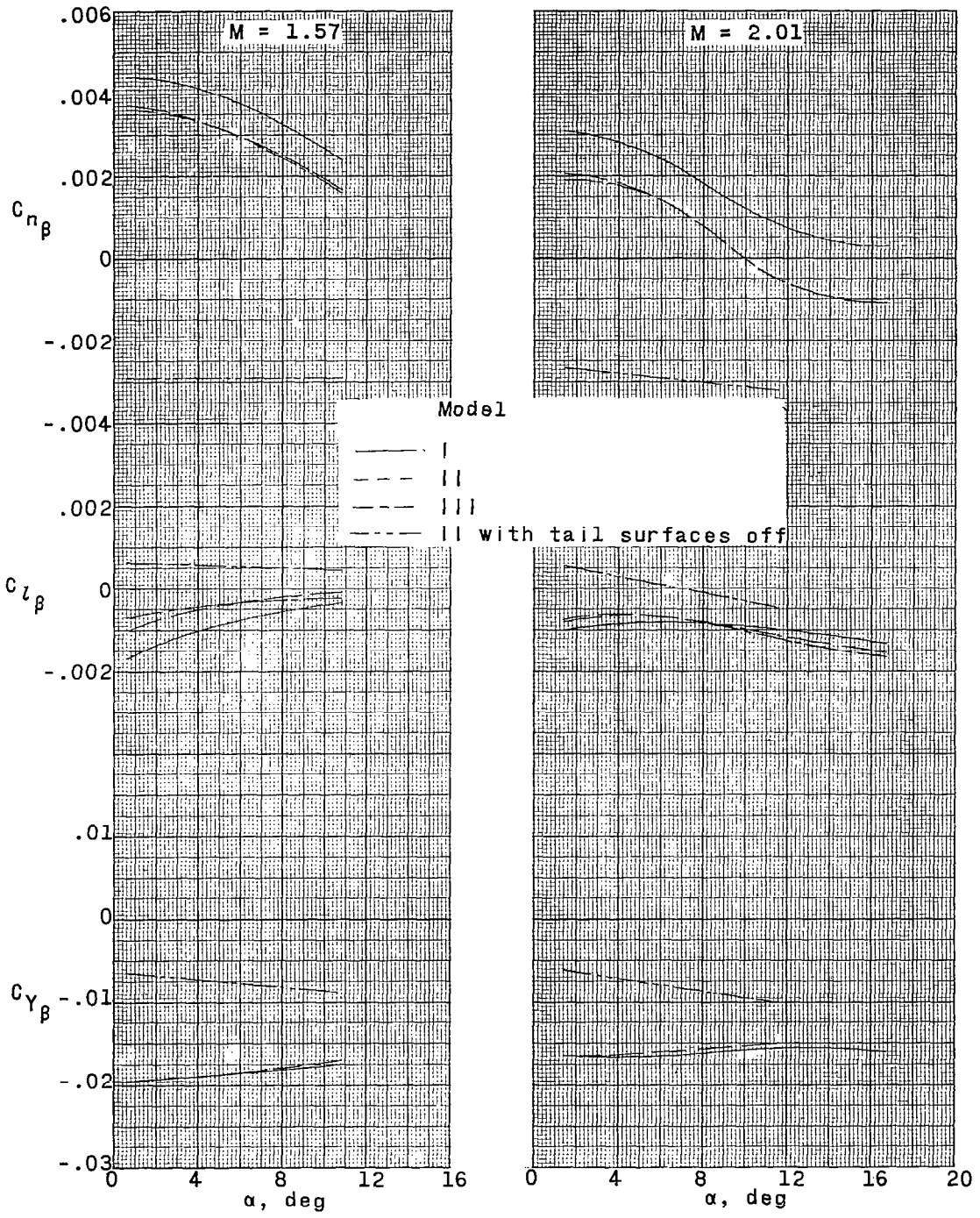

Figure 18.- Summary of directional and lateral stability derivatives for the three model configurations.

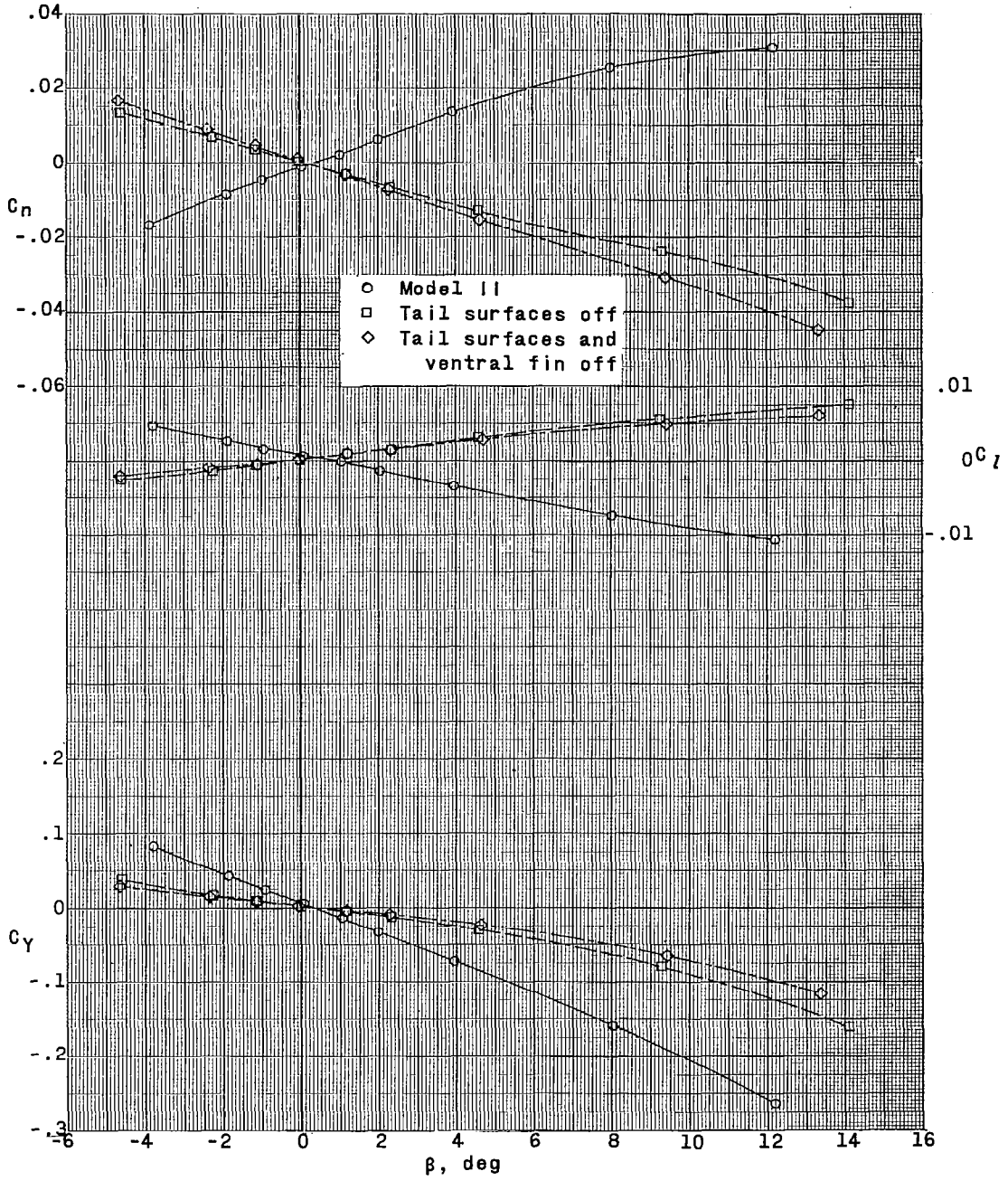

(a) $M = 1.57$; $\alpha \approx 0.6^{\circ}$.

Figure 19.- Effect of tail surfaces and ventral fin on aerodynamic characteristics in sideslip.

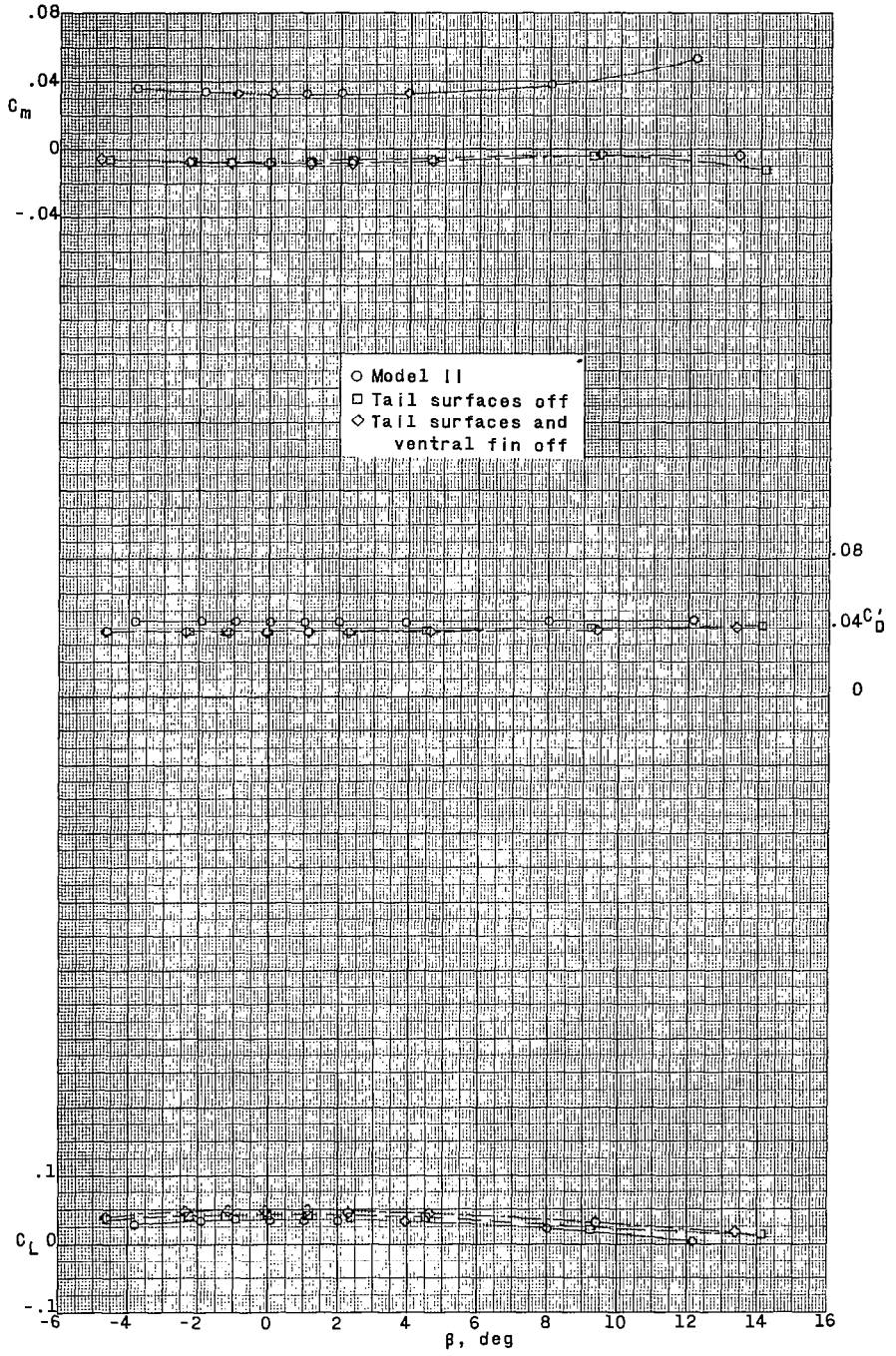

(a) Concluded.

Figure 19.- Continued.

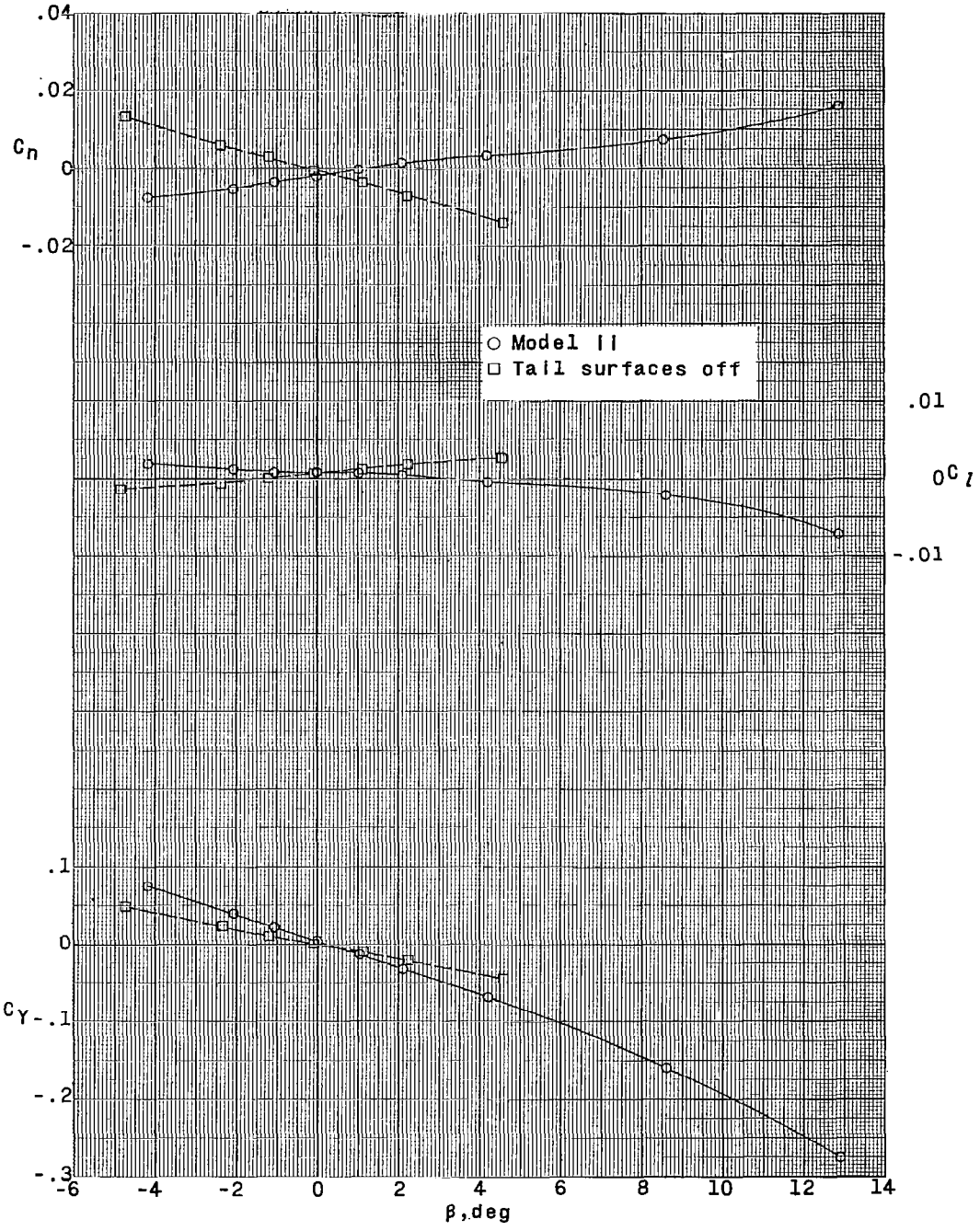

(b) M = 1.57; $\alpha \approx 10.8^{\circ}$.

Figure 19.- Continued.

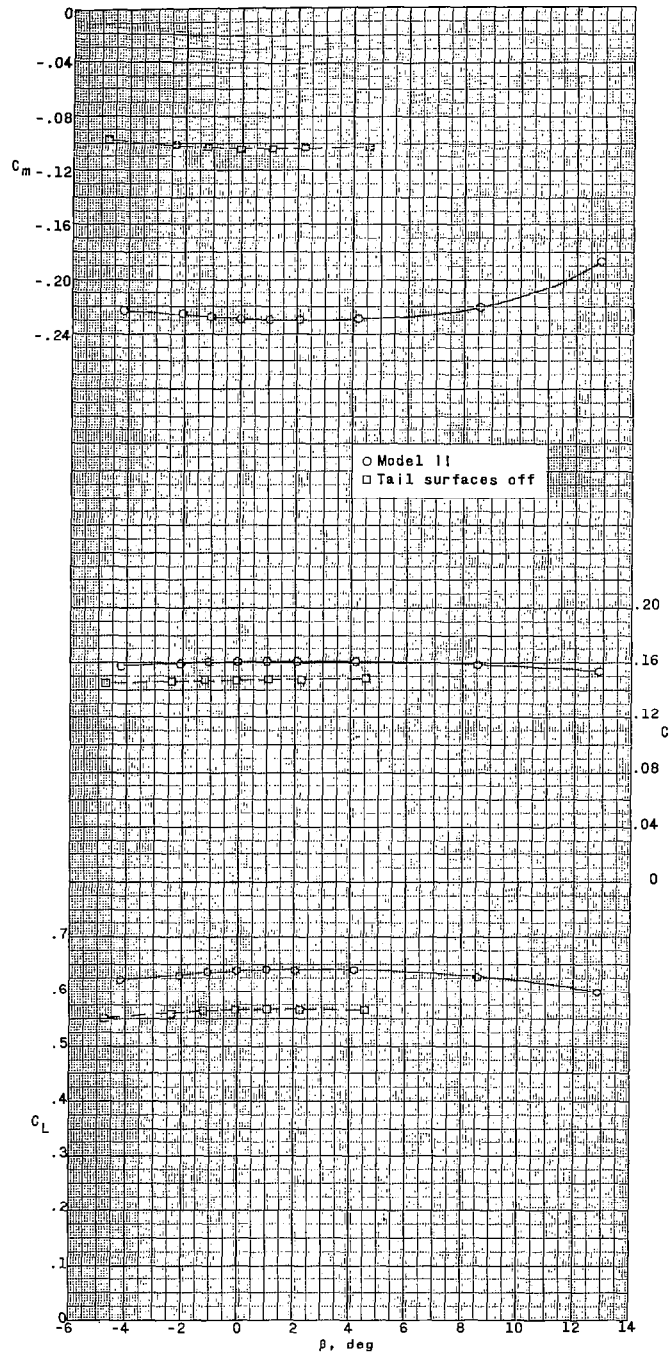

(b) Concluded.

Figure 19.- Continued.

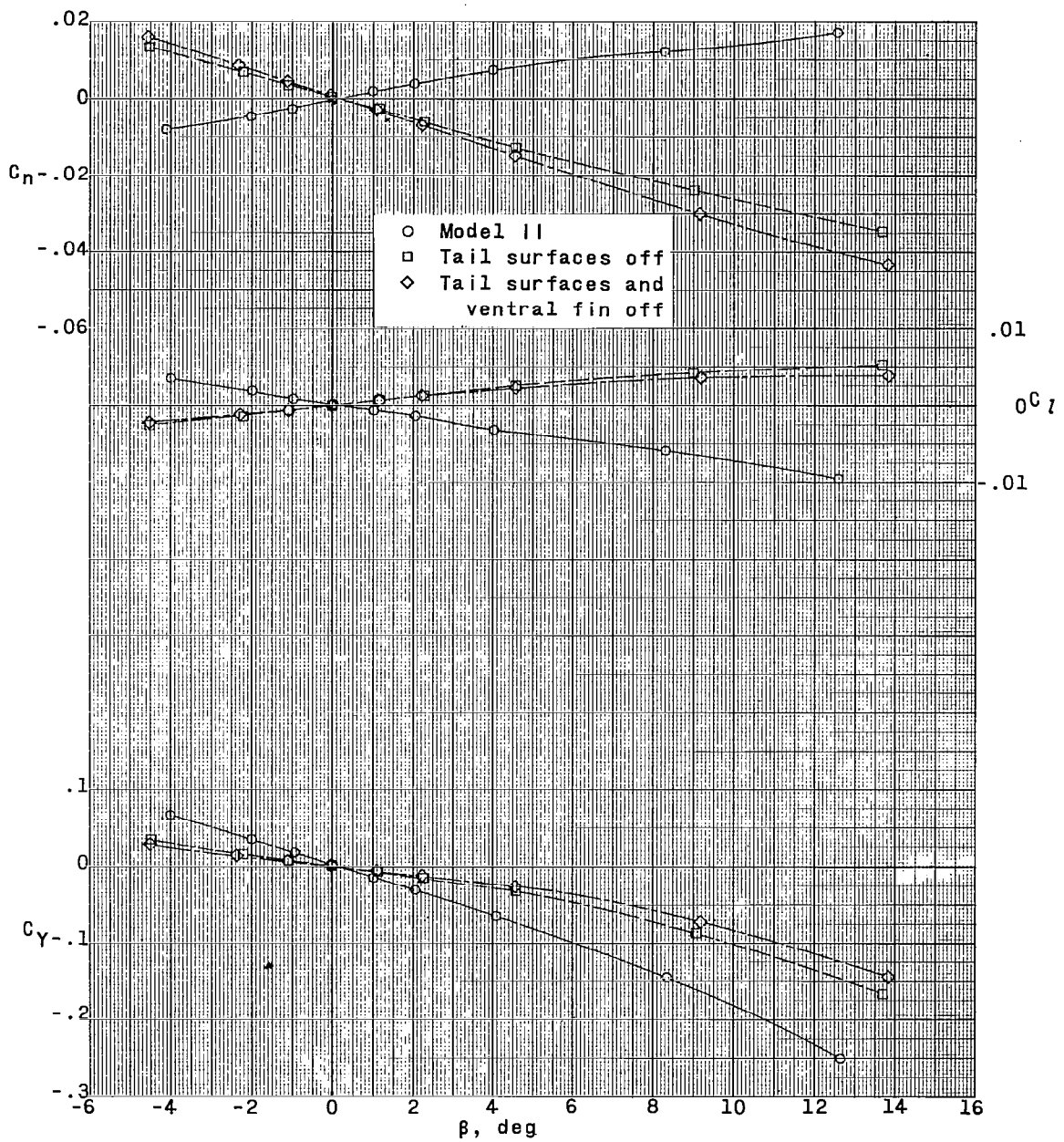

(c) M = 2.01; $\alpha \approx 1.4^{\circ}$.

Figure 19.- Continued.

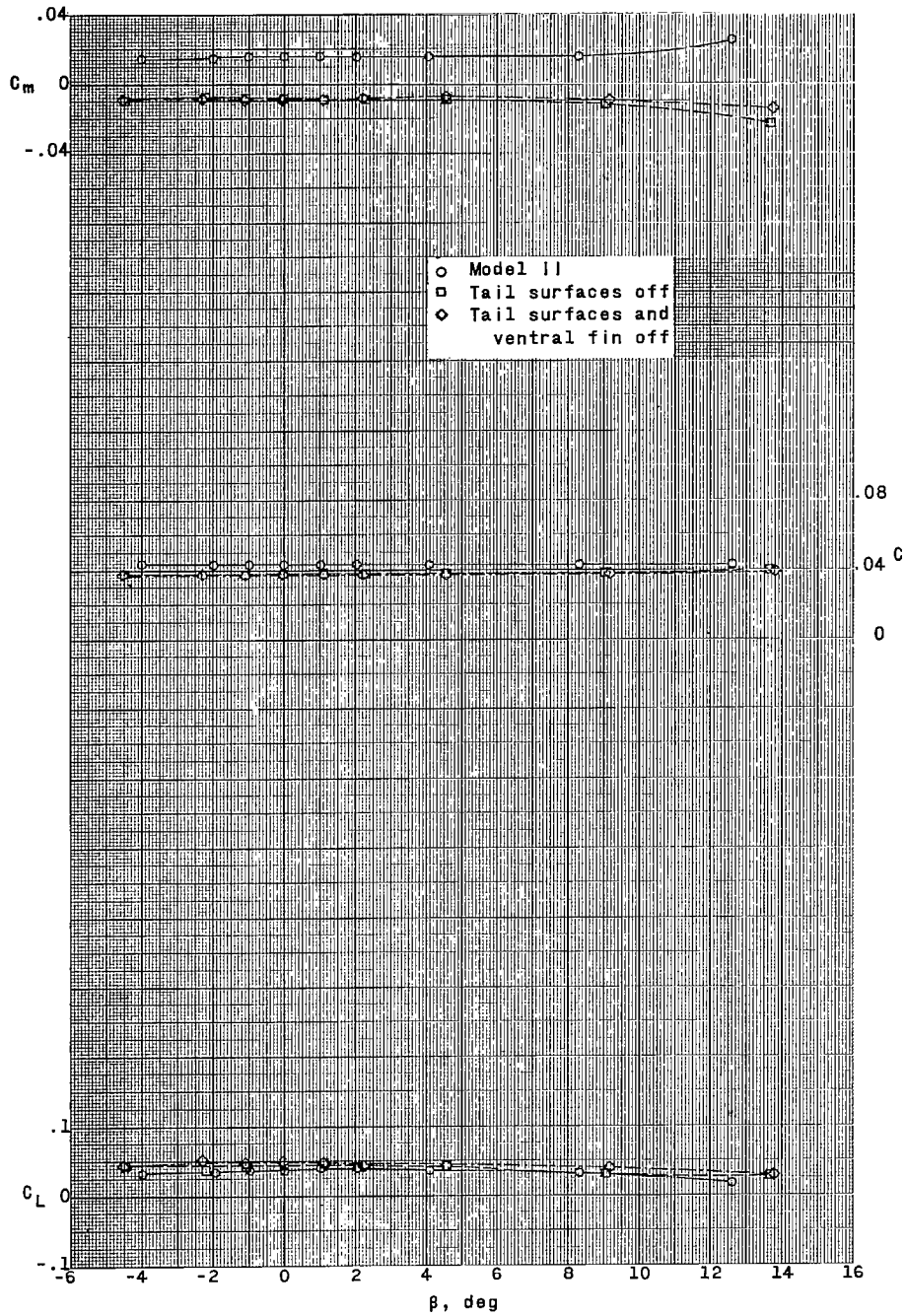

(c) Concluded.

Figure 19.- Continued.

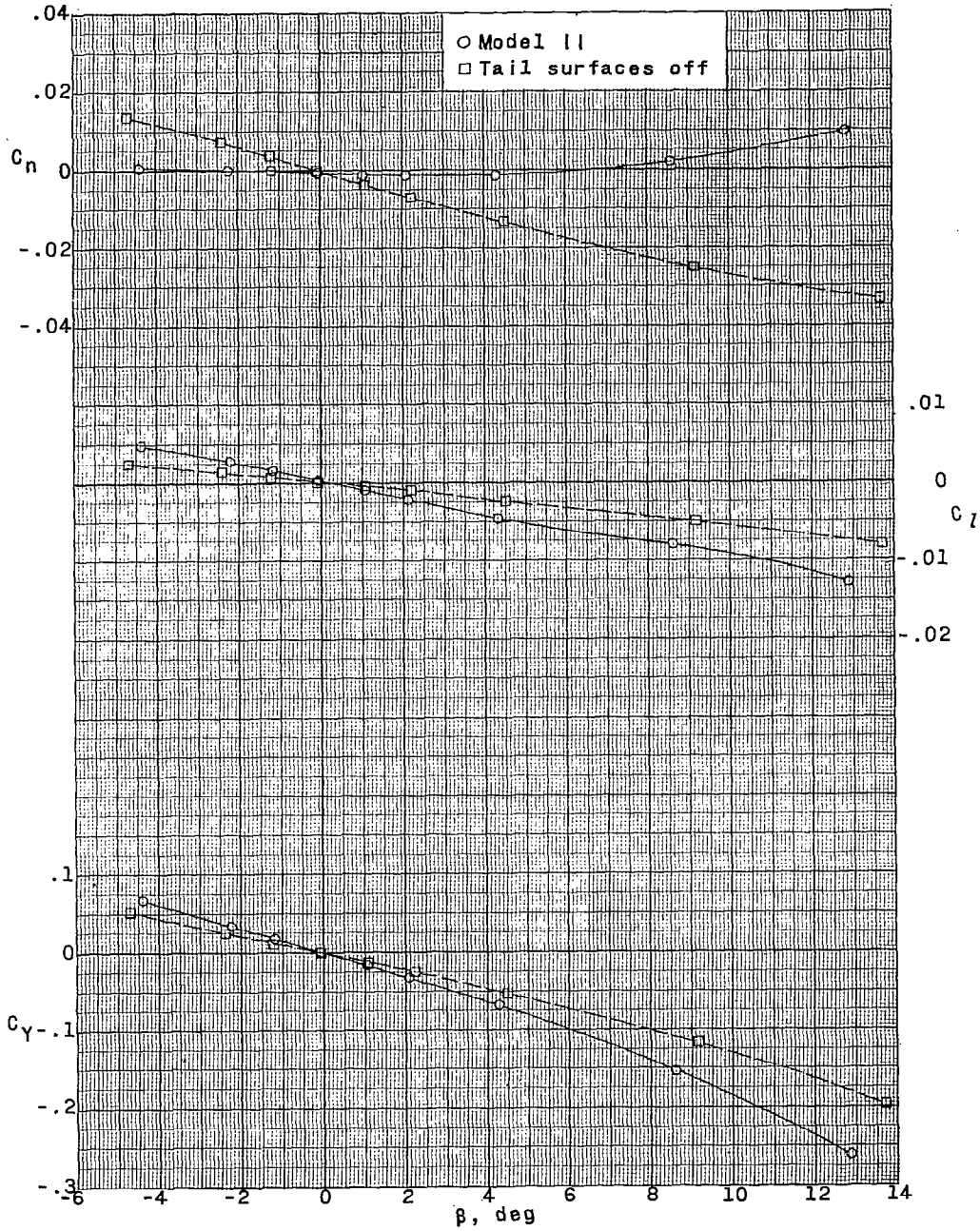

(d) M = 2.01; $\alpha \approx 11.6^{\circ}$.

Figure 19.- Continued.

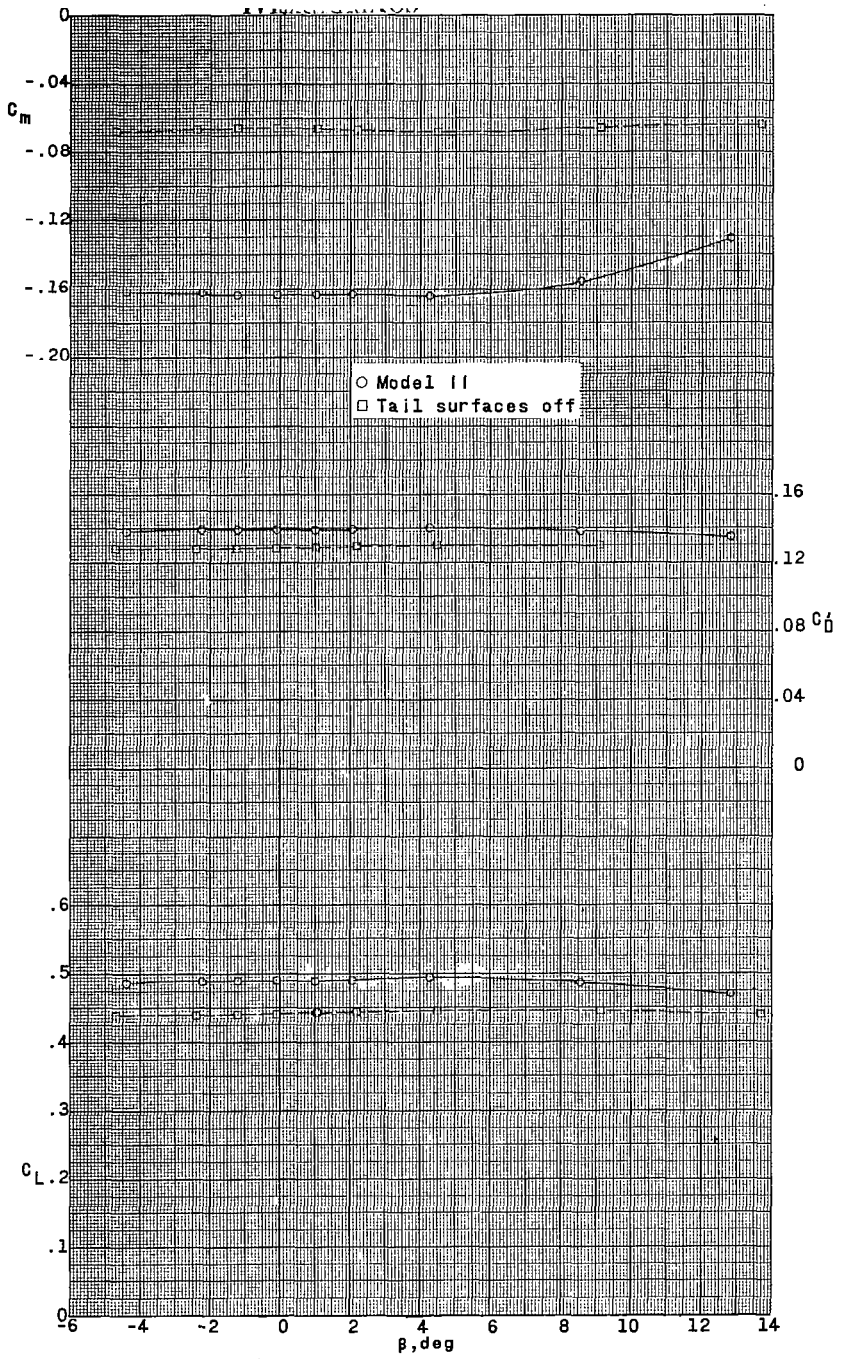

(d) Concluded.

Figure 19.- Concluded.

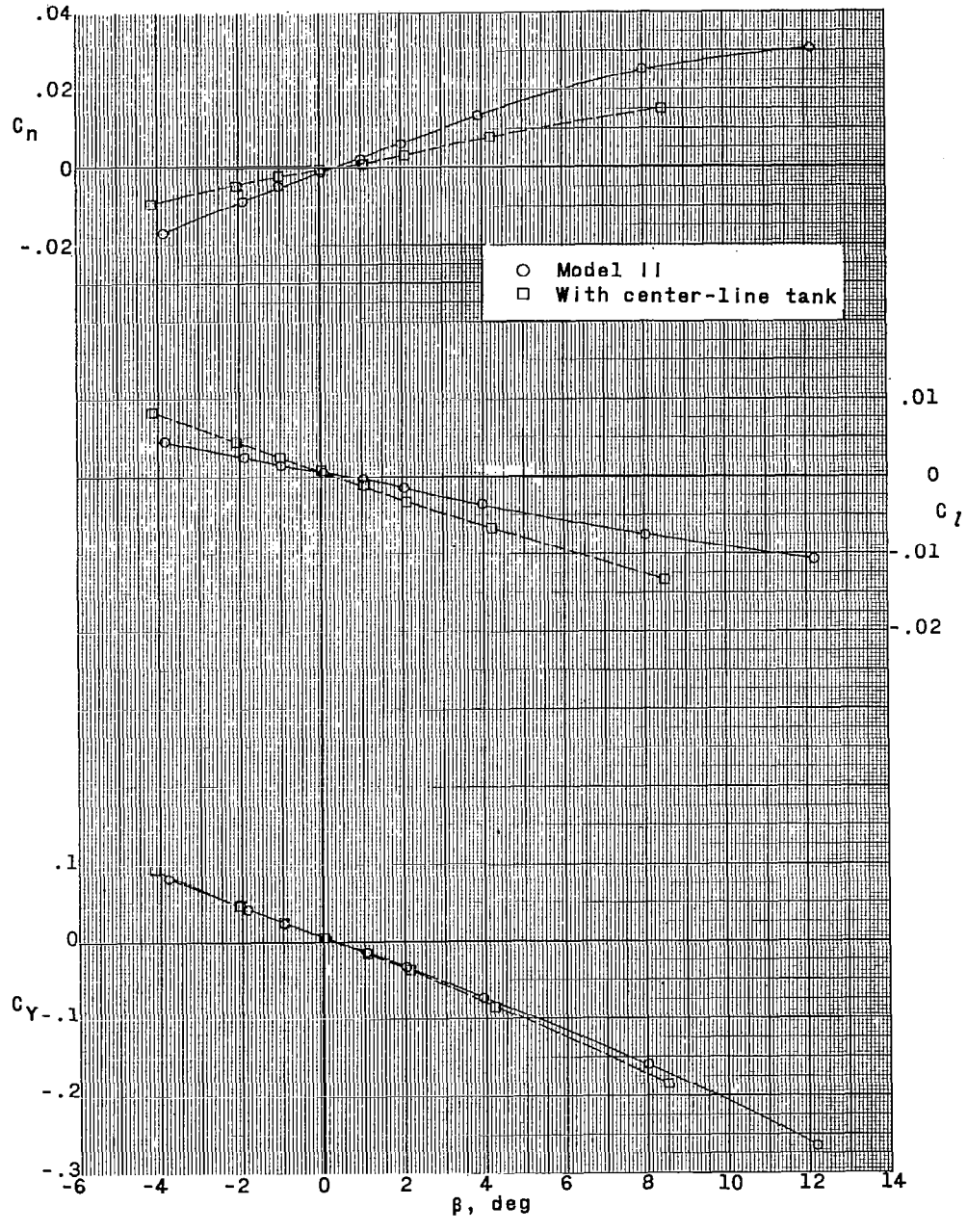

(a) $M = 1.57$; $\alpha \approx 0.6^{\circ}$.

Figure 20.- Effect of external stores on aerodynamic characteristics in sideslip.

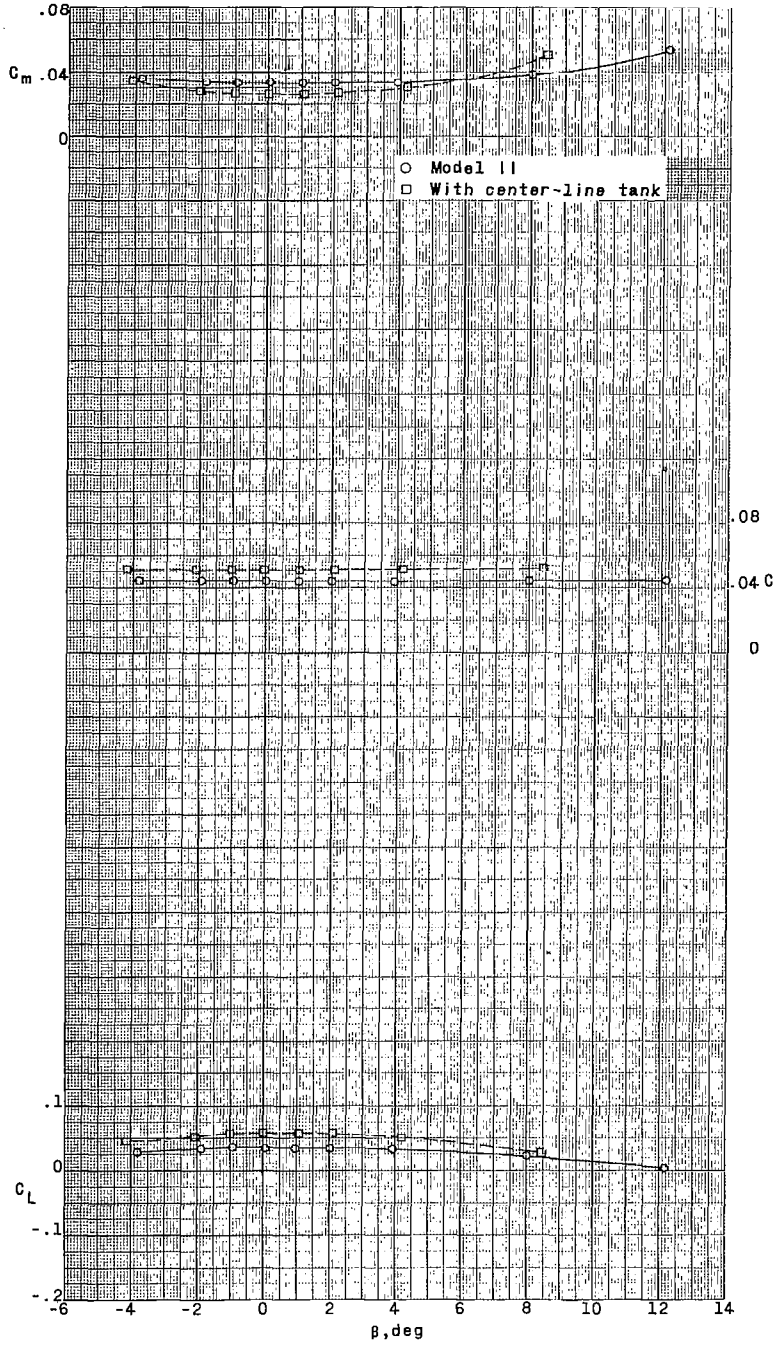

(a) Concluded.

Figure 20.- Continued.

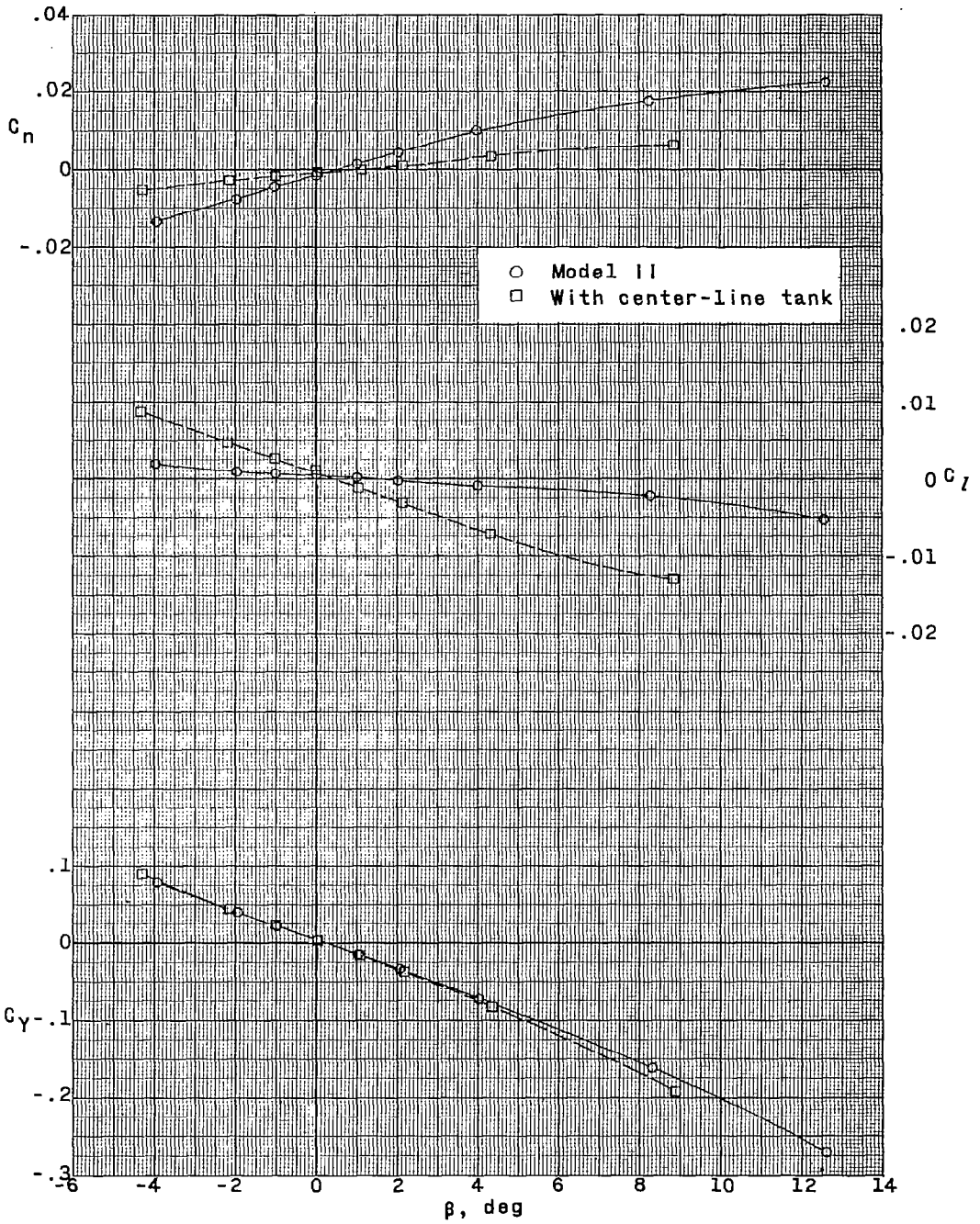

(b) M = 1.57; $\alpha \approx 5.8^{\circ}$.

Figure 20.- Continued.

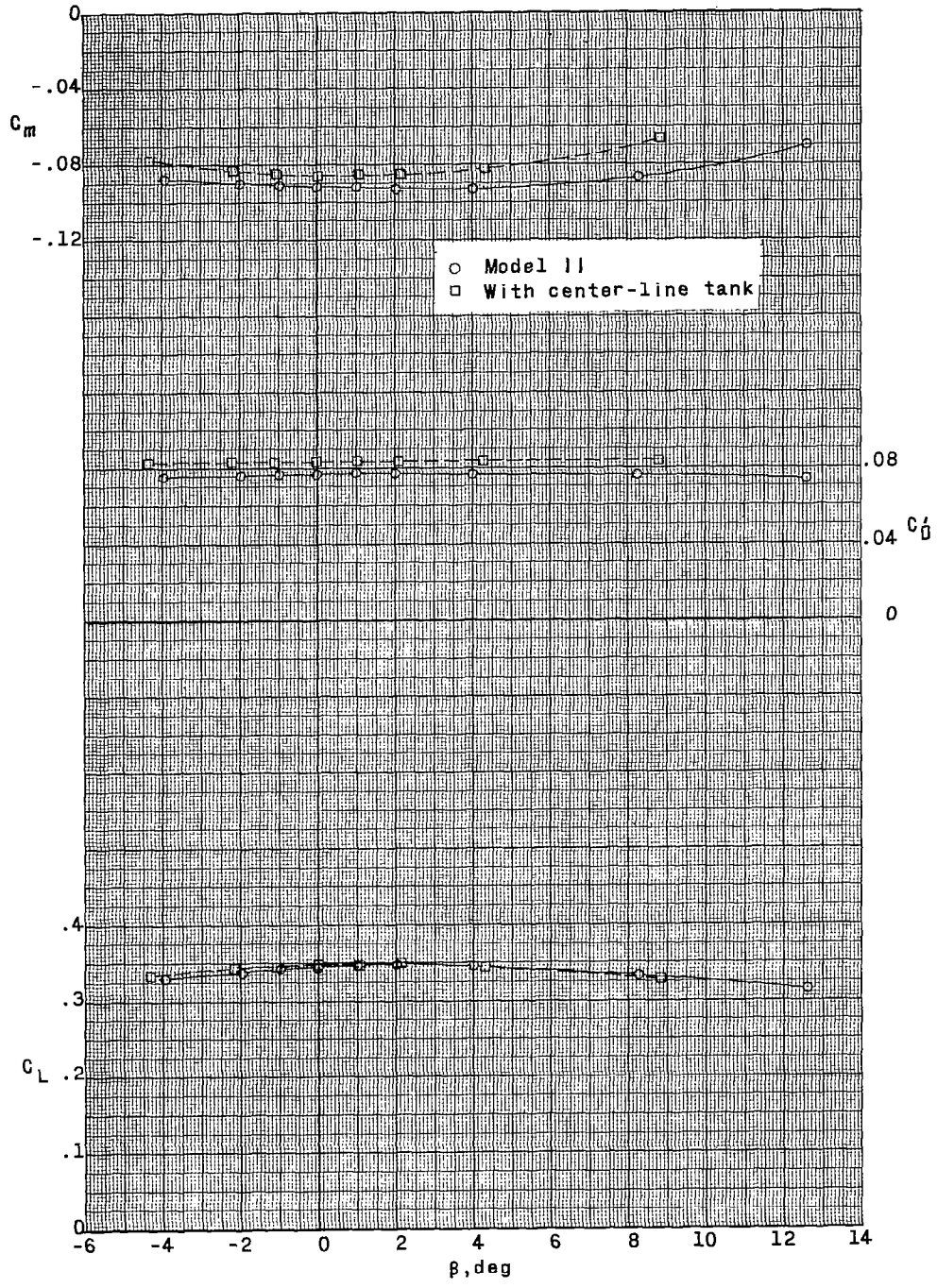

(b) Concluded.

Figure 20.- Continued.

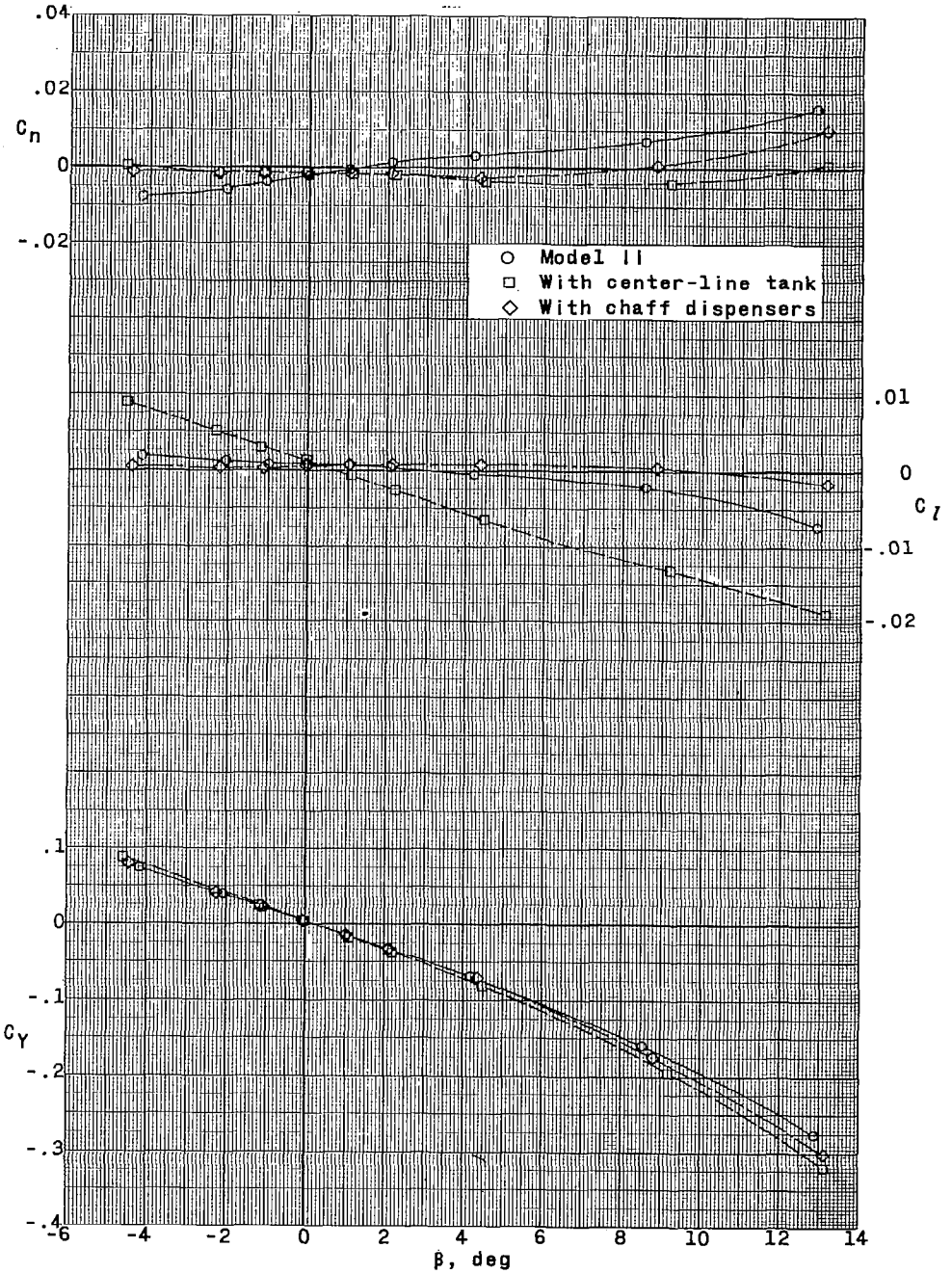

(c) $M = 1.57$; $\alpha \approx 10.8^{\circ}$.

Figure 20.- Continued.

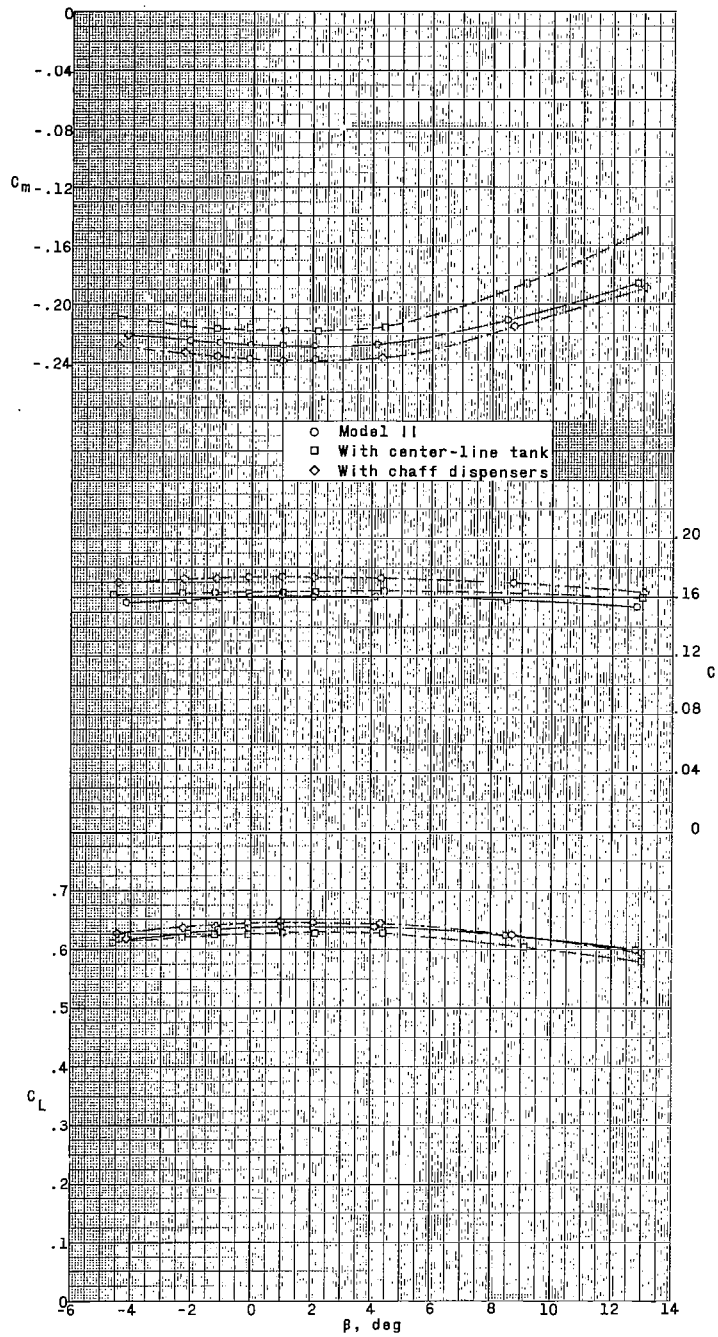

(c) Concluded.

Figure 20.- Continued.

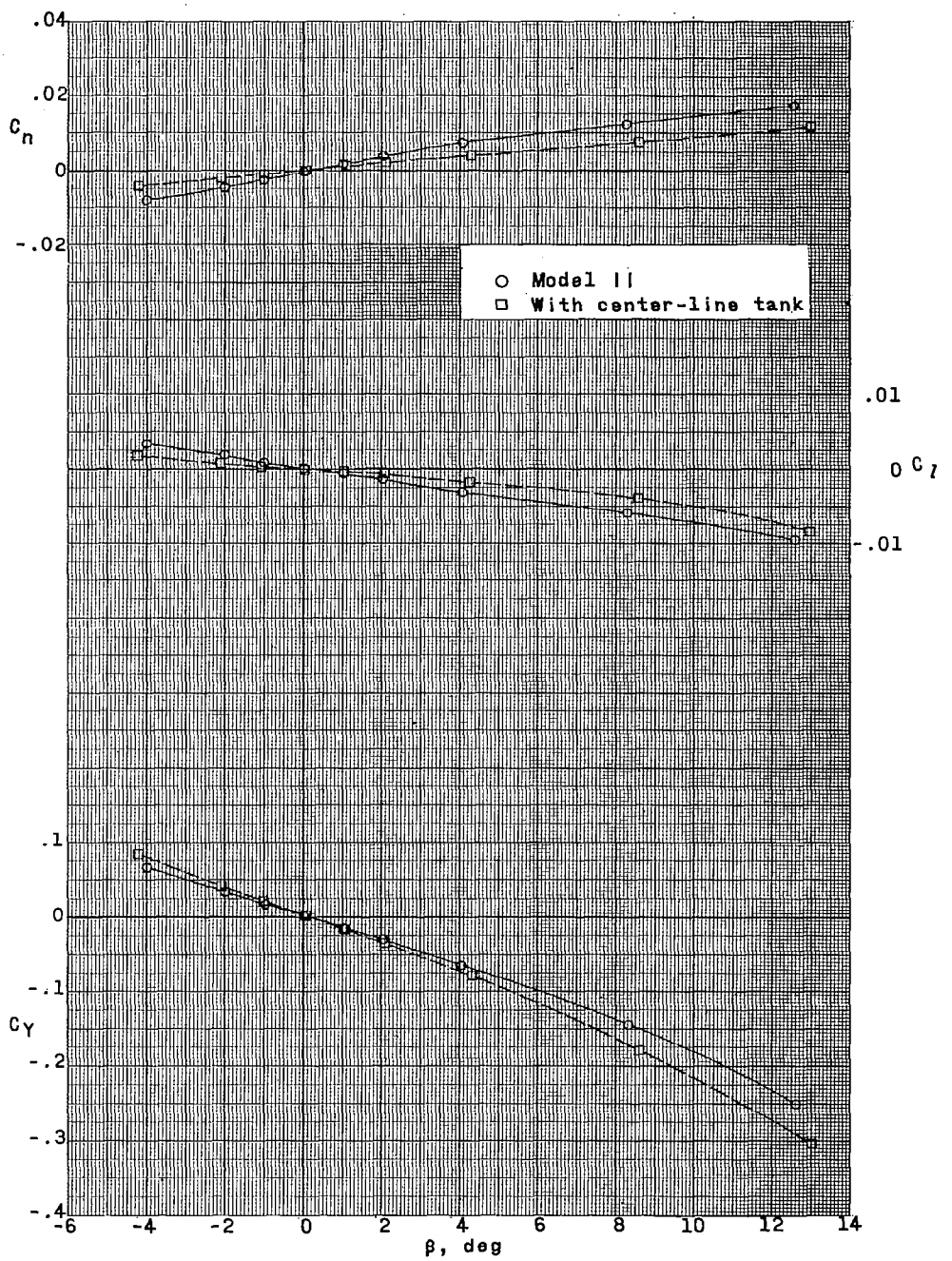

(d) M = 2.01; $\alpha \approx 1.4^{\circ}$.

Figure 20.- Continued.

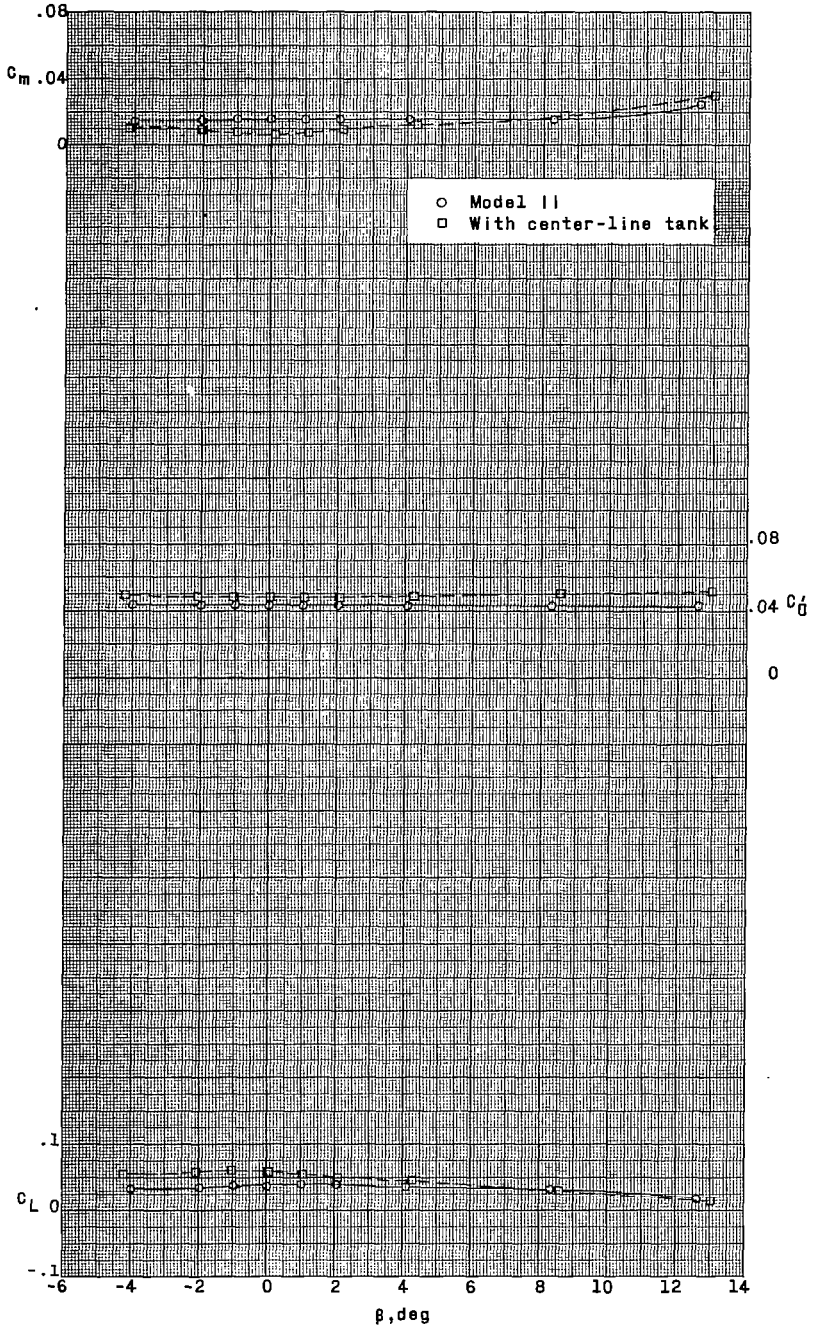

(d) Concluded.

Figure 20.- Continued.

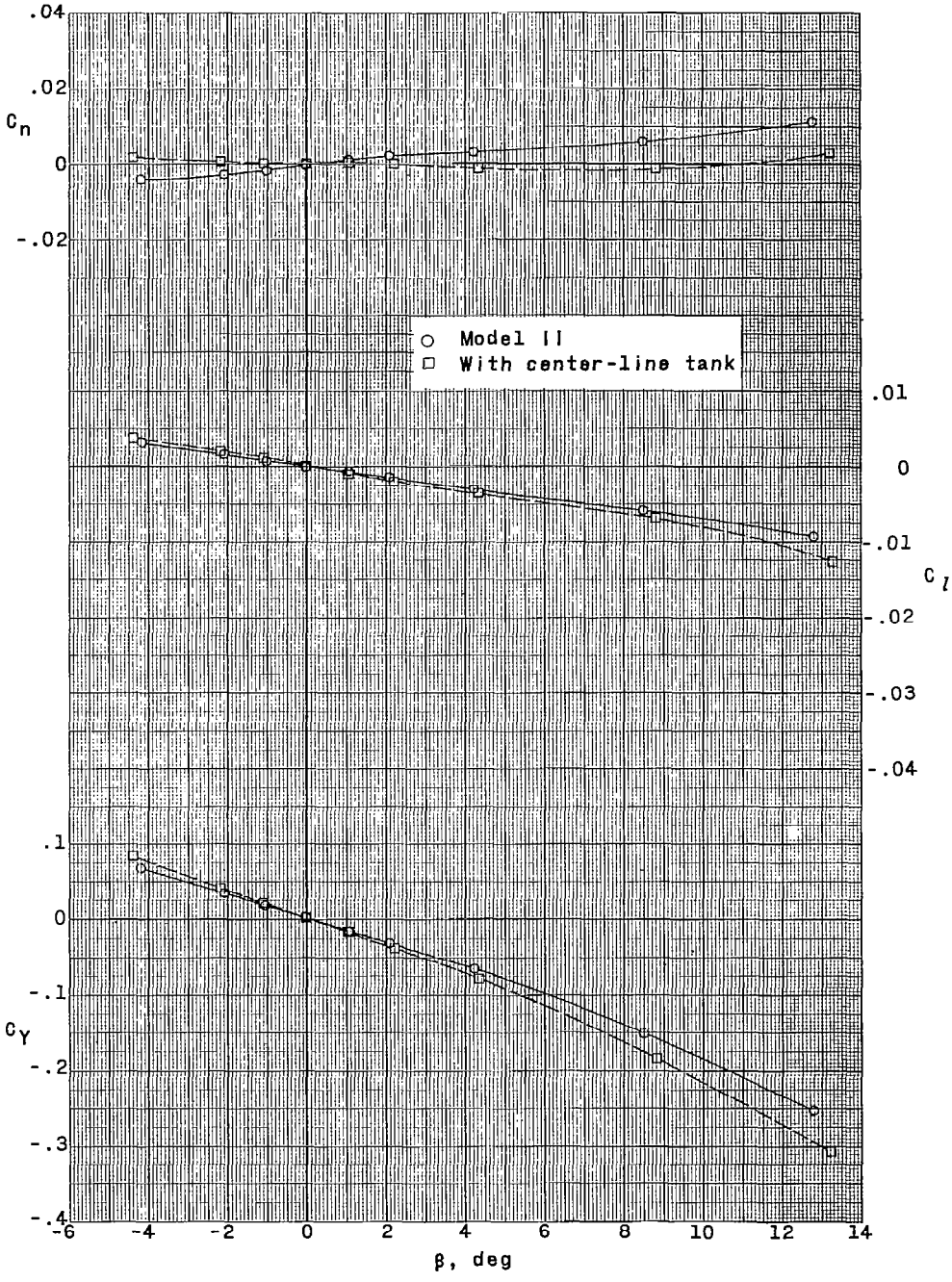

(e) M = 2.01; $\alpha \approx 6.5^{\circ}$.

Figure 20.- Continued.

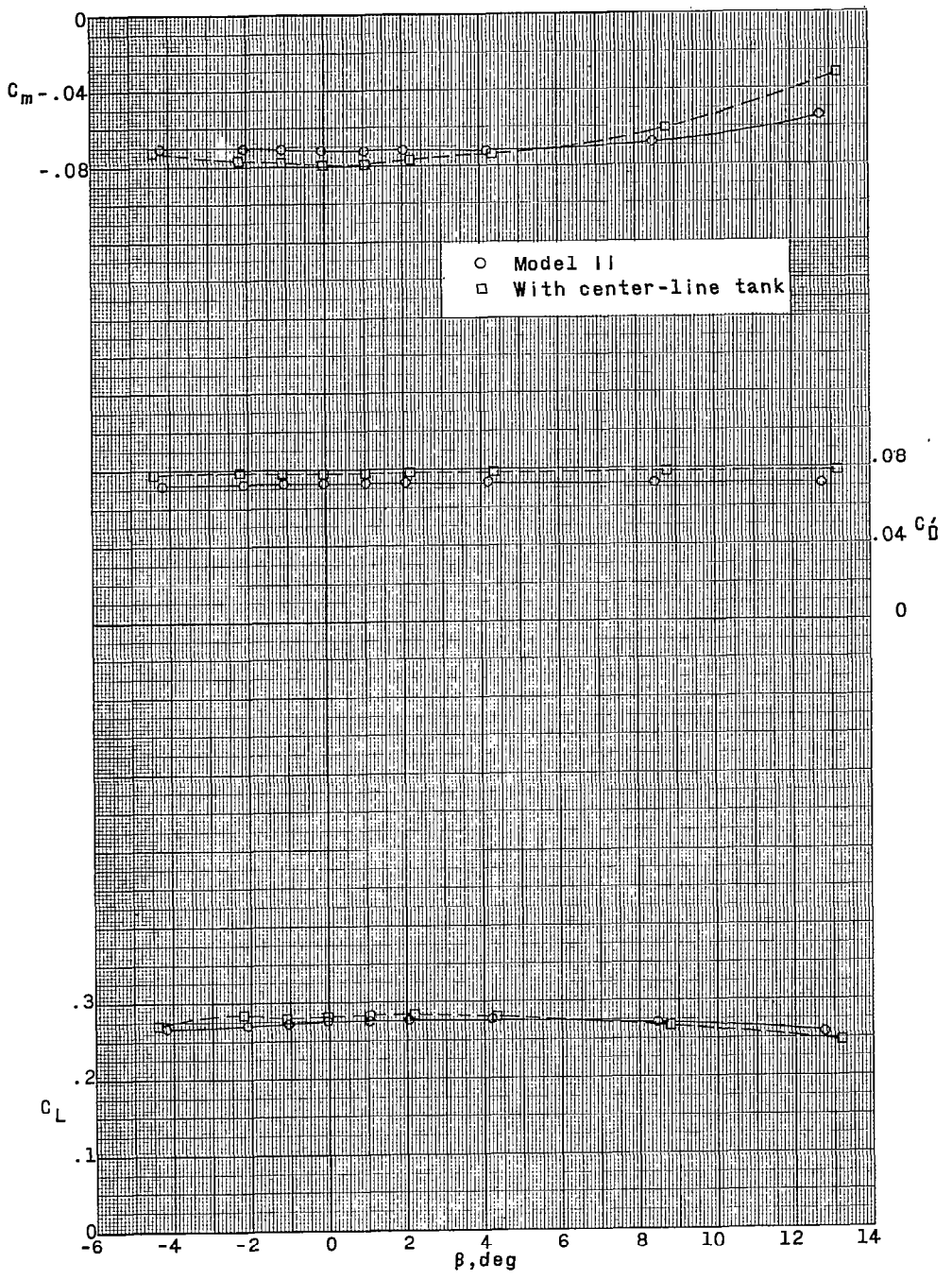

(e) Concluded.

Figure 20.- Continued.

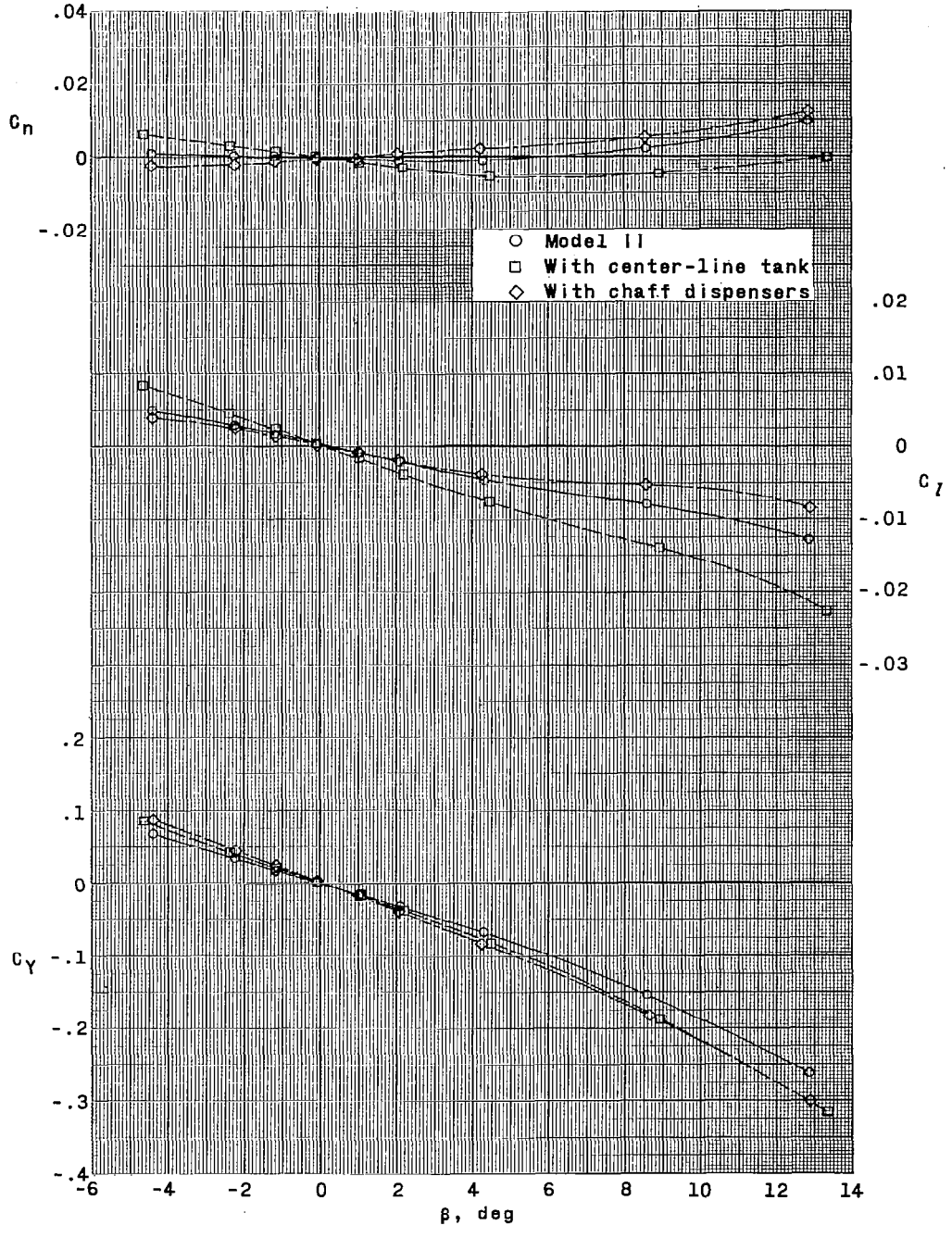

(f) M = 2.01; $\alpha \approx 11.6^{\circ}$.

Figure 20.- Continued.

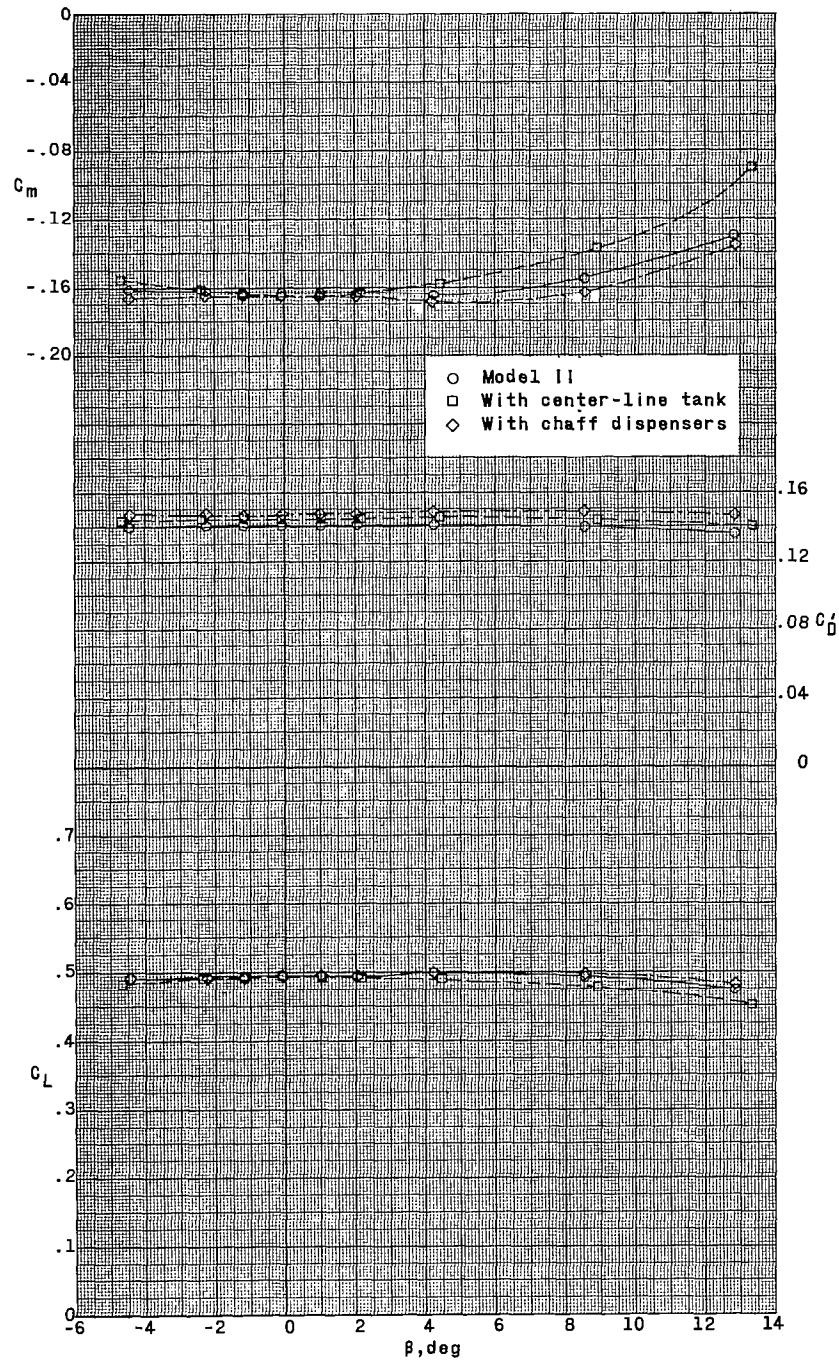

(f) Concluded.

Figure 20.- Continued.

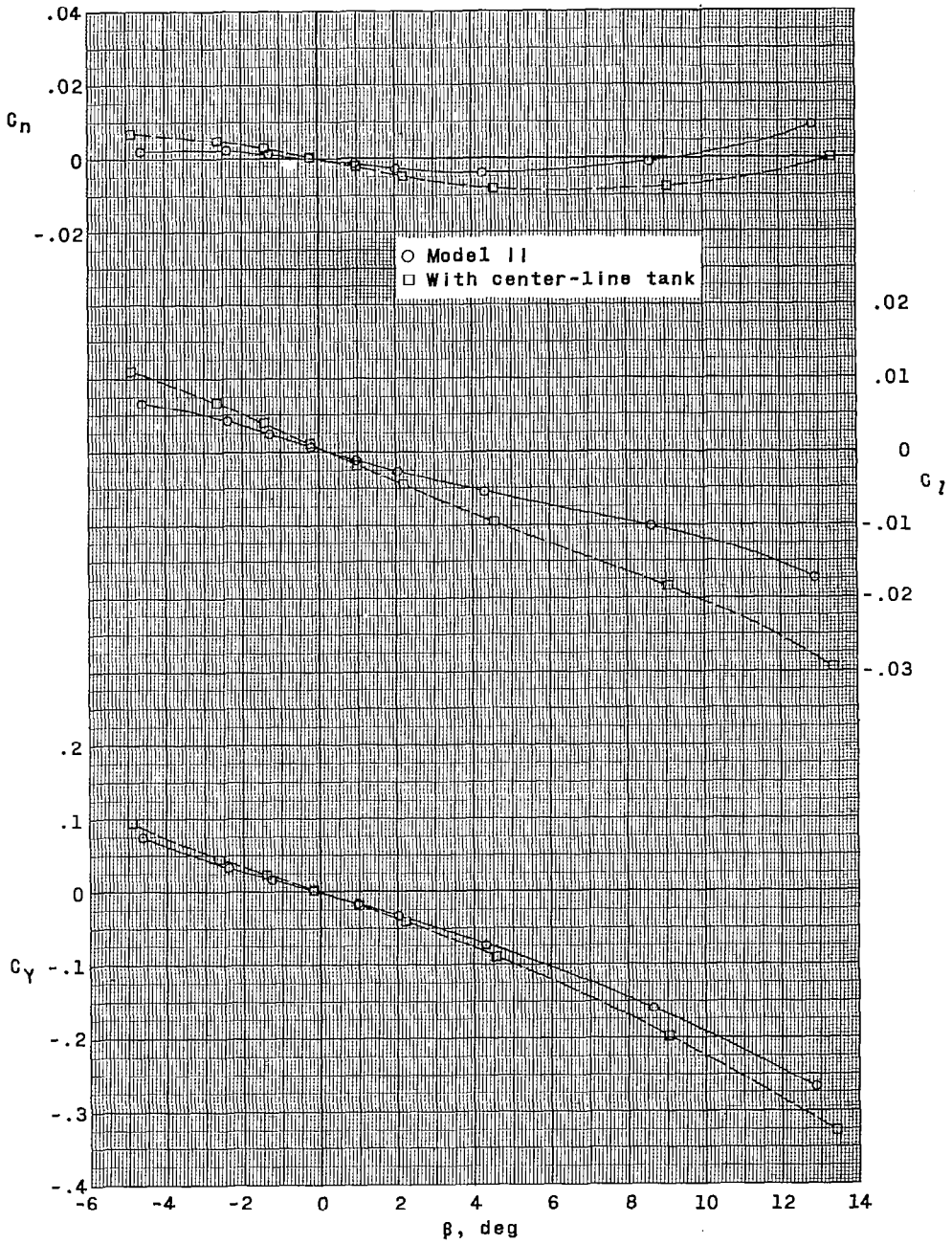

(g) M = 2.01; $\alpha \approx 16.7^{\circ}$.

Figure 20.- Continued.

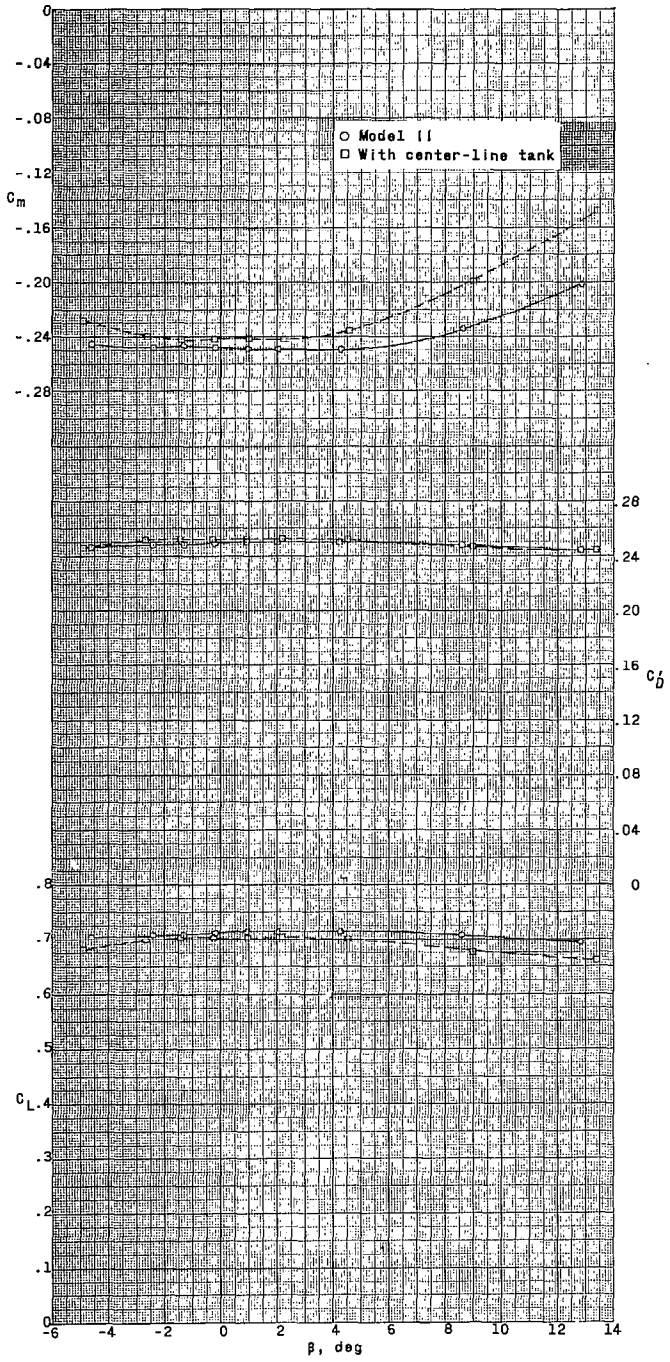

(g) Concluded.

Figure 20.- Concluded.

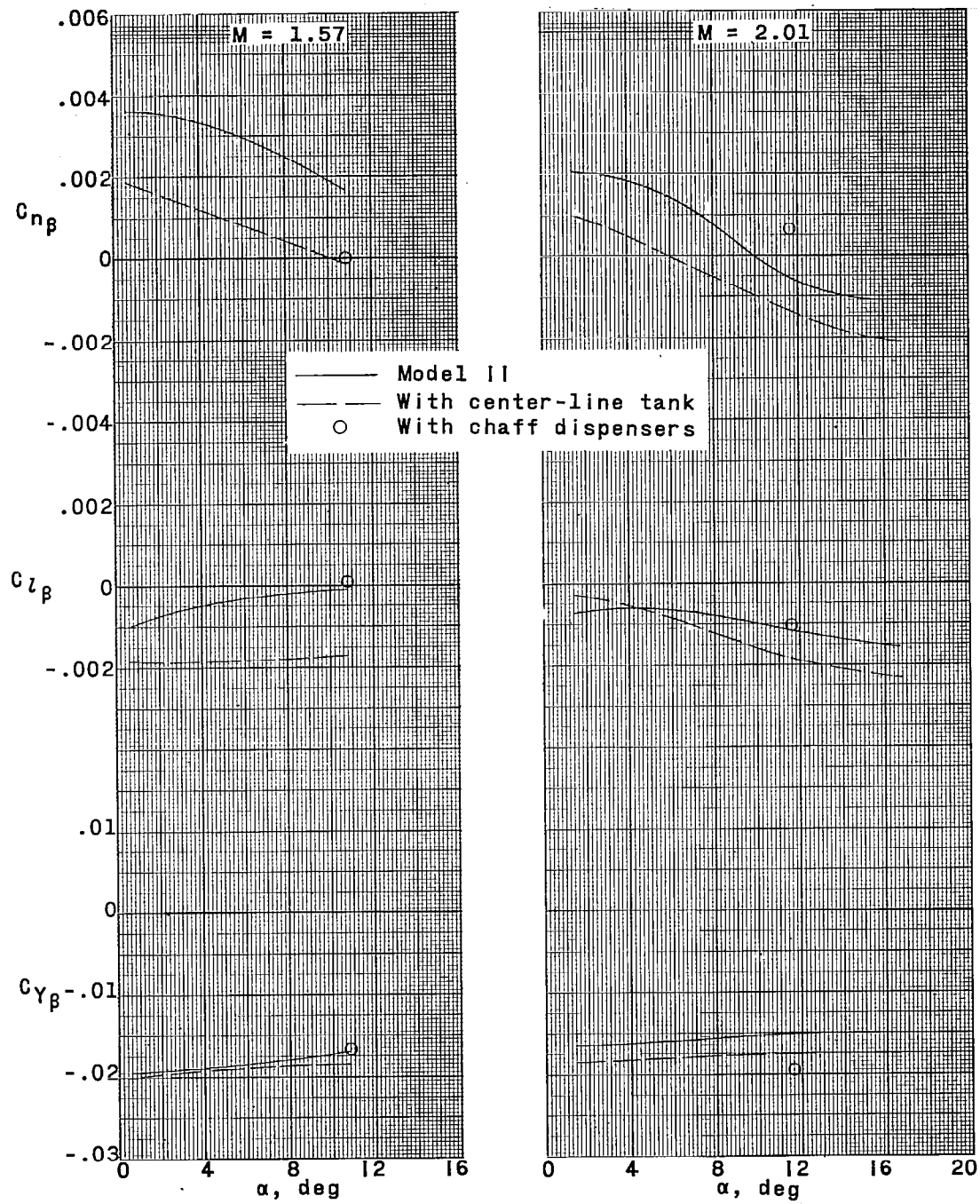

Figure 21.- Summary of directional and lateral stability derivatives for the model with external stores.

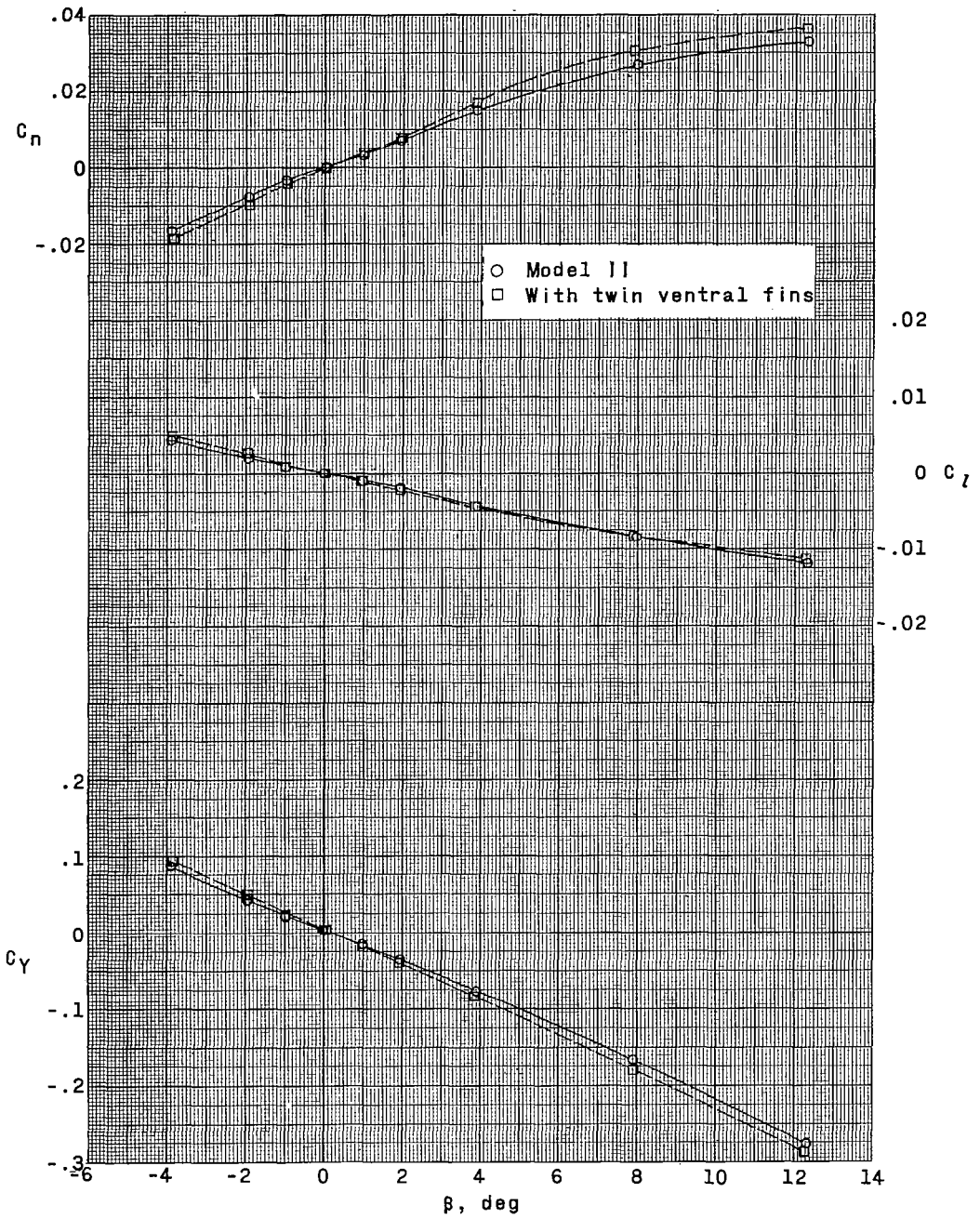

(a) $M = 1.57$; $\alpha \approx 0.6^{\circ}$.

Figure 22.- Effect of twin ventral fins on aerodynamic characteristics in sideslip for model II.

L-107

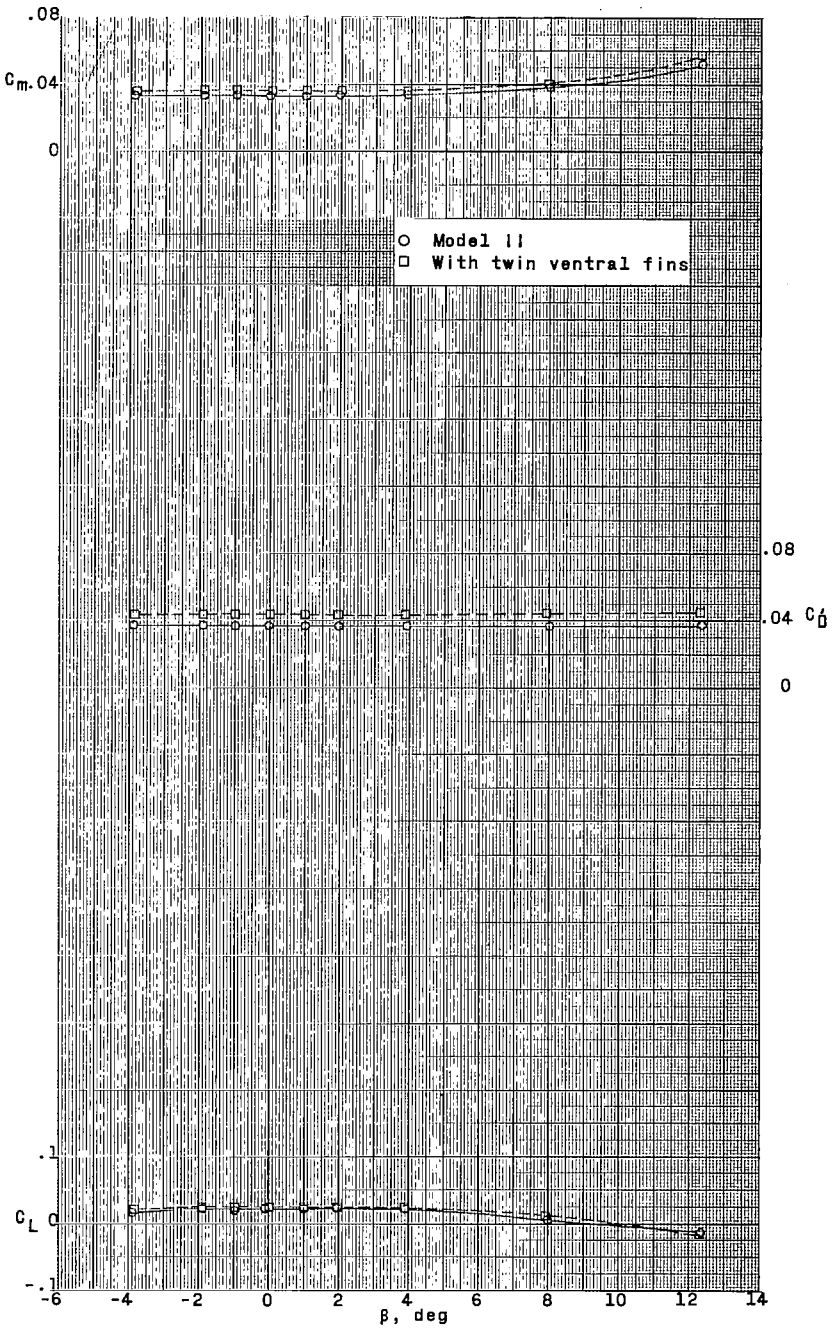

(a) Concluded.

Figure 22.- Continued.

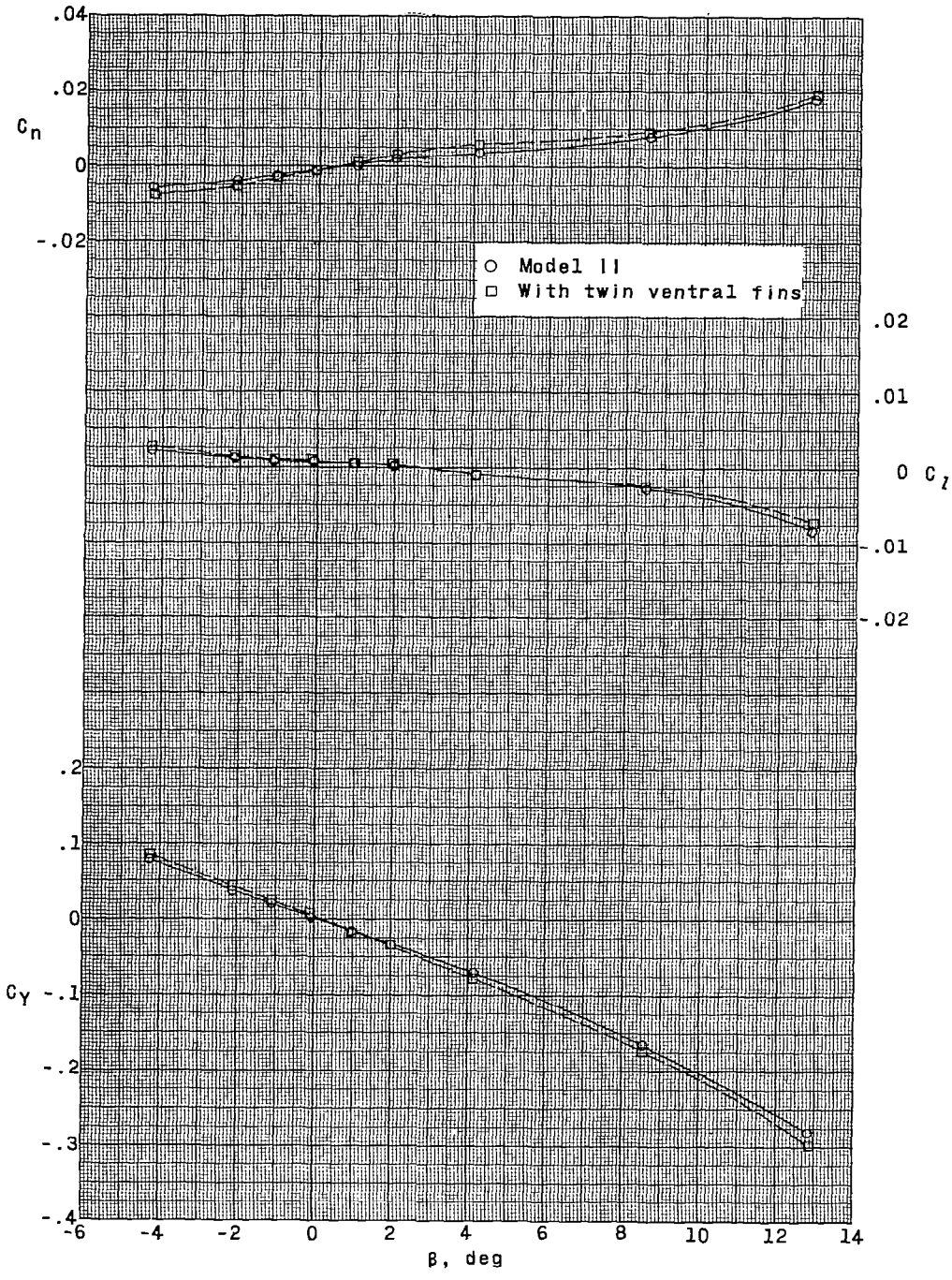

(b) $M = 1.57$; $\alpha \approx 10.8^{\circ}$.

Figure 22.- Continued.

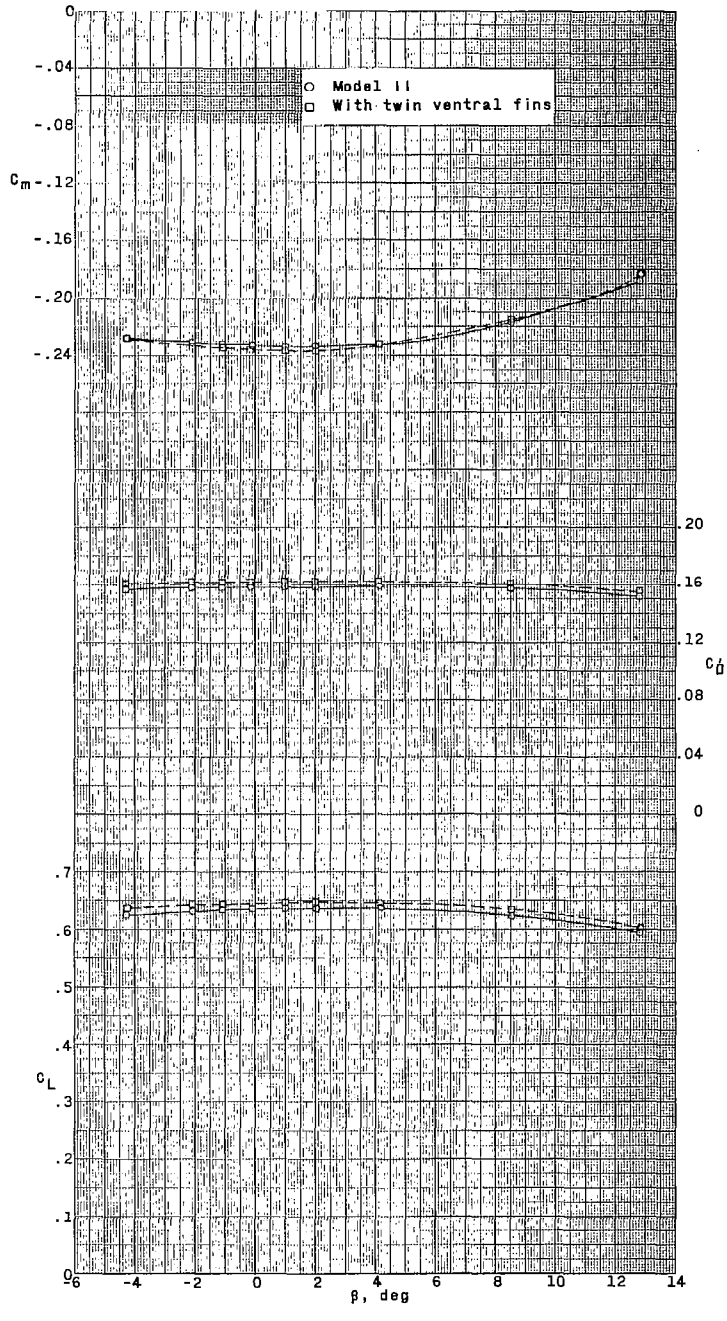

(b) Concluded.

Figure 22.- Continued.

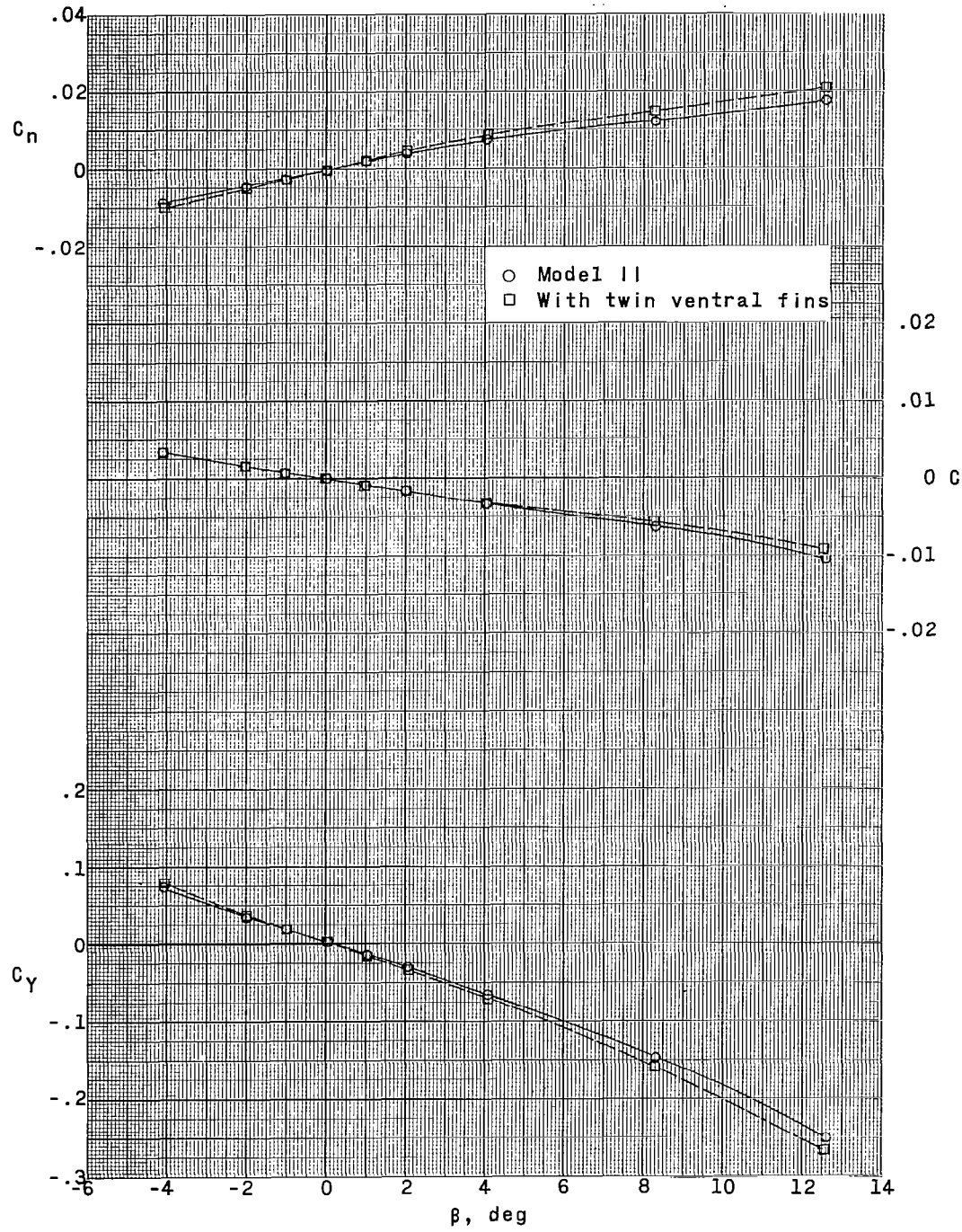

(c) M = 2.01; $\alpha \approx 1.4^{o}$.

Figure 22.- Continued.

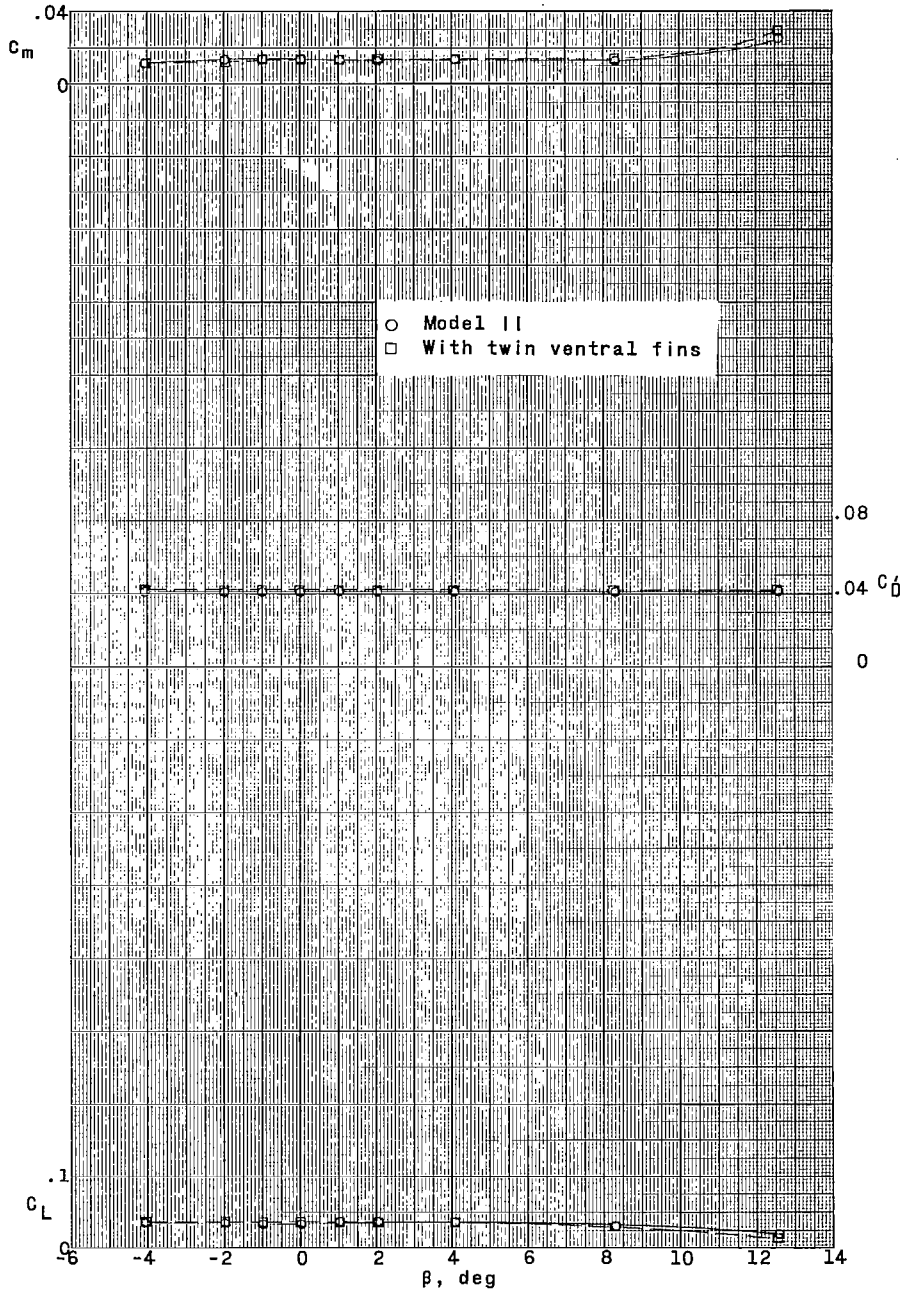

(c) Concluded.

Figure 22.- Continued.

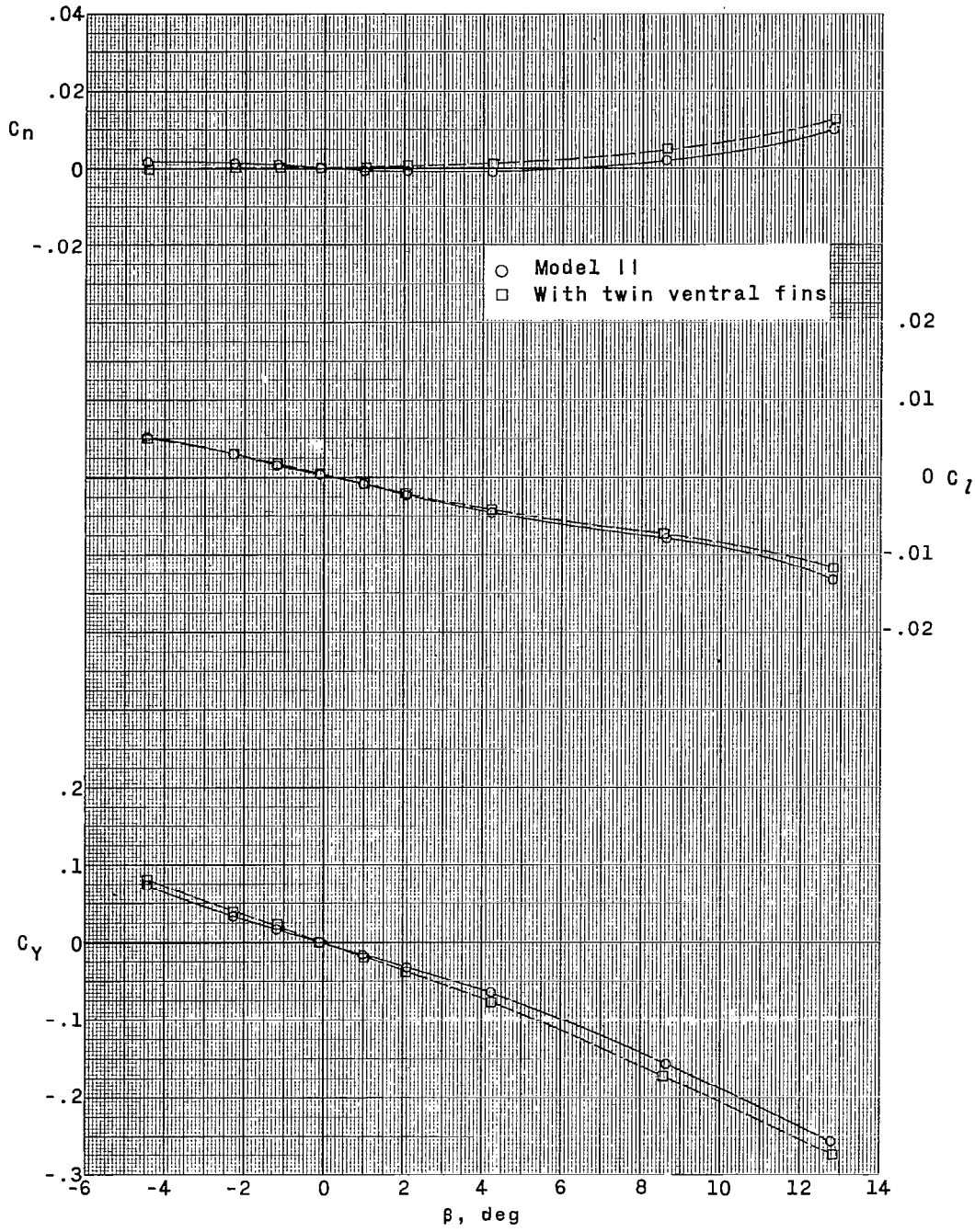

(d) M = 2.01; $\alpha \approx 11.6^{\circ}$.

Figure 22.- Continued.

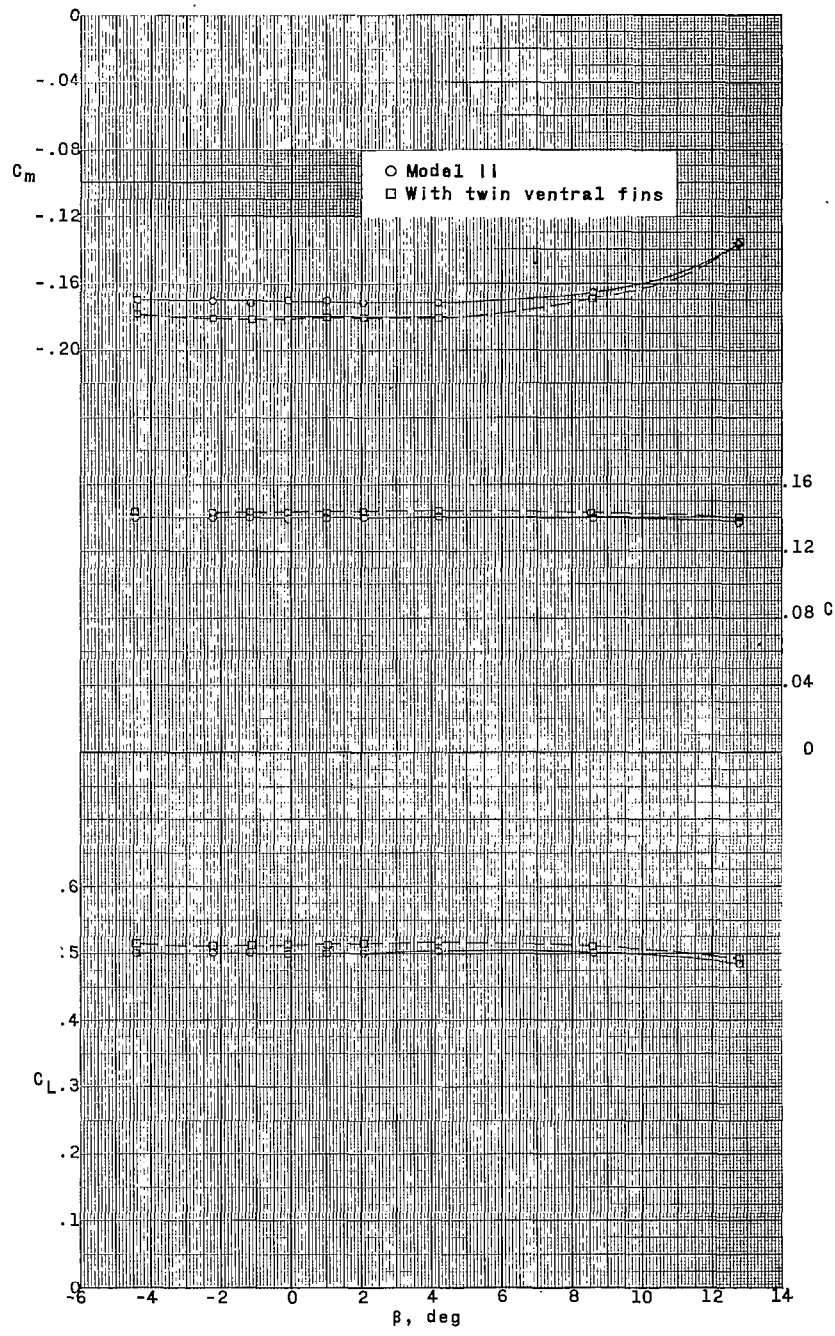

(d) Concluded.

Figure 22.- Continued.

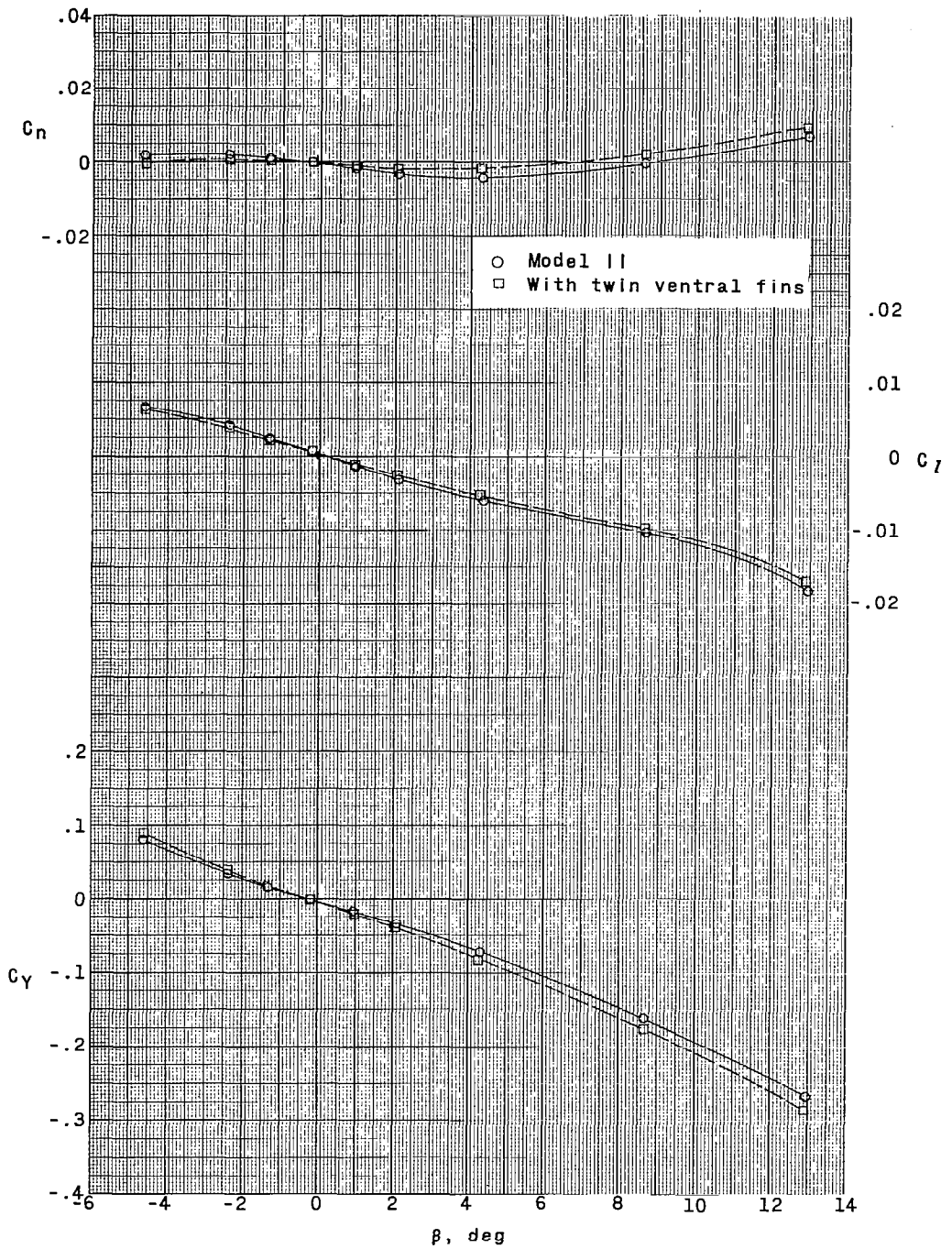

(e) M = 2.01; $\alpha \approx 16.7^{\circ}$.

Figure 22.- Continued.

i3H

L-107

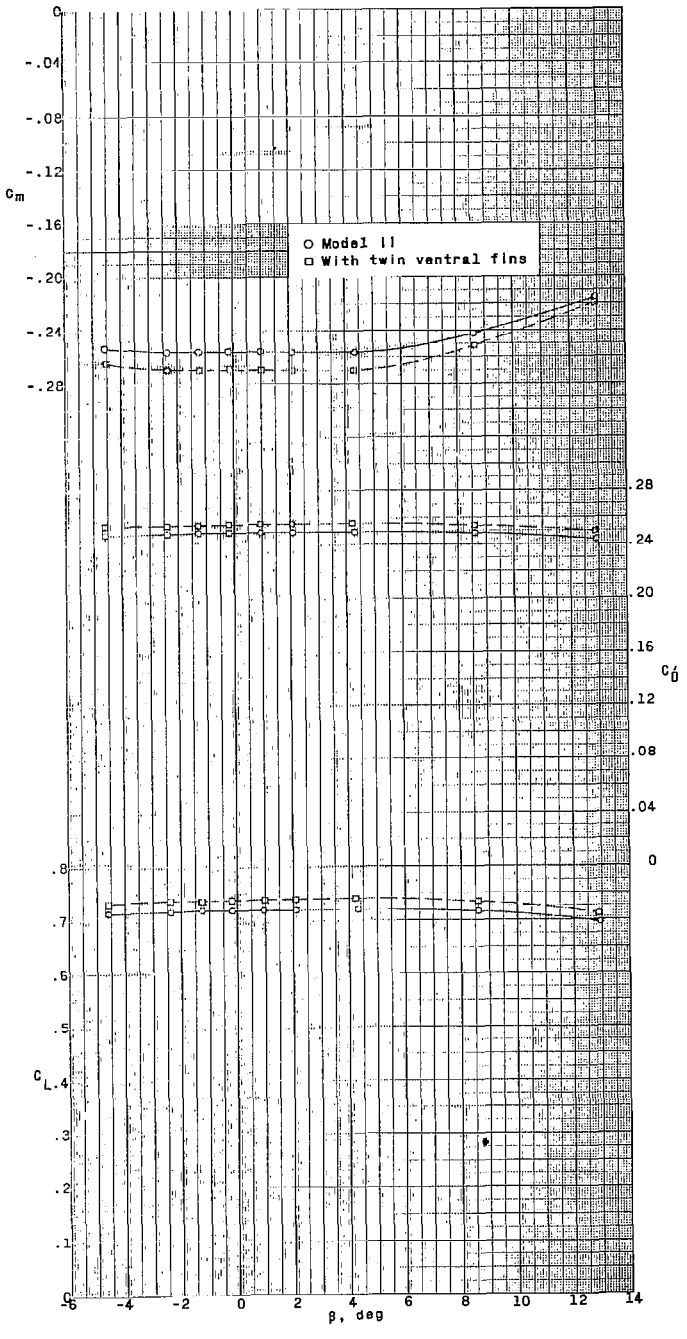

(e) Concluded.

Figure 22.- Concluded.

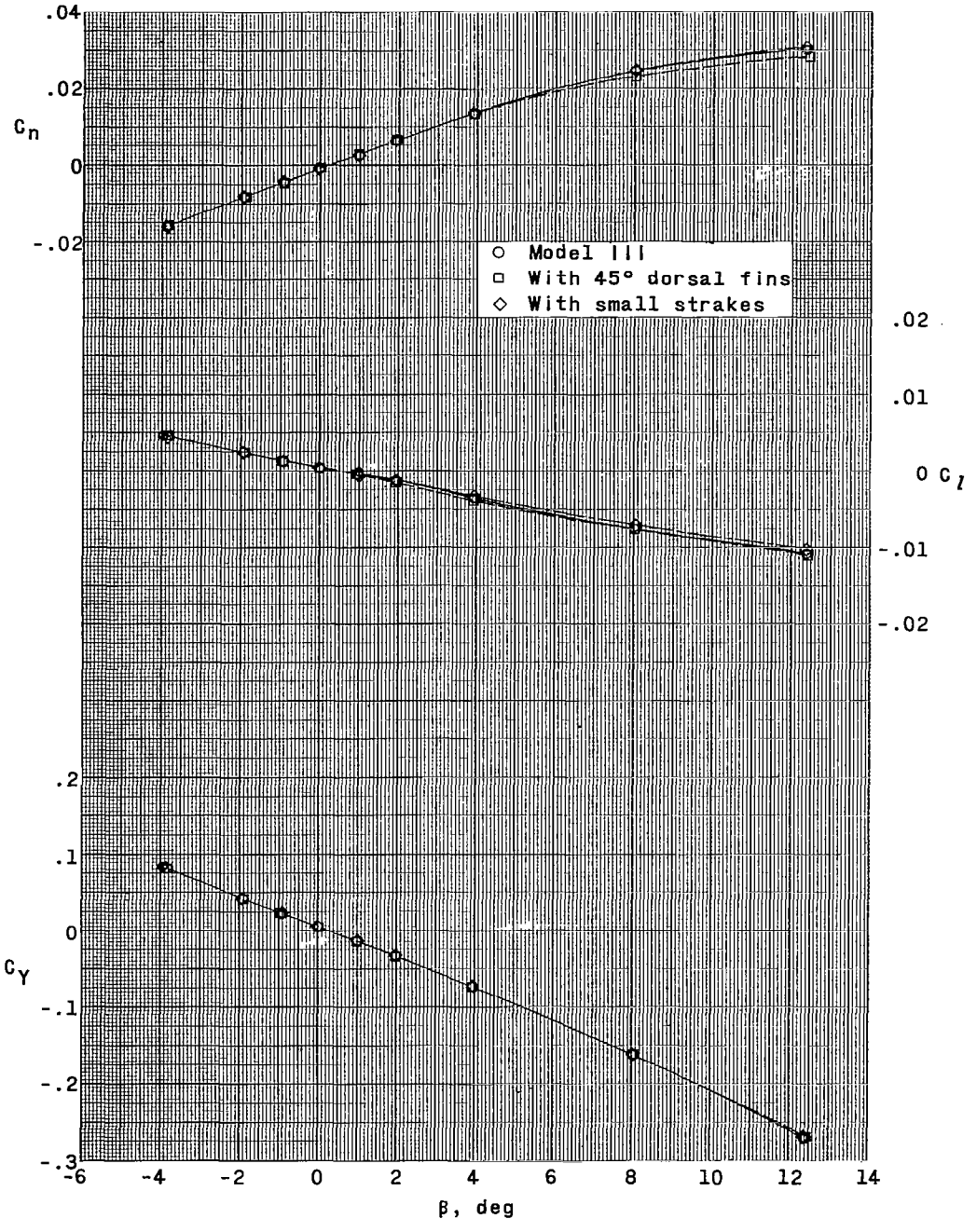

(a) M = 1.57; $\alpha \approx 0.6^{\circ}$.

Figure 23.- Effect of lateral stability control devices on aerodynamic characteristics in sideslip for model III.

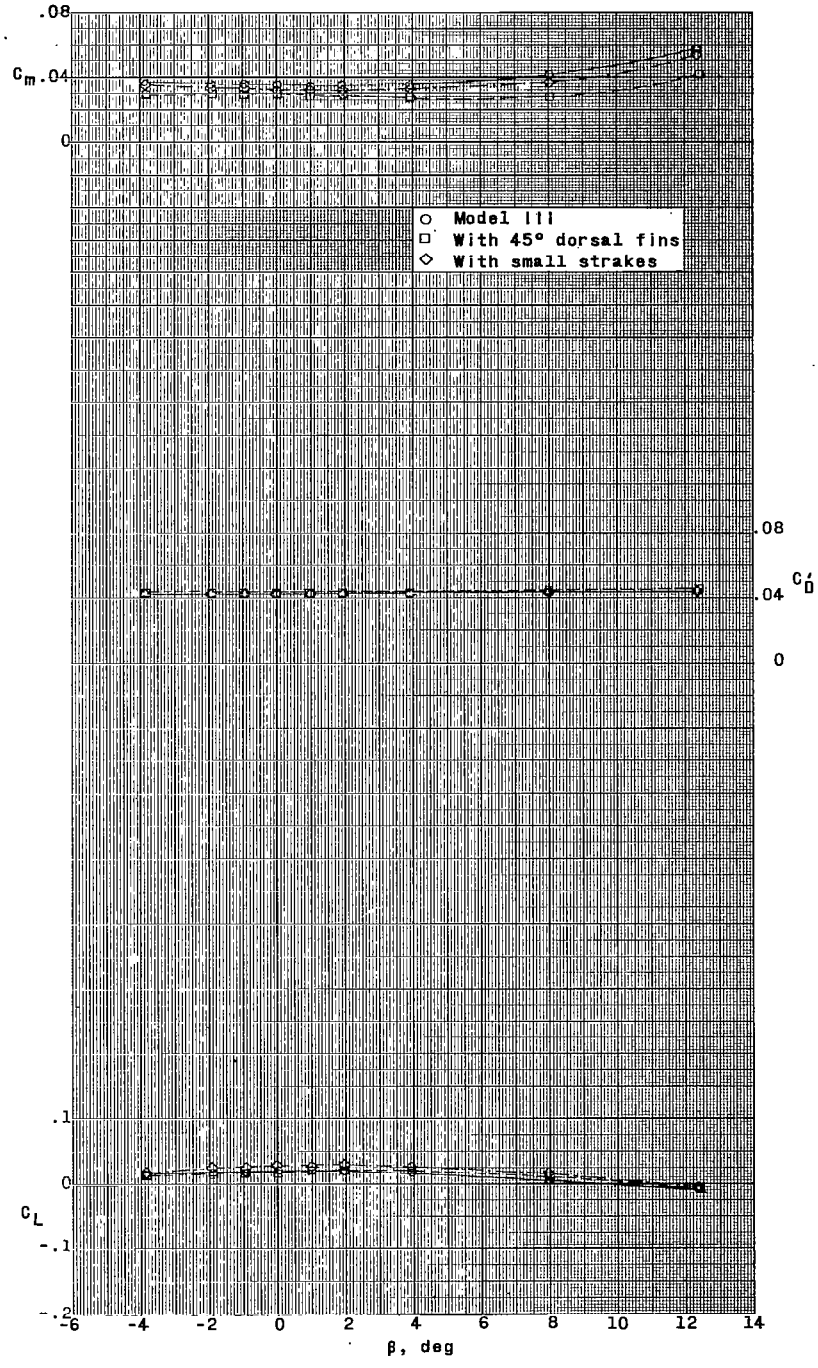

(a) Concluded.

Figure 23.- Continued.

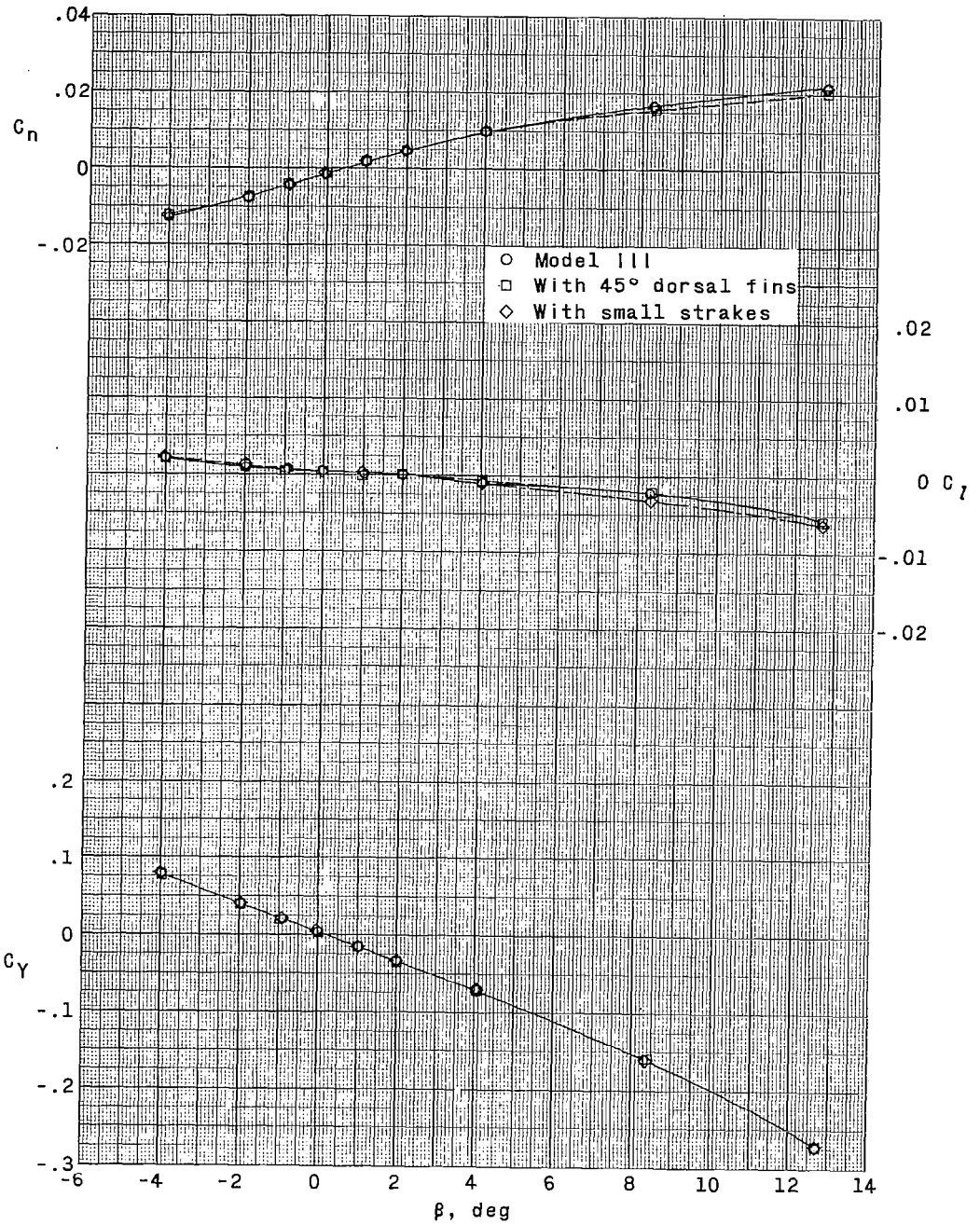

(b) $M = 1.57$; $\alpha \approx 5.8^{\circ}$.

Figure 23.- Continued.

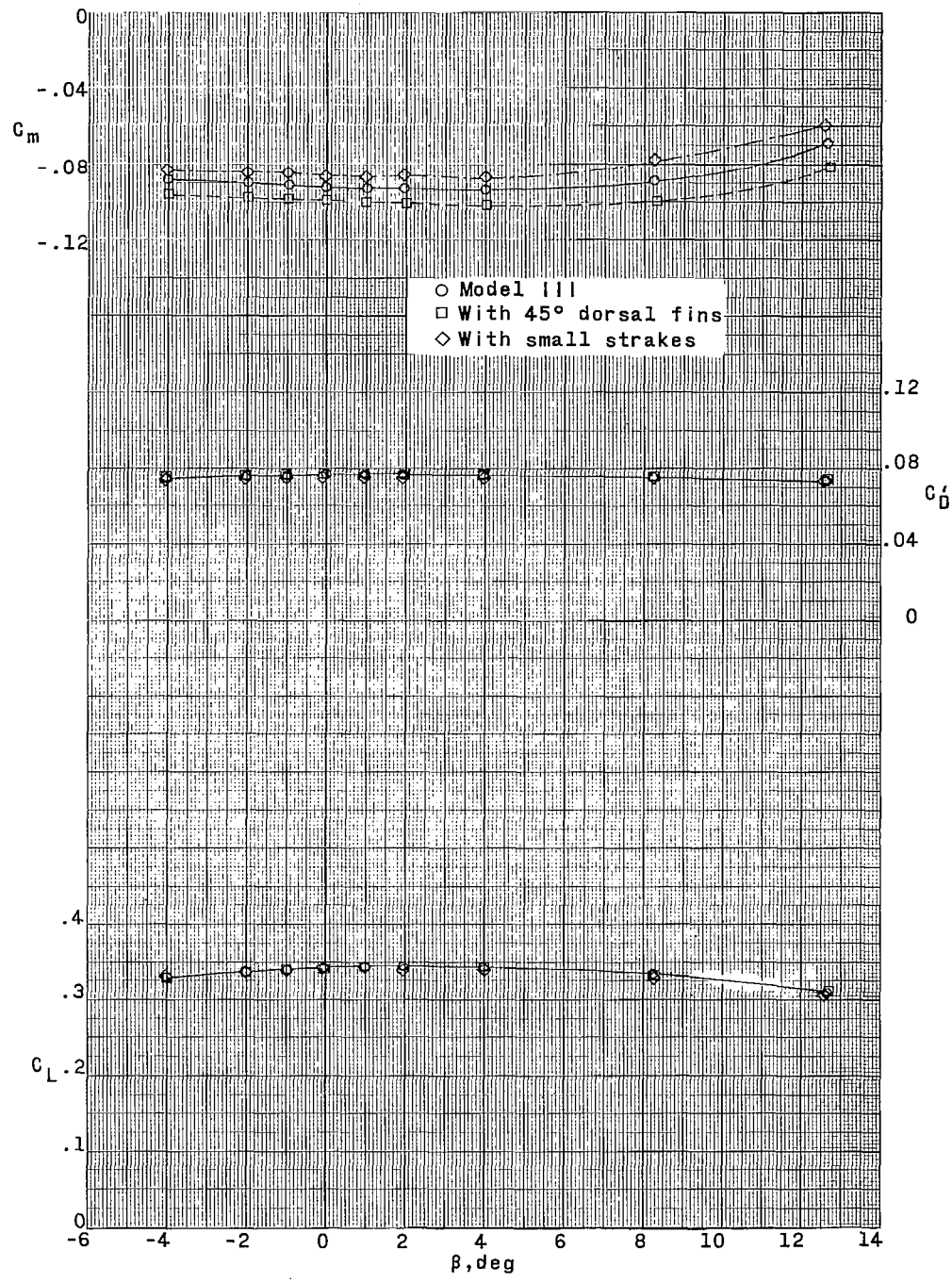

(b) Concluded.

Figure 23.- Continued.

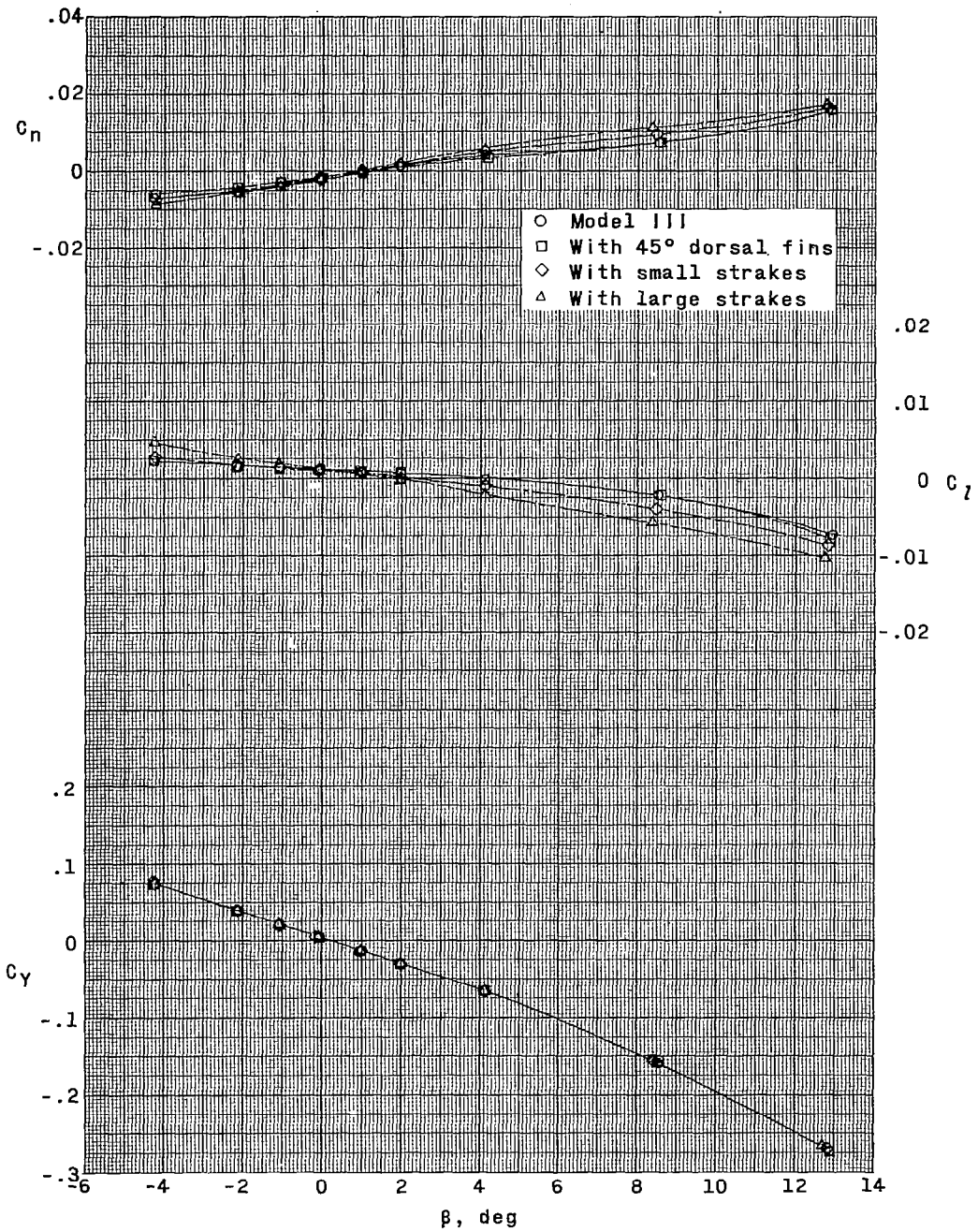

(c) M = 1.57; $\alpha \approx 10.8^{\circ}$.

Figure 23.- Continued.

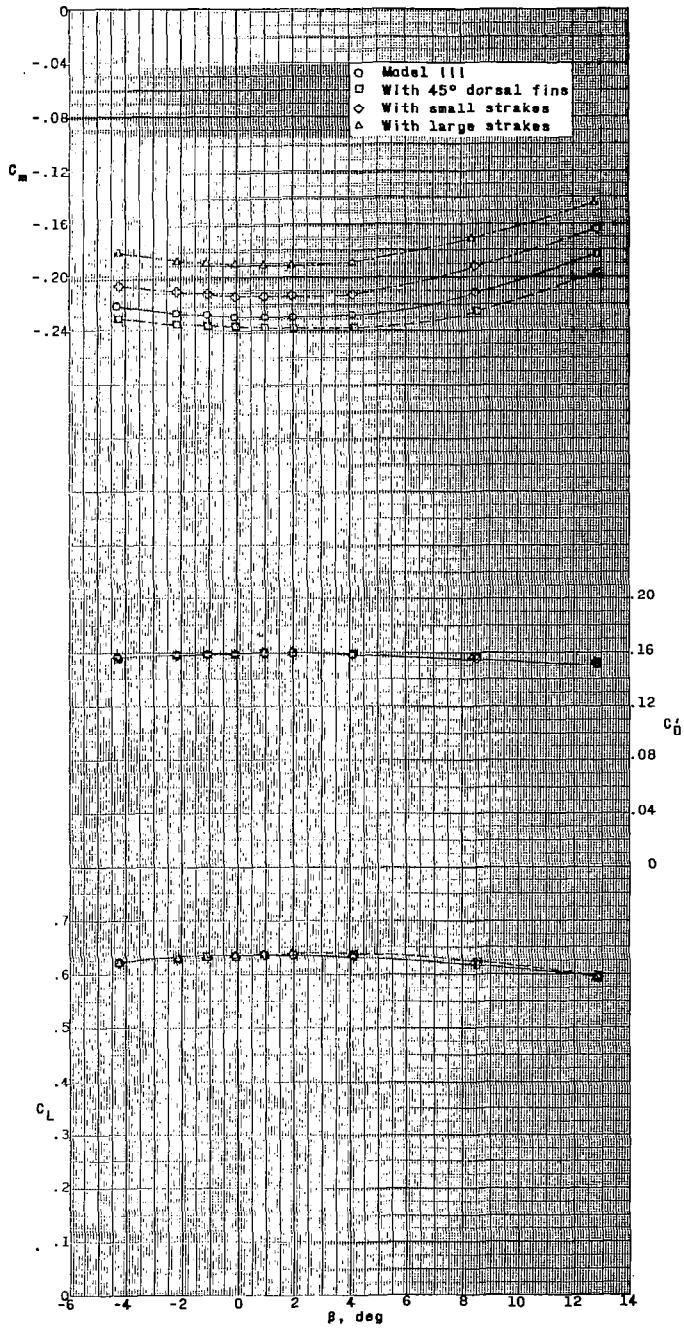

(c) Concluded.

Figure 23.- Continued.

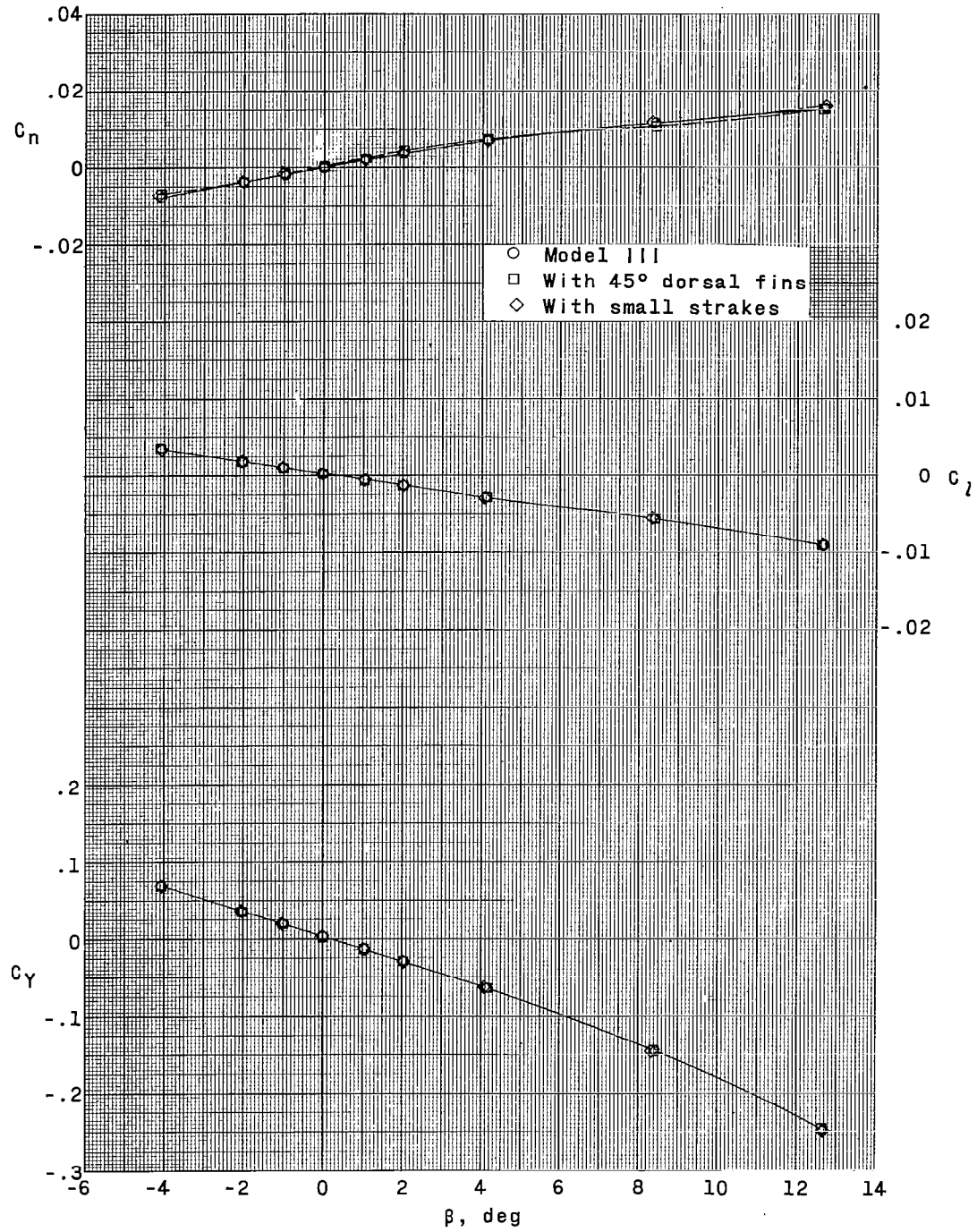

(d) M = 2.01; $\alpha \approx 1.4^{\circ}$.

Figure 23.- Continued.

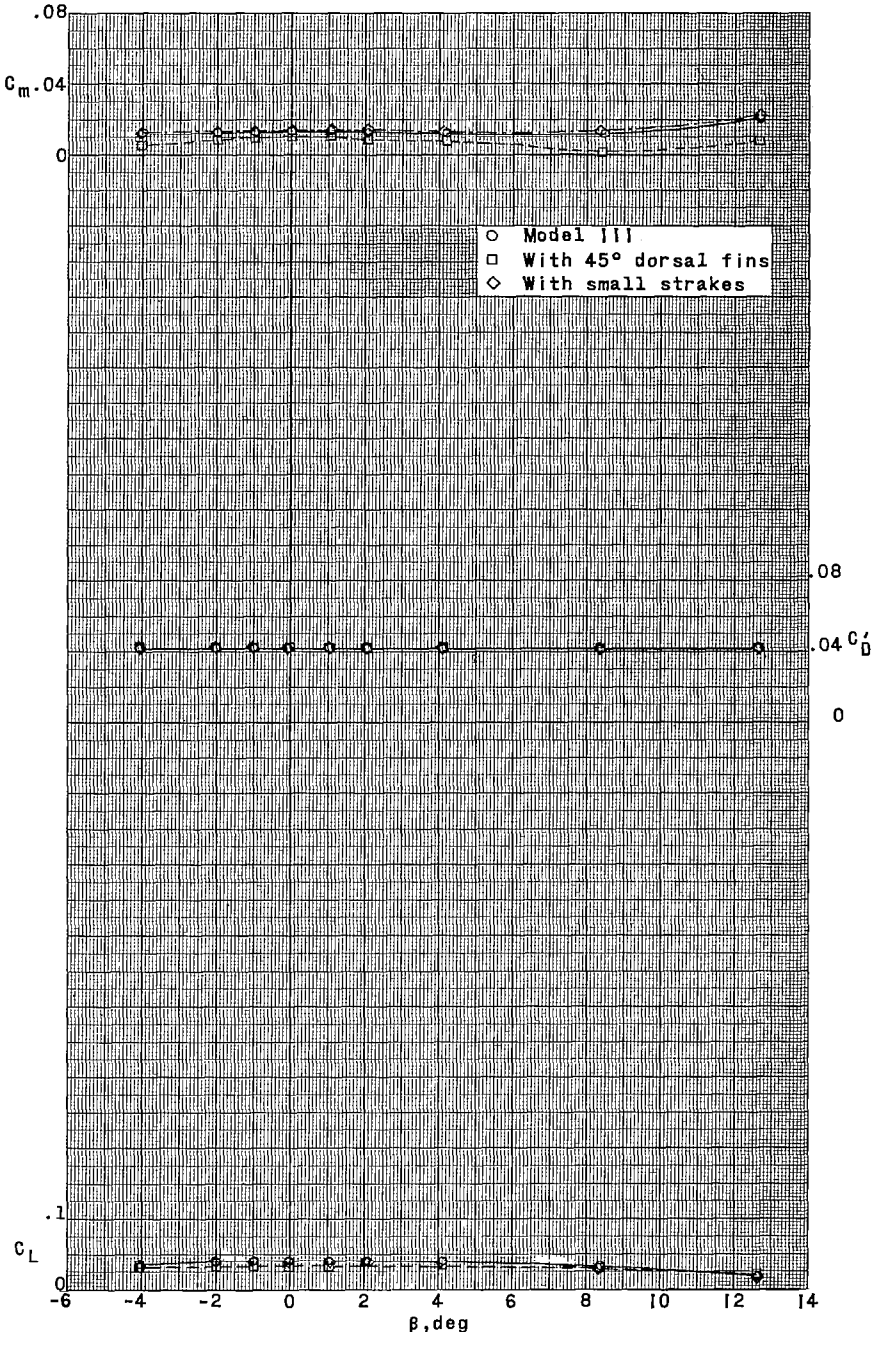

(d) Concluded.

Figure 23.- Continued.

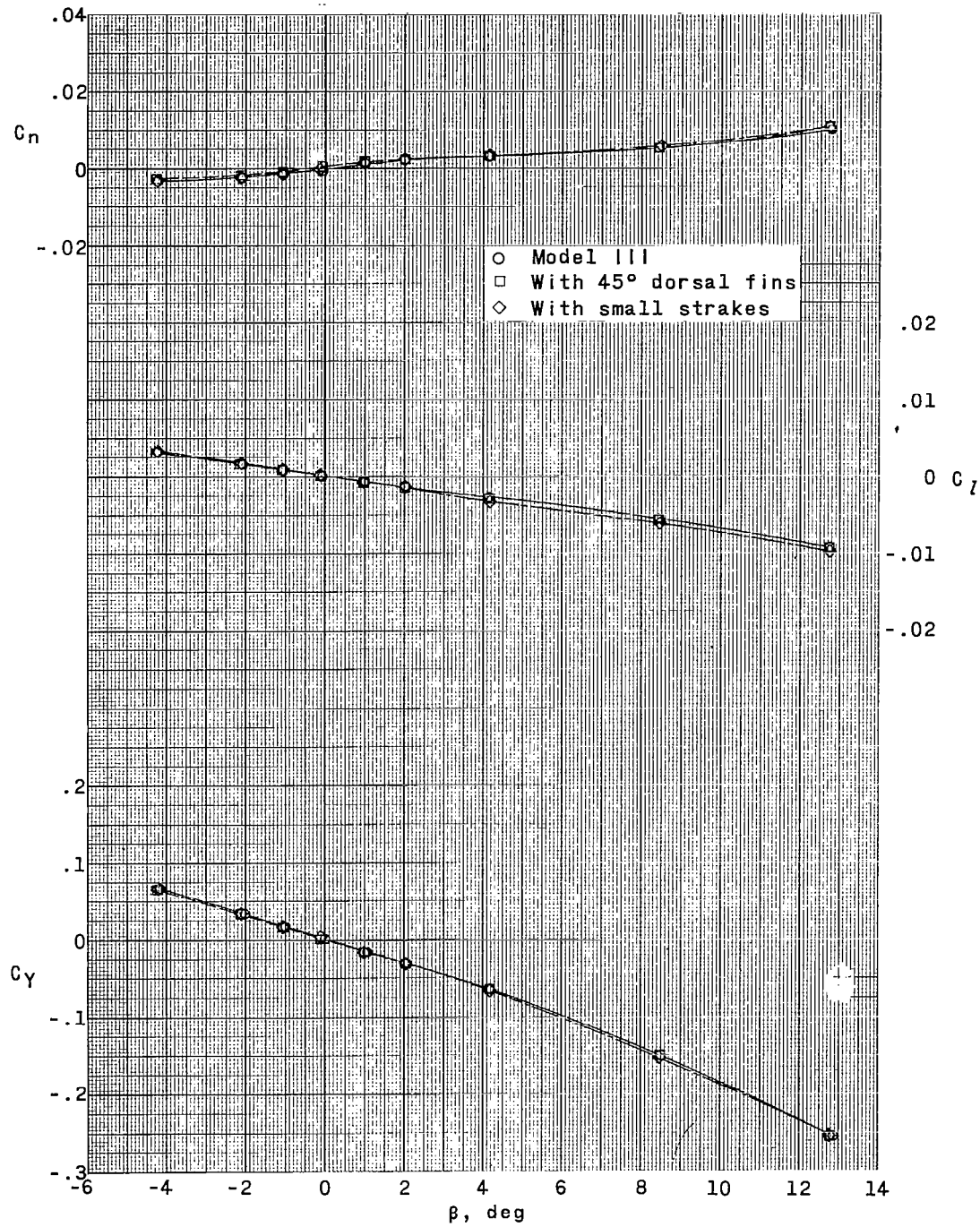

(e) M = 2.01; $\alpha \approx 6.5^{\circ}$.

Figure 23.- Continued.

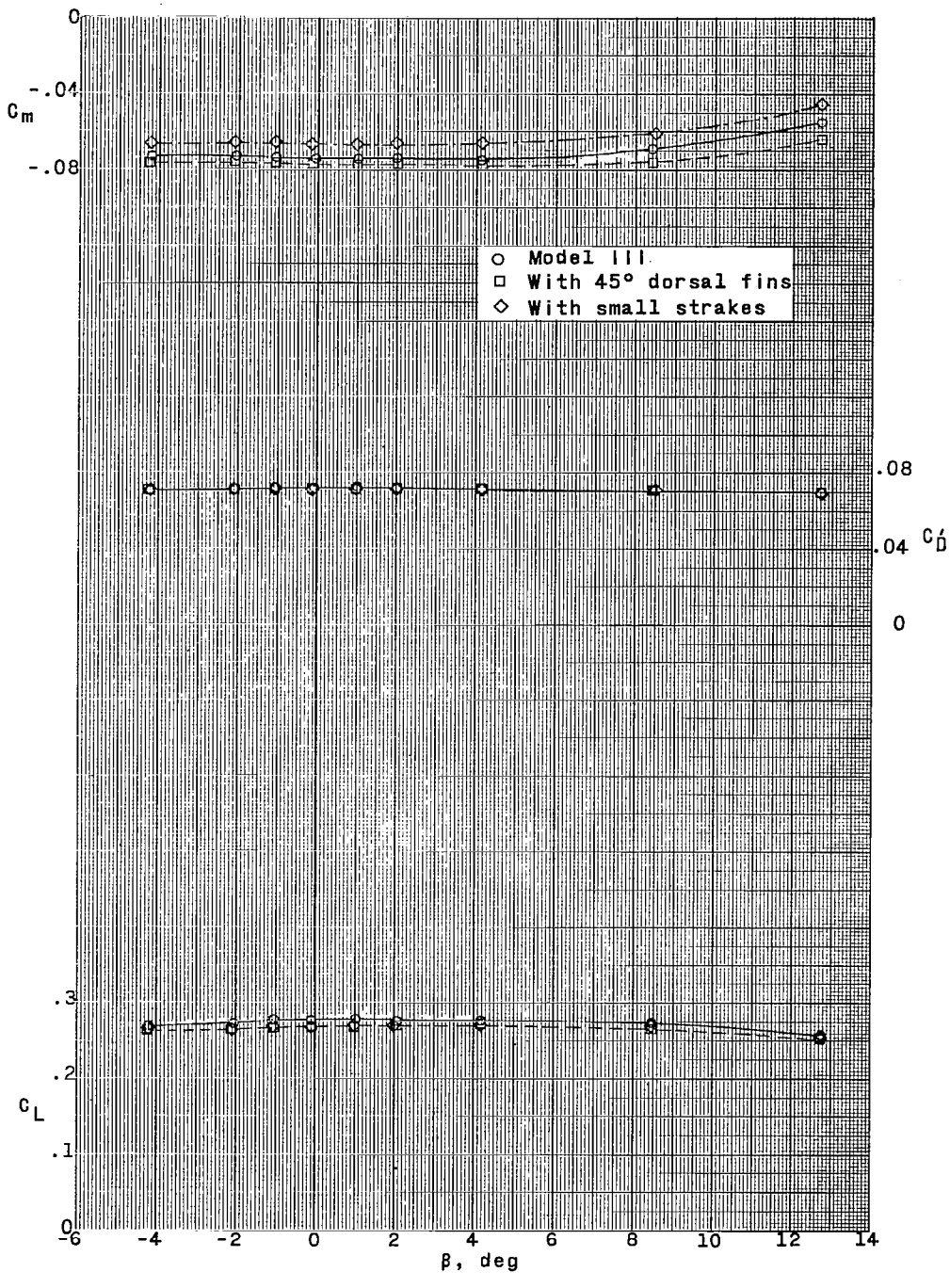

(e) Concluded.

Figure 23.- Continued.

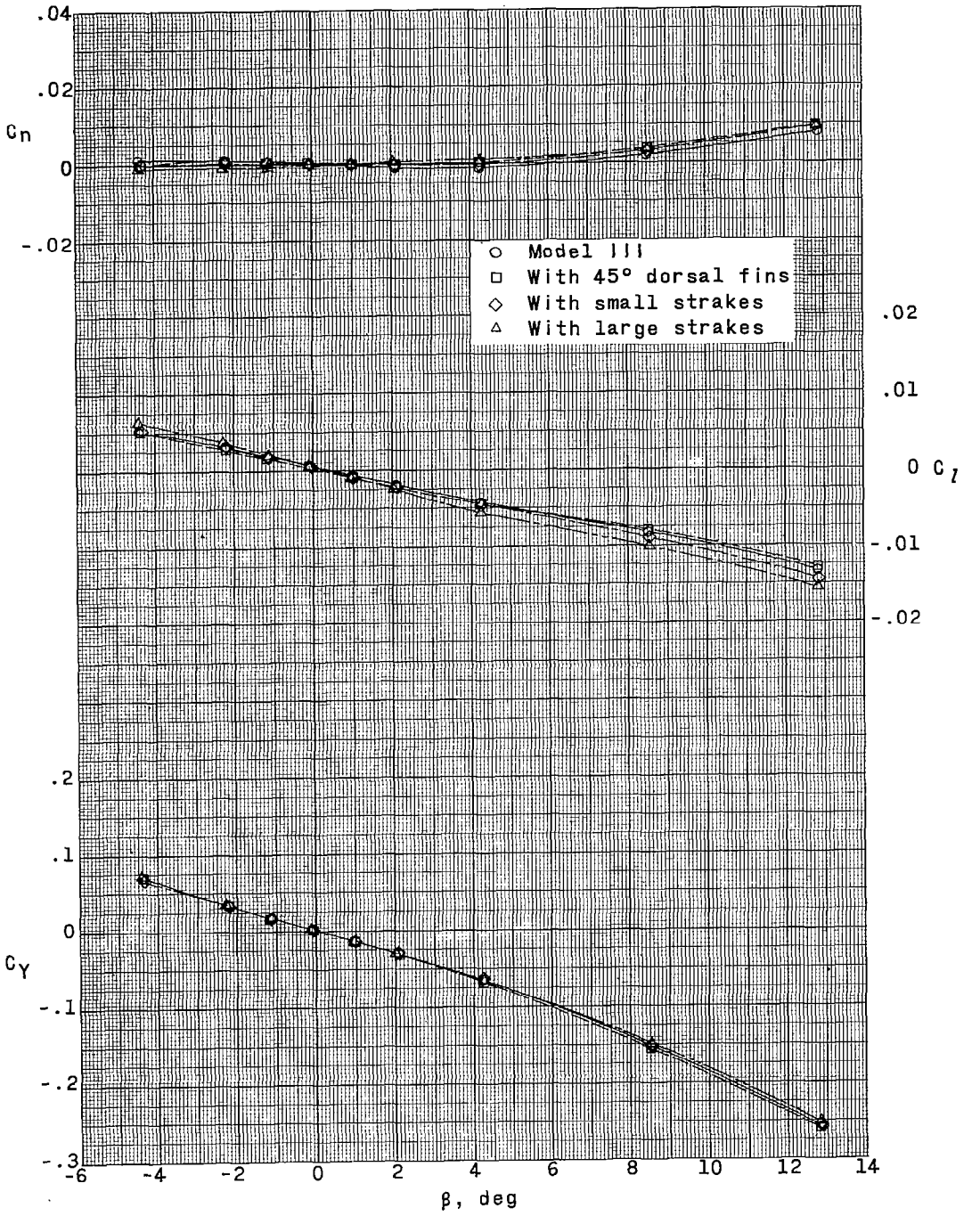

(f) M = 2.01; $\alpha \approx 11.6^{\circ}$.

Figure 23.- Continued.

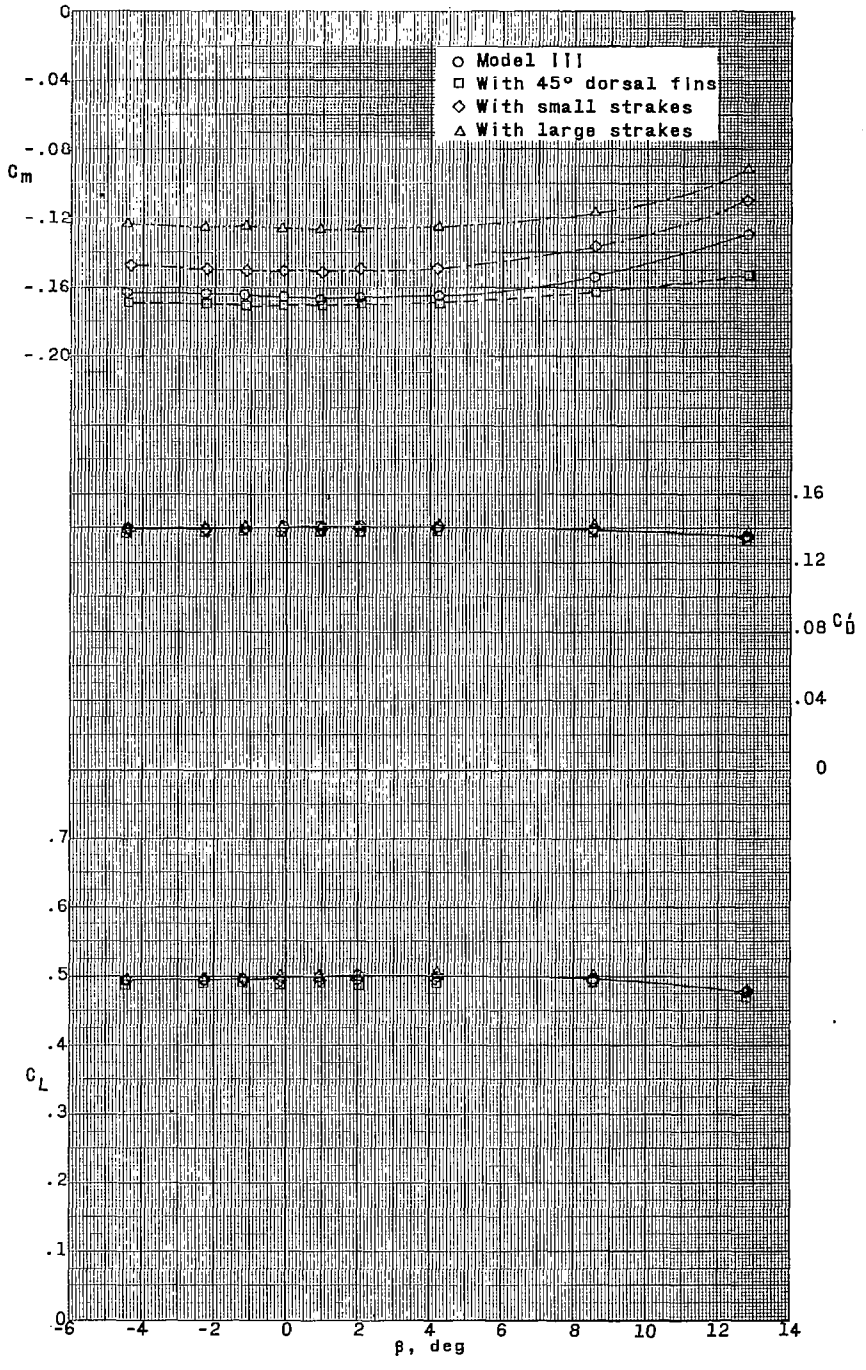

(f) Concluded.

Figure 23.- Continued.

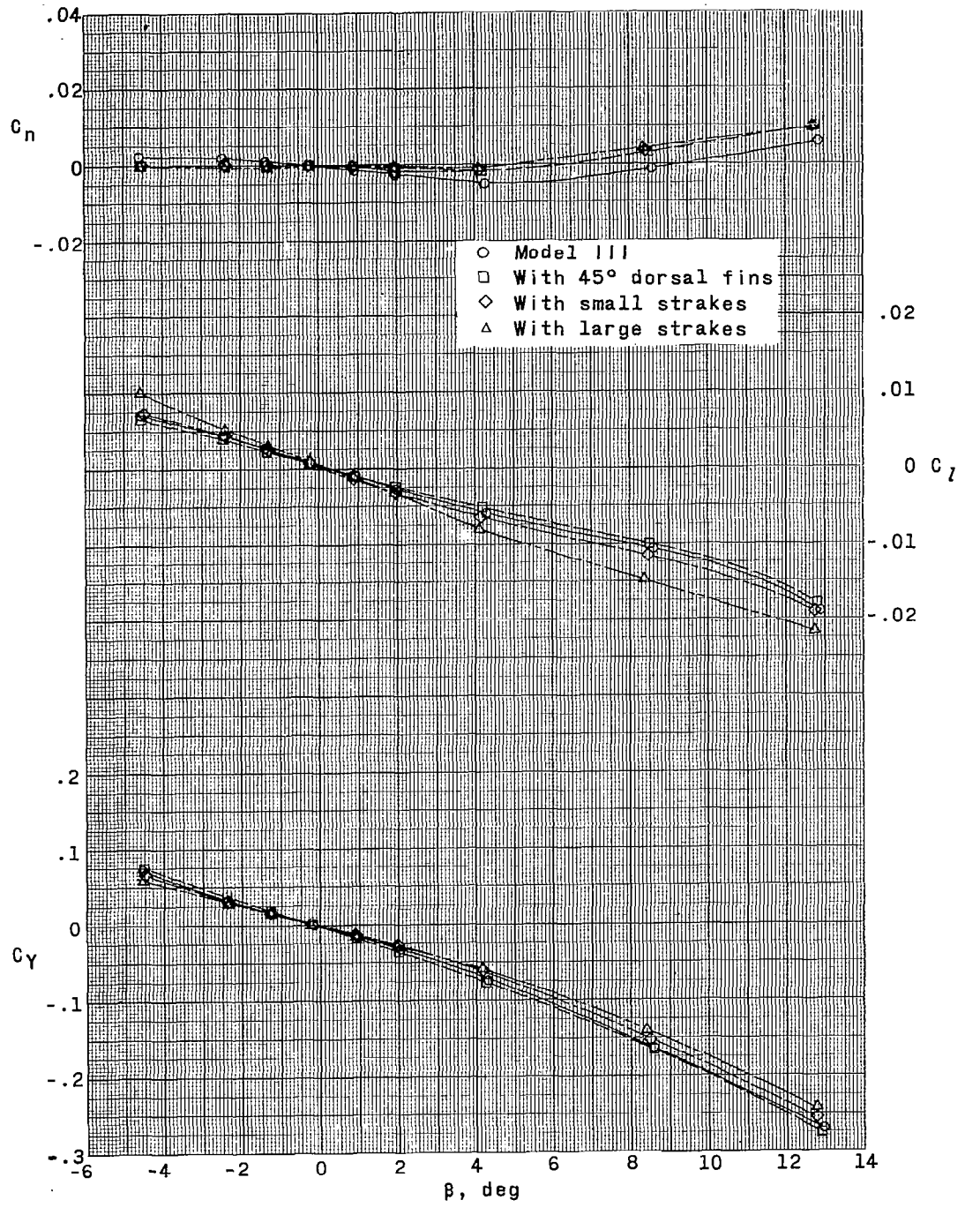

(g) M = 2.01; $\alpha \approx 16.7^{\circ}$.

Figure 23.- Continued.

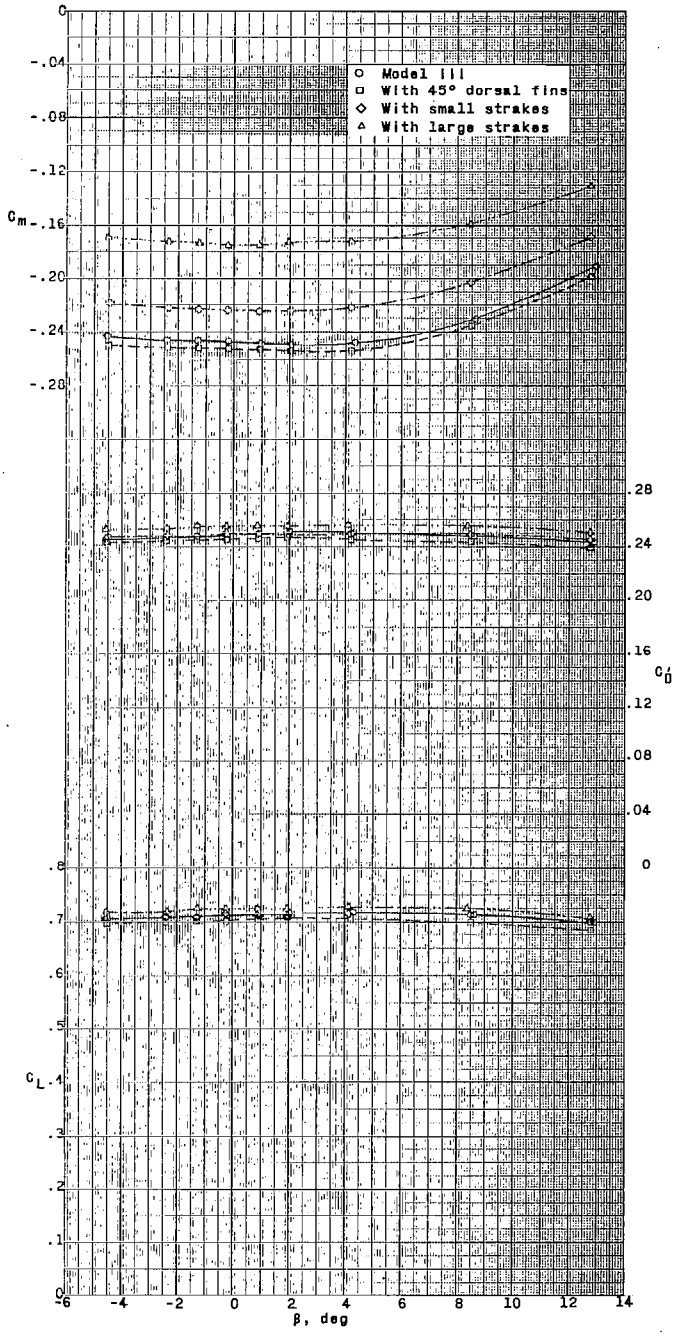

(g) Concluded.

Figure 23.- Concluded.

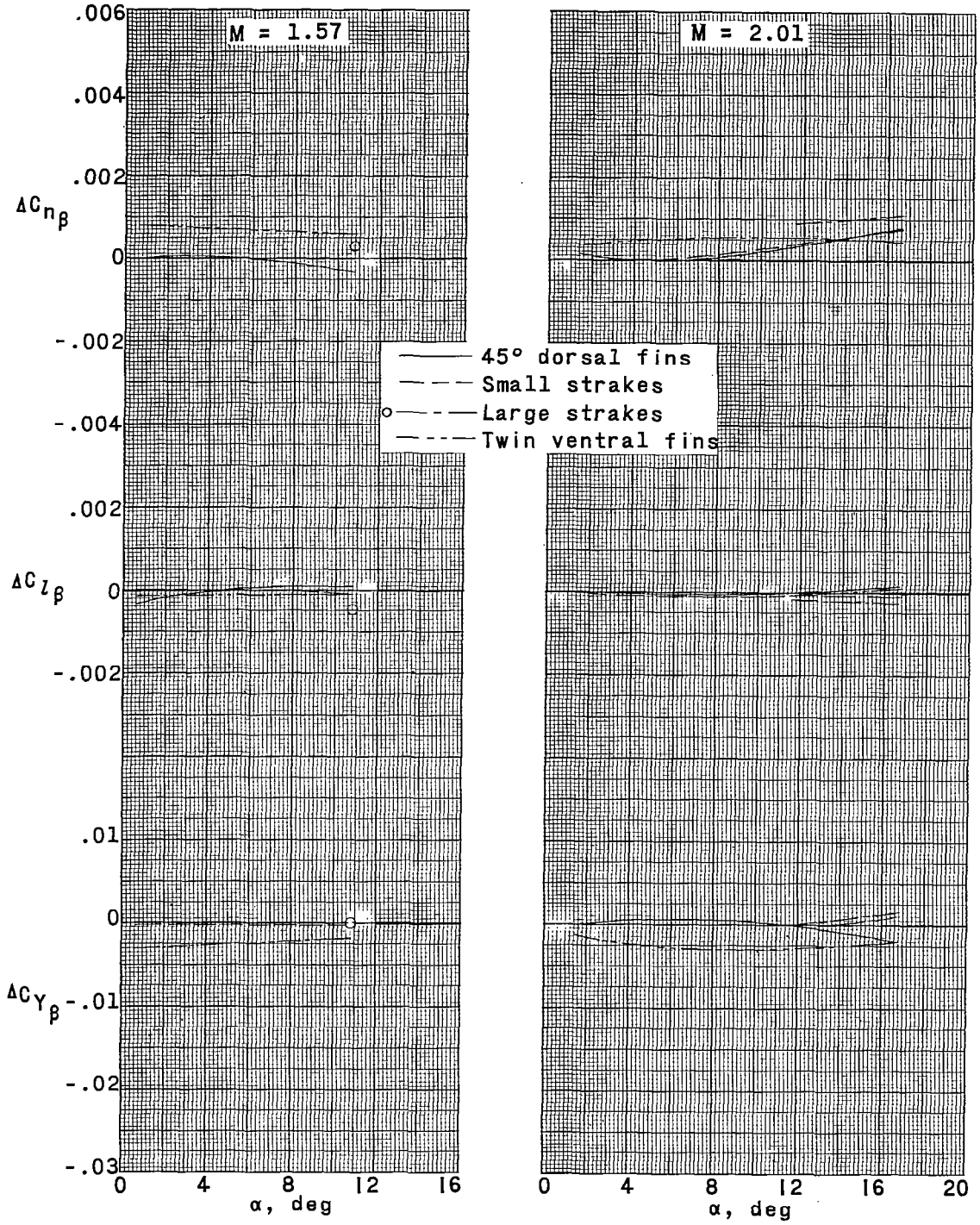

Figure 24.- Increment of directional and lateral stability parameters provided by control devices.